# Geochemical Evolution of Fracture Filling Minerals from the Chalk River Laboratory Site, Ontario, Canada

by

Long Tian

A thesis

presented to the University of Waterloo

in fulfillment of the

thesis requirement for the degree of

Master of Science

in

Earth Sciences

Waterloo, Ontario, Canada, 2016

# Author’s Declaration

I hereby declare that I am the sole author of this thesis. This is a true copy of the thesis, including any required revisions, as accepted by any examiners.

I understand that my thesis may be made electronically available to the public.

# Abstract

The isotope geochemistry combined with fluid inclusion studies of several generations of fracture minerals from the Chalk River Laboratory site (CRL) has been applied to investigate the past fluid evolution including hydrothermal processes and hydrogeochemical evolution of the rock mass. Typical fracture minerals found at the CRL site include chlorite, quartz, dolomite, and calcite. Fracture mineral investigations use oxygen and carbon isotopes from calcites combined with fluid inclusion information such as homogenization temperatures (Th), and melting temperatures (Tm) to calculate temperature and salinity of calcite forming fluids. By combining Th with oxygen isotopic data, we were able to use $\delta^{18}O$ geothermometry calculations to estimate past isotopic characteristics and composition of the fluids responsible for calcite precipitation.

From petrologic evidence, calcite from the CRL site mainly includes four varieties: fibrous calcite, metasomatic calcite, crystal calcite, and vuggy calcite. Fibrous calcite precipitated at a temperature of 78 to 128 $^{o}C$ with a $\delta^{13}C$ signature of -4.91 to -7.88 ‰ (VPDB) and a $\delta^{18}O$ signature of -9.36 to -17.34 ‰ (VPDB). These calcites were formed at an elevated temperature, in a low salinity, Na-Cl fluid that could have been a mixture of hydrothermal water derived from meteoric fluids or seawater. Metasomatic calcite precipitated at 62.1 to 90.0 $^{o}C$ with a $\delta^{13}C$ signature of -4.64 to -8.59 ‰ (VPDB) and a $\delta^{18}O$ signature of -11.98 to -15.08 ‰ (VPDB). These fluids were elevated in temperature, had higher salinity and a Ca-Na-Cl composition similar to a sedimentary basinal brine.

Crystal calcite separated into three groups according to fluid inclusion analyses and results, which are (a) elevated-temperature (67 to 113 $^{o}$C) low-salinity calcite (lower than 15.14 wt. %), (b) elevated-temperature (73.7 to 91.7 $^{o}$C) high-salinity (30 to 40 wt. %) calcite, and (c) higher-temperature (179.6 to 199 $^{o}$C) low-salinity (lower than 7.33 wt. %) calcite. Group (a) has a $\delta^{13}$C isotopic signature of -5.61 to -10.42 ‰ (VPDB) and a $\delta^{18}$O signature of -8.35 to -16.04 ‰ (VPDB), Group (b) has a $\delta^{13}$C isotopic signature of -4.64 to -8.60 ‰ (VPDB) and a $\delta^{18}$O signature of -12.34 to -15.04 ‰ (VPDB), and Group (c) has $\delta^{13}$C signature of -5.59 to -8.06 ‰ (VPDB) and a $\delta^{18}$O signature of -10.03 to -16.17 ‰ (VPDB). Group (a) most likely formed from a hydrothermal fluid with a meteoric water origin, Group (b) could have formed during hydrothermal fluid mixing with an evaporated seawater or basinal brine, and group (c) seems to have formed as a result of a mixture of meteoric and lower salinity metamorphic or crystalline rock fluids. Vuggy calcite precipitated at 85 to 89 $^{o}$C with a $\delta^{13}$C signature of -7.47 to -9.04 ‰ (VPDB) and a $\delta^{18}$O signature of -9.32 to -10.59 ‰ (VPDB). This case is from a high temperature, high Ca-Na-Cl salinity fluid which is hydrothermal fluids mixed with basinal brines.

Strontium isotopic ratios, thorium-uranium ratios and REE data associated with the fracture calcites show that they have a limited water/rock interaction with the host bedrock. Some elevated thorium or uranium concentration were sourced from specific rock types such as pegmatite intrusions in the site.

# Acknowledgments

I would like to thank my advisor Dr. Shaun K. Frape for his guidance and patience in the lab and all the thesis edits. Thanks for giving me a chance to participate in this project and helping me with all my confusion.

I would like to thank Rhys Gwynne for helping me in the Environmental Isotope Laboratory and fluid inclusion experiments. I would like to thank Lori Labelle, and Yinze Wang for the assistance of my thesis.

I would like to thank my parents for all the support of my master study. I appreciate my mom Nai Zhang to help me in fluid inclusion experiments and analyses in China.

I would like to thank Karen Sharp for answers of my questions and assistance of my thesis.

I would like to thank my committee, Brian Kendall and Lingling Wu for your help, feedback and constructive comments.

# Table of Contents

# List of Figures

# List of Tables

# Introduction

In the final stages of bedrock cooling, secondary and late stage minerals are often precipitated in open fractures and voids. In later stage evolution of the bedrock groundwater chemistry, pressure, and temperature are major factors that control weathering reactions and the formation of additional secondary fracture mineral phases after the initial magmatic cooling of the bedrock. Therefore, fracture minerals are useful as indicators to evaluate the origin and historical evolution of fluids in the subsurface. As a result these mineral phases are used to evaluate hydrogeochemical stability at sites proposed for the long term storage of radioactive waste in crystalline bedrock (Tullborg, 1989a; Bottomley and Veizer, 1992; Frape et al., 1992; Blyth et al., 2004, 2009). In addition, fracture minerals occupy the most significant pathways for radionuclide migration from potential repositories and are therefore important to nuclide transport in deep crystalline rock environments (Blyth et al., 2009).

The motivation behind this project was to assess the suitability of crystalline bedrock at the Chalk River Laboratories as a potential site for the disposal of low and intermediate level radioactive waste. In order to do this the history of the rock mass and the potential for hydrogeochemical transport within the system had to be evaluated. Stability of the site depends on rock fracture and matrix porosity (Blyth et al. 2009). Fracture mineral analysis has been applied to assess subsurface stability in radioactive waste disposal projects in many countries such as Canada, the United States, France, Finland, and Sweden (Blyth et al., 2004 and 2009). The ability of these sites to prevent nuclide migration should last for at least 100 ka (Carlson et al., 1996). The

selection of radioactive waste disposal sites should consider current hydrogeology, geochemical characterization, long-term geologic stability, far-field natural characteristics, and hydrothermal history (Frape et al. 1992; Bottomley and Veizer 1992; Blyth et al., 2009; Neymark et al. 2013).

The Chalk River Laboratories (CRL) which is the focus of this study, is near Deep River, Ontario on the Quebec border located approximately 200 km northwest of Ottawa (Fig. 1). A large number of research projects by Atomic Energy of Canada Limited (AECL) on the geologic and hydrogeologic conditions at the CRL site have been conducted. Fracture mineral investigations at the CRL have assisted the understanding of paleo-groundwater flow and geochemical evolution in crystalline rock environments (Frape et al., 1992; Bottomley and Veizer, 1992; Blyth et al., 2009).

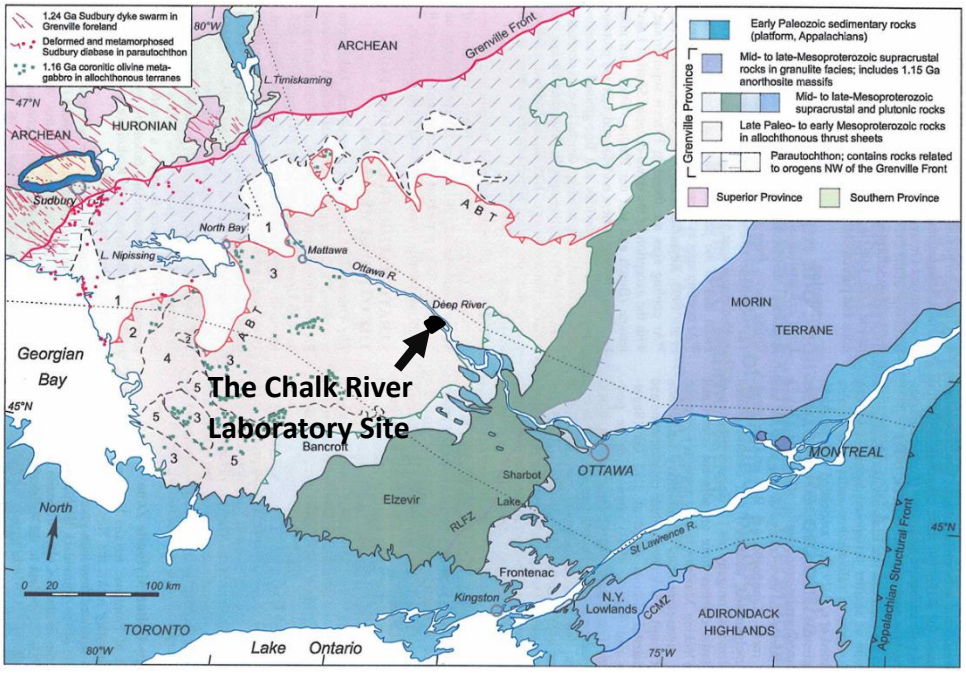

Figure 1. Map of the Chalk River Nuclear Laboratory site

Fracture filling minerals from the CRL bedrock are dominated by carbonate minerals, especially calcite (Bottomely, 1987). Analyses of fracture minerals from the

CRL generally have focused on calcite because it is widely present and forms at environmental temperature from a few degrees to several hundred degrees Celsius (Bottomely, 1987; Blyth et al., 2009). Calcite and other fracture minerals are evaluated in the rock record as indicators of geologic processes such as magmatic and hydrothermal activity. More recently some authors have suggested that hydrogeochemical events such as glacial water intrusion into the deep bedrock may impact fracture mineral precipitation and/or dissolution (Bottomley, 1987; Bukata, 2000).

This study analyzes and compares the petrography, geochemistry, stable isotopic composition ($\delta^{18}O$ and $\delta^{13}C$), fluid inclusions, strontium isotope, and rare earth element (REE) data from core material, taken from a series of recently drilled boreholes at the site, with previous studies to ascertain past geologic and hydrogeologic conditions. The specific objectives of this thesis are: 1) to assess long-term fluid history and stability of the site by using fluid inclusion geothermometry and geochemistry of fracture calcites; 2) to assess if there is any evidence of calcite crystallization under present day, cold climate, glacial conditions or low temperature recrystallization of the calcite at the site; and 3) to evaluate the types of calcites and compare the data from this study to the calcite emplacement history obtained by previous investigations (Bottomley et al., 1987, Bottomley and Veizer, 1992, Bukata, 2000, and Blyth et al. 2009).

Previous studies identified five major factors that influence the hydrostatic conditions of the CRL site: 1) deeper regional groundwater flow; 2) groundwater

mixing between upper modern recharge and deeper saline water; 3) fracture mineral dissolution along major faults; 4) mineral dissolution in the shallow environment; and 5) modern recharge of $O_2$ rich glacial melt water (Bottomley, 1987, Bukata 2000, Blyth et al., 2009, Neymark et al., 2013). Fluid sources identified by these studies and distinguished by chemical and isotopic properties are listed on Table 1.

Table 1. The range of isotopic values from calcite mineralogy for fluid sources suggested by previous studies at the CRL site.

| Source | $\delta^{18}O$ ‰VPDB | | $\delta^{18}O$ ‰SMOW* | | $\delta^{13}C$ ‰VPDB | | Reference |
|---|---|---|---|---|---|---|---|
| | min | max | min | max | min | max | |
| Hydrothermal water | -23 | -18 | 7 | 12 | -8 | -7 | Bukata, 2000 |
| Glacial water | -57 | -47 | -28 | -18 | -23 | -15 | Bukata, 2000 |
| Champlain Sea | -42 | -40 | -12.3 | -10 | -23 | -15 | Bukata, 2000 |
| Meteoric Water | -40 | -39 | -10 | -9 | -23 | -15 | Blyth et al., 2009 |
| Basinal Brines | -49 | -20 | -20 | 10 | -30 | -10 | Blyth et al., 2009 |
| Magmatic/Metamorphic fluid | -27 | -12 | 3 | 19 | -6 | -3 | Blyth et al., 2009 |

* $\delta^{18}O$ ‰ SMOW calculated by $\delta^{18}O$ ‰ VPDB follow by equation:
$\delta^{18}O$ ‰SMOW = $\delta^{18}O$ ‰VPDB*1.03091+30.91
VPDB is the short of Vienna Pee Dee Belemnite; SMOW is the short of Standard Mean Ocean Water;

Previous studies suggested that the $\delta^{13}C$ and $\delta^{18}O$ isotopic results reflect two different origins for the fracture mineral calcite at the CRL site: re-precipitated calcite with depleted $\delta^{13}C$ and enriched $\delta^{18}O$ and hydrothermal higher temperature calcite with elevated $\delta^{13}C$ and depleted $\delta^{18}O$ (Fig. 2). Bottomley (1987) found that most $\delta^{13}C$ values for calcite ranged between -5.5‰ and -8.0‰ (PDB) while the $\delta^{18}O$ values ranged between -8‰ and -17‰ (PDB). Bukata (2000) obtained some additional

elevated $\delta^{13}C$ measurements that extended the range to +2‰ and suggested a magmatic source, although $\delta^{13}C$ values from that study were mostly between -7‰ to -23‰ possibly from mixing between sources (Table 1, Fig. 2). Stable isotopic measurements from Bukata (2000) were similar to those found for many Canadian Shield sites (Blyth et al., 2009). Some studies from other sites such as Simpevarp area and Forsmark in Sweden also found some calcites have overlapping isotopic data (Drake and Tullborg 2009; Sandstrom and Tullborg 2009). For example, Drake and Tullborg (2009) found that calcite has $\delta^{13}C$ values between -2.1‰ and -16‰ (PDB) while the $\delta^{18}O$ values ranged between -9.5‰ and -23.5‰ (PDB). In another study, Sandstrom and Tullborg (2009) found that calcite has $\delta^{13}C$ values between -1.6‰ and -30‰ (PDB) while the $\delta^{18}O$ values were between -7‰ and -24‰ (PDB).

In order to constrain the temperature of formation and further understand the origin of calcites in fracture systems, fluid inclusion analyses were introduced as a geothermometry tool (Blyth et al, 1998 and 2009; Drake and Tullborg 2009; Sandström and Tullborg 2009). The temperature of calcite formation has been measured using fluid inclusion geothermometry by previous studies at the CRL site as well as this study (Bukata, 2000). Previous studies identified three different families of calcites using fluid inclusions analyses, 1) those having high homogenization temperatures (approximately 200 ℃) with low salinities, 2) calcites with low homogenization temperature (70 ℃ to 120 ℃) and low salinity, and 3) low homogenization temperature (70 ℃ to 120 ℃) and high salinity (Bukata, 2000). In addition, it was reported that the presence of the laumontite as a fracture mineral was associated with hydrothermal

calcite, having depleted $\delta^{18}O$ values, probably formed at more than 300 ℃ (Bottomely, 1987; Bottomely and Veizer, 1992). The fluid inclusion data confirmed many of the high temperatures suggested by homogenization temperature (Bukata, 2000; Blyth et al., 2009).

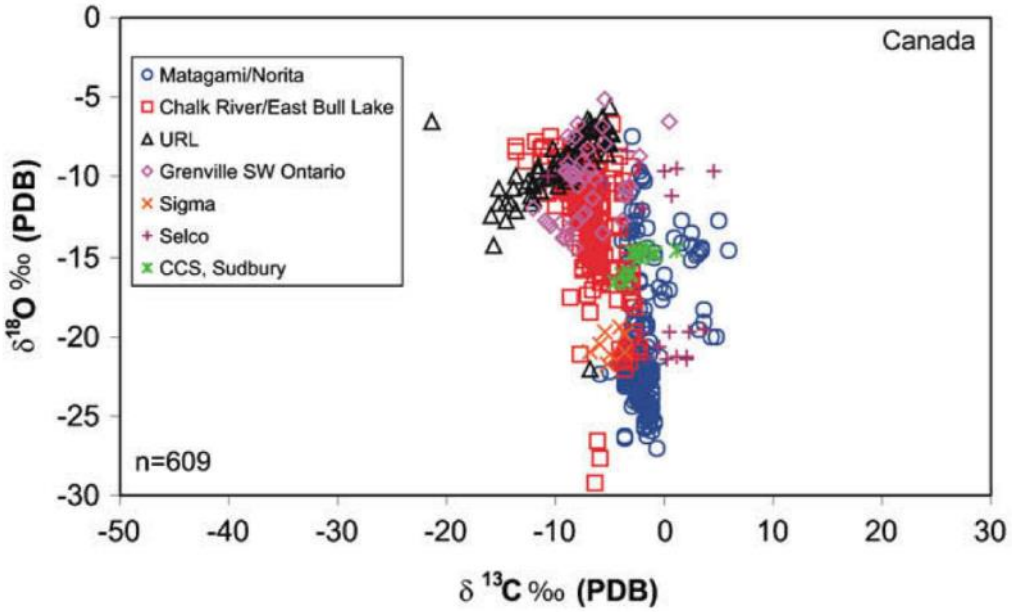


Figure 2. The range of isotopic measurements on fracture calcites from other Canadian sites compared to Chalk River calcites measured in previous studies at the site. Also shown are the potential end members; hydrothermal or modern/meteoric source water (after Blyth et al., 2009)

Uranium-series measurements were widely obtained on fracture calcites in the past, in order to provide observation on the long-term stability of the current hydrological events and the crystallization age of the calcites (Milton, 1987; Milton and Brown, 1987; Neymark et al., 2013). The ages of calcites deposited at the CRL site have been estimated from 5000 to 500,000 years BP by uranium and thorium ratio dating (Milton, 1987; Milton and Brown, 1987). Bukata (2000) estimated the calcite age range from < 9 ka to >350 ka by thorium/uranium ratios which is similar to the Milton (1987) study. Neymark et al. (2013) analyzed the calcite and obtained ages from 400 ka to 1500 ka

with uranium and thorium dating. These studies speculated that the high uranium activity ratios observed at the CRL site were probably due to extensive post glacial bedrock fracturing and groundwater movement (Milton, 1987; Neymark et al., 2013).

**Bedrock Geology at CRL**

The Chalk River Laboratory site is located within the central gneissic belt (CGB) of the Grenville Province which formed 1-1.8 Ga ago within the Canadian Shield (Bukata, 2000, Blyth et al., 2009, Neymark et al., 2013). It is located at the intersection of the Ottawa – Bonnechere graben and Allochthonous terrane which is between the Composite Arc Belt and Parautochthonous terrane (Fig. 3). The CGB is believed to be transported from the southeast allochthonous lithotectonic and northern parautochthonous crust, which originally came from the pre-Grenvillian Laurentian margin (Ketchum and Davidson, 2000; Neymark et al., 2013). The bedrock of the CRL area is mostly amphibolite to granulite facies gneisses (Catto et al., 1982; Neymark et al., 2013).

The geologic history of the CGB of the Grenville Province can be described using a time sequence (Fig. 4). The first intruded plutons are believed to have occurred between 1740-1650 Ma ago during the Late Paleoproterozoic Central Plains Orogen (Sims and Peterman, 1986). The crust mainly developed in the Algonquin Terrain of the CGB during that time (Bukata, 2000). The second intruded plutons are believed to have occurred from 1460-1340 Ma ago into the Mid-Mesoproterozoic Granite-Rhyolite Province (Sims and Peterman, 1986; Neymark et al., 2013). There is

evidence of orthogneisses crystallizing in the CGB during this period (Davidson and Van Breement, 2001; Neymark et al., 2013). Felsic magmatism and metamorphism under granulite facies conditions occurred between 1450 Ma and 1420 Ma in the Algonquin terrain (Bukata et al., 2000).

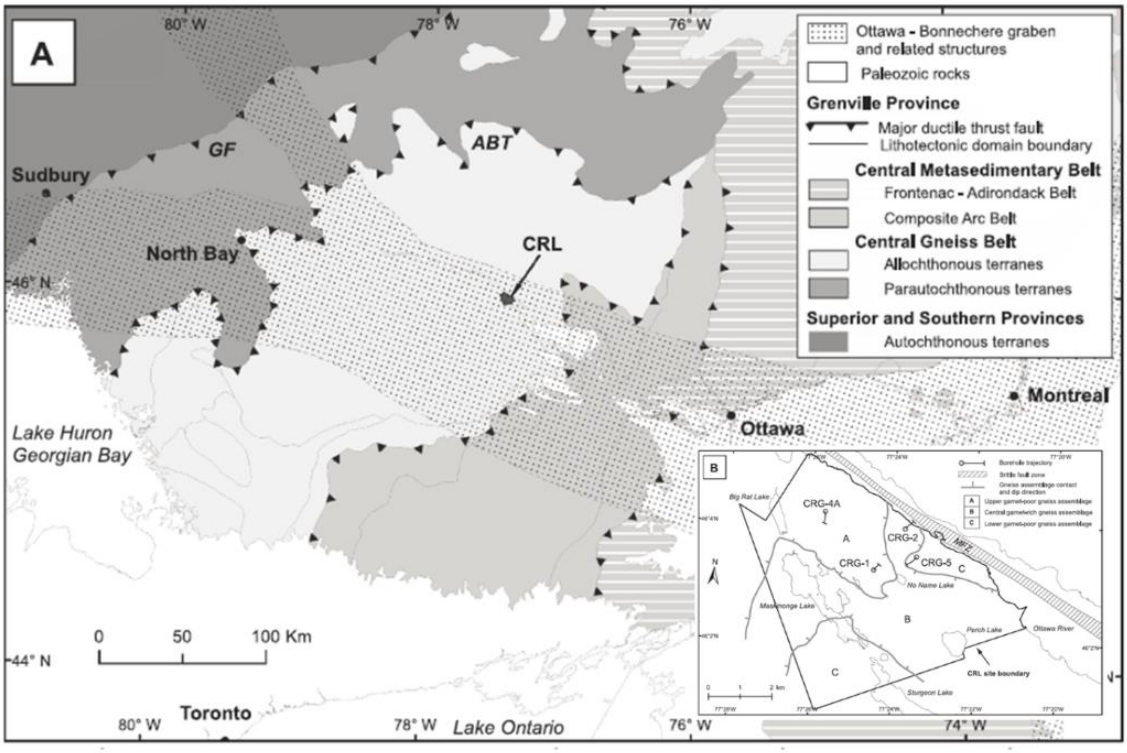


Figure 3. A) Lithotectonic subdivision of the southwestern Grenville Province and the Ottawa-Bonnechere graben including the location of the Chalk River Laboratories site (CRL) (Davidson, 1998; Neymark et al., 2013). B) Site geology of the CRL site showing three different gneiss assemblages from A to C (Thivierge et al., 2011).

Grenville orogenies that probably affected the site were the Elzevirian (1350-1180 Ma) and Shawinigan (1190-1140 Ma) to the southwest of the area. The Grenville orogeny included two province wide collisional events named the Ottawan orogen (1090-1020 Ma) and Rigolet orogeny (1000-980 Ma) (Neymark et al., 2013, Mclelland et al., 2010). After these two collisional events, the Grenville orogenies became more stable and cooling, uplift and erosion occurred over the next 1000 Ma (Bukata, 2000).

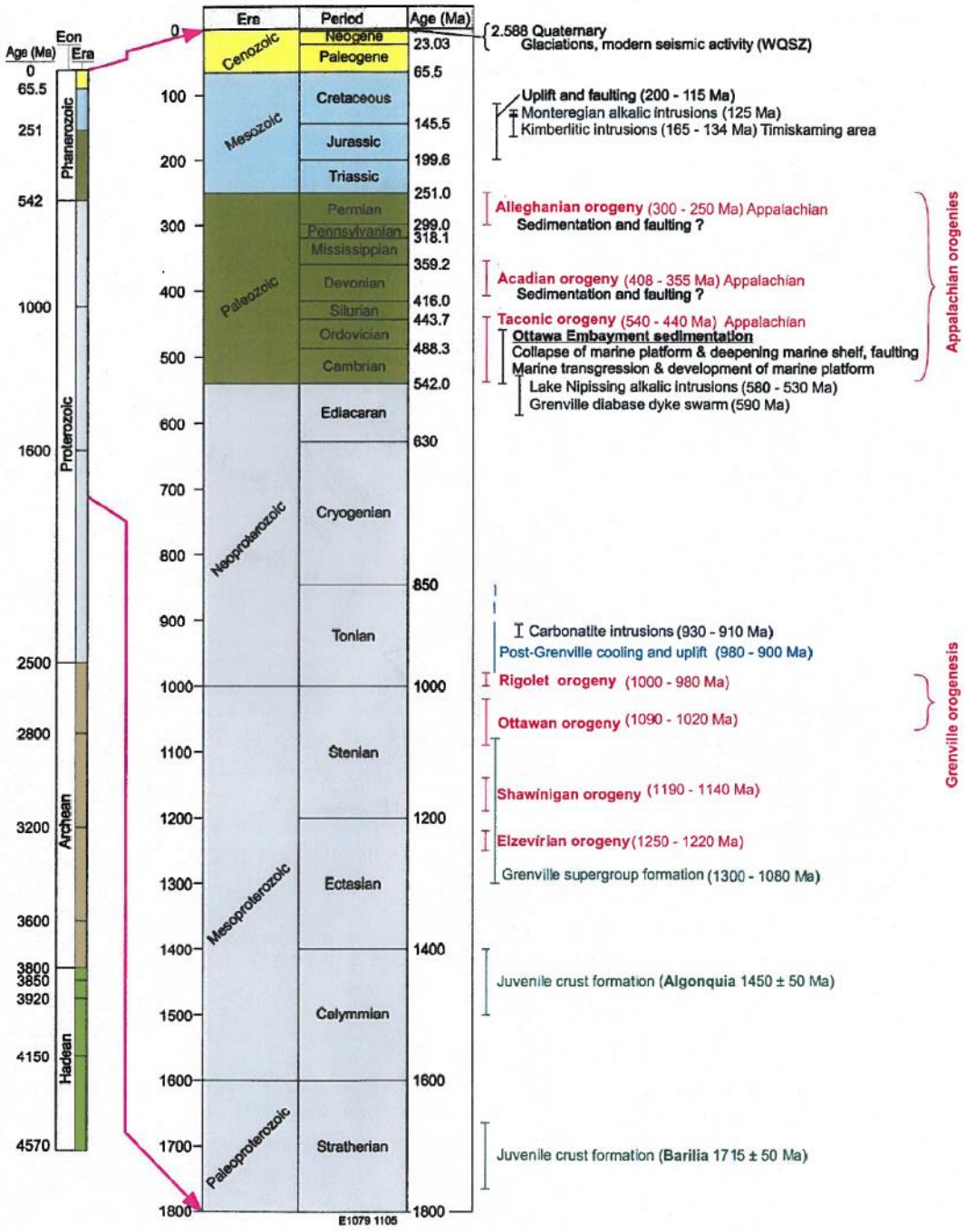


Figure 4. Stratigraphic column for the CRL site showing geologic ages and information and tectonic events that occurred in the area (from Thivierge et al., 2011).

The Grenville orogenic belt was a peneplain by the Early Paleozoic (Easton, 2000). Several dyke swarms in the Ottawa-Bonnechere graben system, which may have

impacted fracture mineral formation at the CRL site, occurred prior to and during the Early Paleozoic (Fig. 3 and 4). The Ottawa-Bonnechere graben system is a seismically active north-west-north striking fault system (Fig. 3) (Bukata, 2000, Neymark et al., 2013). A major diabase dyke swarm intrusion happened during the Late Neoproterozoic around 590 Ma at the CRL site (Fig. 4). The carbonatitic and Lake Nipissing alkali plutonic rocks evolved in this area after the diabase dykes around 530-580 Ma (Kamo et al., 1989, Bukata, 2000, Neymark et al., 2013). The Taconic, Acadian and Alleghanian orogenies dominate the Paleozoic Era from 540-440 Ma, 408-355 Ma and 300-250 Ma respectively (Fig. 4). The Taconic orogeny covers the time period of Cambrian marine transgression and Ordovician development and collapse of the marine platform into a deepening marine shelf (Neymark et al., 2013).

The Mesozoic and Cenozoic are the last periods of bedrock building. Uplift and faulting dominated the Mesozoic from 200 Ma to 115 Ma. The Mesozoic Era involved two intrusions which are the Monteregian Alkali Intrusions around 125 Ma and Kimberlitic intrusions around 165-134 Ma. Previous studies in the area suggested that geologic activity at the CRL site was dormant during the Cenozoic. Geologic evidence from the site shows that there is a lack of either sedimentary or igneous rock deposition or major tectonic activity at this time (Neymark et al., 2013). At the surface there are Quaternary sediments covering large areas of the site (Fig. 4).

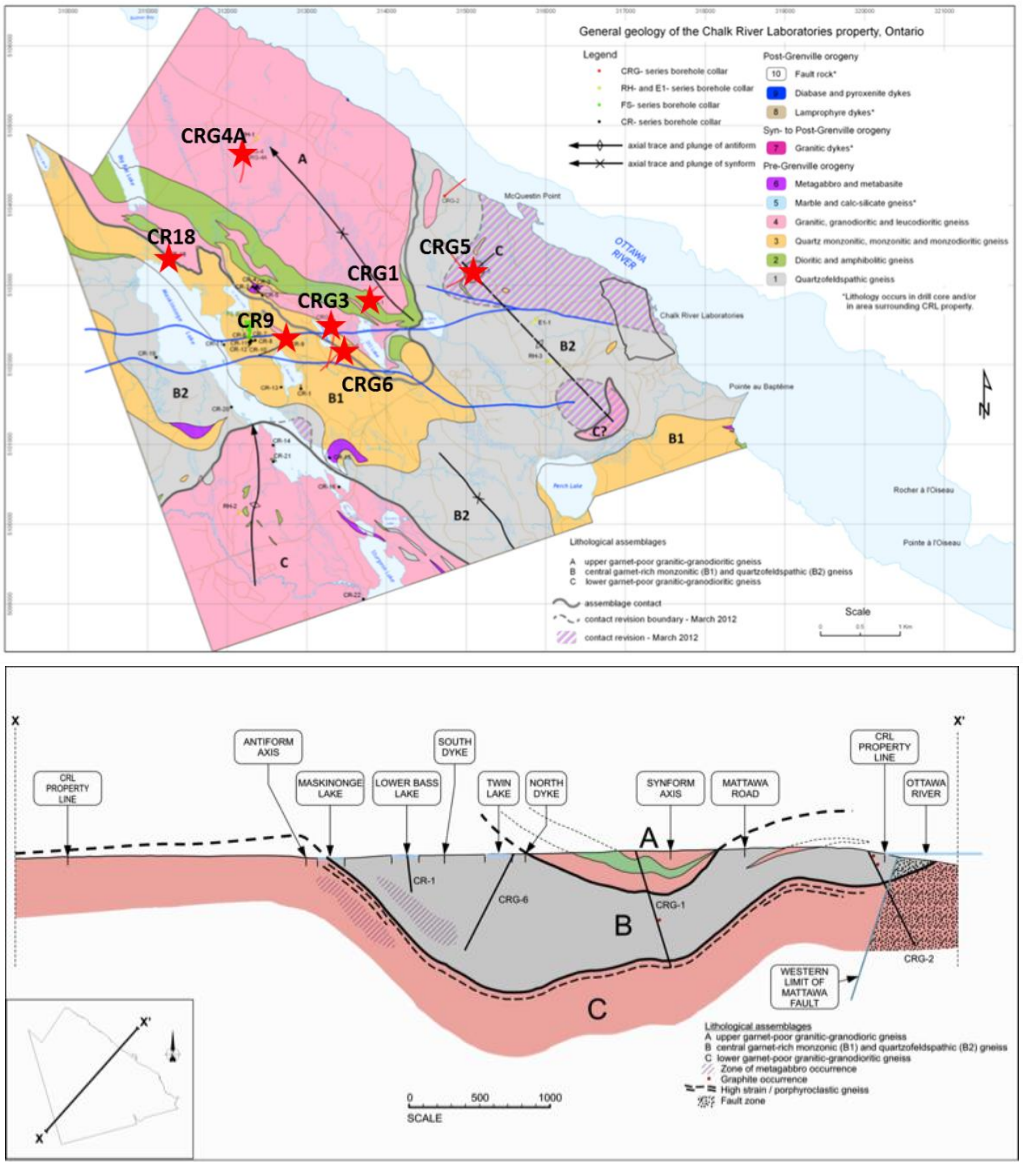


Figure 5. Lithostructural configuration of the CRL site including the three bedrock assemblages recognized by CRL personal and a cross section showing the geologic divisions (from Thivierge et al., 2011)

The CRL site is located in the Ottawa-Bonnechere graben system which is a long rift valley system (Bukata, 2000). The study site is adjacent to the Mattawa Fault Zone (Fig. 3B) next to the Ottawa River (Fig. 5) (Thivierge et al., 2011). At the site there is an anticlinal and a synclinal system running from SW to NE (Fig. 5). The lithostructure of the CRL site can be divided into three gneissic assemblages: (A) an

upper garnet-poor gneissic assemblage, (B) a central garnet-rich gneissic assemblage, and (C) a lower garnet-poor gneissic assemblage (Fig. 5).

The lithofacies of assemblage (A) is dominated by hornblende-biotite quartz-feldspar gneiss of granitic to granodioritic composition. Accessory rocks in this assemblage are biotite-hornblende-rich mafic bands and lenses comprised of amphibolites, metadiorite, metagabbro, and metabasite (Neymark et al., 2013). There is also some calc-silicate gneiss with mesocratic and biotite-hornblende monzodiorite to diorite gneiss units close to the base of the upper gneiss assemblage.

Assemblage (B) is a garnet-rich gneiss and involves distinctive garnet-bearing leucocratic units and mafic units. The lithofacies of (B) is dominated by biotite-garnet-hornblende quartz monzonitic, monzonitic, monozodioritic gneiss and grey garnet-biotite quartz-feldspar gneiss (Neymark et al., 2013). Both quartz monzonitic and monzodioritic gneisses contain more hornblende than other rock types. They appear to contain recrystallized megacrystic plutonic textures.

Assemblage (C) has heterogeneous, grey or pink migmatitic magnetite-biotite granitic to granodioritic gneiss which is mixed with mafic magnetite-biotite-hornblende metadiorite/amphibolites or metabasite bands within the top 500 meters of the upper contact (Neymark et al. 2013). There are several porphyroclastic gneissic zones within the top 200 meter thick section of assemblage (C). Under the upper 500 meters is the deeper part of assemblage (C) which has more homogeneous, pink foliated magnetite-biotite metagranite generally lacking mafic lenses compared to the upper parts (Neymark et al. 2013).

**Fracture minerals**

At the CRL site more than 20 different types of fracture minerals have been identified by this study and previous researchers. The most common minerals are calcite, chlorite, quartz, dolomite, and clay. Hematite in fracture mineral assemblages at the site most likely indicates oxidizing groundwater conditions, whereas graphite and sulphides occur in other fractures indicating reducing conditions in the past (Neymark et al., 2013). Calcite predominates in the A and B assemblage as a primary fracture filling.

As the Canadian and Fennoscandian shield have similar host rock morphologies, the comparison of the host rock and fracture mineralogy from other sites evaluated from radioactive waste programs within the two shields (Table 2) can further assist in a comparison of the mineralogy found at the CRL study site. Fracture minerals at all sites worldwide are dominated by calcite and chlorite. The CRL site also contains zeolites and other silicates similar to several other sites in the Canadian and Fennoscandian shields.

Table 2. A comparison of sites from the Canadian and Fennoscandian shield where calcite geothermometry studies have been conducted. The table includes host rock, fracture rock mineralogy, and calcite type. (Blyth et al. 2009; Bottomley, 1987; Fritz et al., 1989, Tullborg 1989a; Larson and Tullborg 1984)

| Country | Site | Rock types | Fracture minerals | calcite type |
|---|---|---|---|---|
| Canada | Matagami/Norita (Jones 1987) | Mafic volcanics and ultramafics | Calcite, quartz, chlorite, clay | Massive veins; sucrosic veins; platy grey coating on open fractures |
| | Sigma (Jones 1987) | Felsic volcanics | Calcite, quartz, chlorite, clay | Not described |
| | East Bull Lake (Bottomley 1987) | Gabbro and anorthosite | Calcite, chlorite, zeolites, clay | Dense coarse crystalline; Fine and friable granular |
| | Copper Cliff South (Bottomley 1987) | Mafic intrusive (norite) | Calcite, quartz, chlorite, clay | Not described |
| | Selco (Macdonald 1986) | Felsic volcanics | Calcite, quartz, chlorite, clay | Anhedral with quartz and euhedral chlorite |
| | URL (Jones 1987) | Granitic gneiss | Calcite, quartz, chlorite, clay, zeolites, epidote, gypsum, iron oxides | Massive veins; sucrosic veins; platy grey coating on open fractures |
| | Chalk River (Bottomley 1987) | Metasedimentary gneiss | Calcite, chlorite, zeolites, silicates | Dense coarse crystalline; fine and friable granular |
| | SW Ontario (Jones 1987) | Metasedimentary gneiss | Calcite, quartz, chlorite, clay | Massive veins; sucrosic veins; platy grey coating on open fractures |
| Sweden | Stripa (Fritz et al. 1989) | Granitic intrusion | calcite, chlorite, epidote, quartz, mica, fluorite | Massive with chlorite/epidote; Massive with fluorite, platy |
| | Klipperas (Tullborg 1989) | Granitic intrusion | calcite, clay, epidote, quartz, chlorite, micas, iron oxides | Closed fracture with epidote, mica, quartz and chlorite; open fracture with chlorite and hematite; open fractures with clays and Fe-oxyhydroxides |
| | Finnsjon (Larson and Tullborg 1984) | Granitic gneiss | calcite, clays, prehnite, chlorite, epidote | Prismatic; Granular |

(Table 2 continue)

| Country | Site | Rock types | Fracture minerals | calcite type |
|---|---|---|---|---|
| Sweden | Taavinunnanen (Larson and Tulborg 1984) | Gabbroic intrusion | calcite, clay, chlorite, quartz, prehnite, zeolite | GenerationaI, sealed fracture; generation II, open and sealed fracture; generation III, Open fracture; open and sealed, relative age determined |
| Finland | Olkiluoto (Blyth 1993 and 2004) | Granitic gneiss | Calcite, clay, chlorite, quartz, zeolites, pyrrhotite | Crystalline veins; Crystalline veins with clays |
| | Palmottu (Blomqvist et al. 1991 and 2000) | Granitic gneiss and schist | Calcite, clay, iron oxides | Massive veins; Crystalline vugs; Powdery coatings on open fractures |
| | Mäntsälä (Ruskeeniemi et al. 1996) | Mafic volcanics and gabbro | Calcite, zeolites, chlorite, clay, iron oxides, prehnite, quartz | Massive veins; Rhombohedral crystals on open fractures |
| | Ylivieska (Blyth 1993) | Mafic and ultramafic intrusions | Calcite, clay, chlorite, serpentine, gypsum, zeolites | Rhombohedral veins; Euhedral crystals on open fractures; Thin, compact crystalline veins; Radiating, elogate crystals on open fractures |
| | Juuka/Miihkali (Blyth 1993) | Ultramafic serpentinite | Calcite clay, chlorite, zeolites magnesite, quartz, serpentine | Thick, compact crystalline veins; Euhedral crystals on open fractures; Thin, compact crystalline coatings on open fractures; Sucrosic coatings on open fractures |

**Quaternary geology**

The thickness of Quaternary sediments in the CRL area is mostly less than 100 m and consist of sand, silt and clays (Catto et al., 1982). Previous studies suggested that much of the Quaternary sediment formed post glaciation (<12000 years BP) and during the Champlain Sea intrusion (Catto et al., 1982; Cloutier et al., 2010). The Champlain Sea covered parts of the area around 12,000 years ago and consisted of a mixture of melting water from the Laurentide Ice Sheet, local precipitation, and salt water from the Gulf of St. Lawrence (Parent and Occhietti, 1988; Bolduc and Ross, 2001). The Champlain Sea was probably present at the CRL site from approximately 11,300 to 11,100 years BP, according to some evaluations of elevation of the marine limit and possible glacial marine clays (Catto et al., 1982).

The last Quaternary glacial cover in the CRL area was deposited about 11,300 years ago consisting of upper-Wisconsinan sediments including glacial till, glaciofluvial sand and gravel (Catto et al., 1982; Bolduc and Ross 2011). The Ottawa River increased its drainage about 10,500 years ago due to the opening of the North Bay drainage route (Boyko-Diankonow and Terasmae 1975). Quaternary sediments in the CRL area can be divided into two parts, an early glaciomarine sequence which deposits probably before 11,000 years and a later fluvial sequence that was deposited before 11,000 years BP. The bottom part of the sequence contained fossiliferous marine clays, silts and thin aeolian sand layers. The shallow upper parts contain channel sands, which includes undergone aeolian reworking, fluvial sand, and gravels from the Ottawa River (Catto et al., 1981).

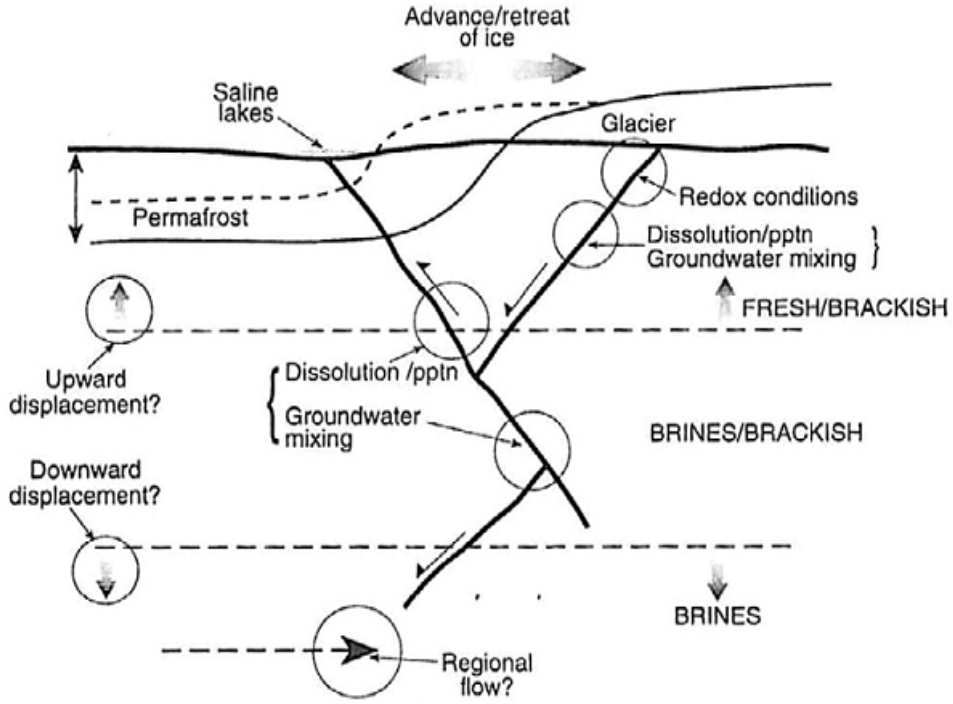


Figure 6. Conceptual model of a typical groundwater scenario that would impact fracture minerals at the CRL site (from Smellie and Frape, 1997). Model shows different fluids mixed in fractures underground.

Glacial and marine sediments on the CRL site such as the sand and gravel layers may have allowed fresh glacial water or marine Champlain Sea fluids to recharge into the subsurface along open fracture zones containing mineralization in the bedrock. A conceptual model that could be used for the site is similar to that proposed by Smellie and Frape (1997) and shown on Figure 6. Recharging glacial fluids would have the potential to dissolve, remobilize and precipitate young calcite in the bedrock at a site. Their presence or absence and location of such mineral phases is a critical issue to site suitability for a potential waste repository.

# Methodology

Four methods were followed to investigate the fracture mineralogy for the present research: petrography, stable isotopic analyses, fluid inclusion analyses, and geochemistry of major and rare earth elements (REE). More than 20 boreholes were drilled and cored at the CRL site and core material from seven of these were used in this study, including CR9, CR18, CRG1, CRG3, CRG4A, CRG5, and CRG6 (Fig. 5).

Petrography in this study was used to identify fracture mineral phases and elucidate the formation sequence of vein fillings. Stable isotopes of $\delta^{13}C$ and $\delta^{18}O$ were used to initially separate the types and possible origins of the calcite mineralogy identified from the petrographic analyses. Fluid inclusion geothermometry was employed to assess and constrain the temperature and salinity of formation fluid or groundwater that was responsible for calcite precipitation. Chemistry data including REE's, cathodeluminescence analyses, thronium-uranium ratios, and strontium isotopic ratios were used to further evaluate the characteristics and geochemical relationship of the fracture minerals with the host rocks at the CRL site.

Petrographic analyses of fracture minerals using the microscope and cathodeluminescence (CL) done for a large suite of samples. The petrography and CL analyses were done at the Laboratory Center of the Research Institute of Petroleum Exploration and Development (RIPED), China. The veins and other fracture minerals in thin sections were observed using a Zeiss AXIOSKOP microscope to analyze the crystallization characteristics of representative samples from varies stages of mineralization. Different colors of calcite in cathodeluminescence photos show the

different stages of calcite mineralization in individual samples from a fracture system (Pagel et al., 2013). The CL analyses used a CL8200 MK5 cathode luminescence system and ORTHOPLAN polarization microscope.

Isotopic analyses for $\delta^{13}C$ and $\delta^{18}O$ ratios of fracture calcites were run at two different facilities, Environmental Isotope Laboratory (EIL) at the University of Waterloo (UW) and earlier analyses were done at Isotope Tracer Technologies ($IT^2$), Waterloo. Material for isotopic analyses was selected from fractures at various depths in the seven cores. For samples run at $IT^2$, calcite samples were prepared using 2 mg for each sample. Samples are weighed into glass reaction vessels, which are flushed with helium, sealed and reacted with 0.1 ml of pure $H_3PO_4$ acid at 46 $^oC$ for 24 hours. The carbon dioxide gas which is created from the reaction was injected into a Delta plus XL Stable Isotope Ratio Mass Spectrometer via a ConFlo III Interface. Most calcite isotopic analyses were performed at the University of Waterloo (UW) Environmental Isotope Laboratory. The method at UW uses 0.2 mg of sample and a similar method to flush and acidify the sample to produce $CO_2$ gas at 90 ℃ after 3 hours of reaction. The carbon dioxide was collected and injected into a Gilson 222 XL LH connected to a GVI IsoPrime-TG/MG mass spectrometer used for sample analyses at UW.

Fluid inclusion analyses involving homogenization temperatures (Th) and melting temperatures (Tm) for selected samples were done at the Laboratory center of the RIPED, China and UW. The instruments for fluid inclusion analyses at RIPED were a Zeiss AXIOSKOP microscope and LINKAM MDS 600 heating and cooling stage

with a temperature range from -190 ℃ to 600 ℃. In this method five primary fluid inclusions in a sample are tested at one time and the size chosen for fluid inclusion analyses was primarily close to 10 μm. The melting temperature (Tm) is recorded to measure the salinity of the fluid from which the calcite formed (Roedder 1984; Zhang 2016). For the melting temperature, the sample is first cooled to -100 ℃ by 20 ℃/min and held at -100 ℃ for one minute. Next the samples are thawed to -50 ℃ by 20 ℃/min then to 5 ℃ by 1 ℃/min. The temperature recorded occurs when the fluid inclusions finished melting, i.e., the temperature at which a free gas bubble forms and just starts to move. In addition, eutectic temperature (Te) was also measured during this step ay the temperature that fluid inclusion started to melt. Te values were applied to analyze the salinity type in the calcite. For example, when the Te values measured around -25 $^{o}$C that probably indicated a Na-Cl salinity otherwise when it was lower than that temperature it was estimated to be a high Ca-Na-Cl salinity in this study (Roedder 1984).

The homogenization temperature (Th) is a measured of the temperature of the fluid from which the calcite formed (Roedder 1984). For the homogenization temperature, all thin sections are put into a refrigerator under -18 ℃ for a 48 hour period to enhance the opportunity for a free gas phase to form as a bubble. Next the sample is heated to 50 ℃ by 10 ℃/min then to 160 ℃ by 2 ℃/min. The homogenization temperature is the temperature at which the free gas bubble disappears in the fluid inclusion. Fluid inclusions selected to measure in this study are primarily gas-liquid primary fluid inclusions, and the gas-liquid ratio is less than 15%. Fluid inclusions that contain gas ratios of more than 15% will mostly have gas bubble when it formed (Roedder 1984,

Zhang 2016). Therefore, this kind of fluid inclusions cannot be used to derive accurate homogenization values. In addition, in any Th-Tm analyses inclusions were not used twice as calcite is a temperature solubility sensitive mineral and inclusion parameters can be altered by heating (Roedder 1984).

Geochemistry analyses of rare earth element data were analyzed at the Analytical Laboratory Beijing Research Institute of Uranium Geology (ALBRIUG) and Actlabs, Canada. Sample powders for REE analyses were prepared using a hydrofluoric acid (1.16 g/mL) and nitric acid (1.42 g/mL) dissolution in a sealed container (Li et al., 2011). Samples were then put on a hot plate to evaporate the hydrofluoric acid. Next 2% nitric acid was used to dissolve the sample in a sealed container. Finally ICP-MS was used to measure the REE concentrations.

A limited number of calcites, groundwater samples and crush and leach samples were subsampled for $^{87}Sr/^{86}Sr$ analyses. These analyses were performed at the University of Waterloo Environmental Isotope Lab using thermal ionization mass spectrometry (TIMS). For carbonate samples, 1 mg of calcite was dissolved using 50% $HNO_3$, leaching any available strontium into solution. This solution was then passed through a strontium selective resin (50-100 μm mesh). A water sample between 20 to 120 mL containing a minimum of 6 μg of aqueous strontium was filtered at 0.2 μm and dried before a similar dissolution in 50% $HNO_3$ and resin extraction. In both cases purified strontium was then redissolved using 0.3 M $H_3PO_4$ and loaded onto 99.999% zone refined, degassed rhenium filaments. Filaments were loaded alongside an additional ionizing filament into a Thermo-Finnegan TRITON thermal ionization mass

spectrometer and ionized at approximately 1500 ℃ for analysis. All values have been measured alongside the NBS international standard material NIST SRM 987 ($^{87}Sr/^{86}Sr$ = 0.710245) and corrected for mass fractionation and $^{87}Rb$ interference using $^{87}Sr/^{86}Sr$ = 8.375209 and $^{87}Rb/^{85}Rb$=0.386 respectively. Absolute ratios are reported with a standard error of ±0.000002 (ThermoFinnigan, 2002).

# Results and Discussion

### Petrography and fracture minerals

In this study, seven boreholes (Fig. 5a) were selected to examine for fracture mineral composition. The geological structure of the CRL site is a complex synclinal structure in cross section from the NE to SW direction (Fig. 5b). As the underlying geological structure is complex, most boreholes were drilled across several different bedrock gneissic types and summary information for each borehole is shown on Figure 7. Values for depth used to describe the sample position indicate the length along the borehole in this study. Some of the values are not the exact depth of sample below the surface but most are similar as most of the boreholes are almost vertical. As shown, boreholes CR18 and CR9, are within bedrock assemblage B. The upper 38.6 m of CRG6 is in bedrock unit A but contained no fracture calcites and unit B occurs in the lower section of borehole. Borehole CRG3 crosses unit A in the upper 96.9 m, consists of unit B from 96.9 m to 1081.1 m and unit C in the lower section. Borehole CRG4A has unit A in the upper 517.97 m, unit B from 517.97 m to 1157 m (bottom). Borehole CRG1 has unit A in the upper 179.2 m, unit B from 179.2 m to 832 m and C

in the lower section below 832 m. All of borehole CRG5 is within rock assemblage C. The samples selected for detailed fracture mineral examination and calcite isotopic analyses from the seven boreholes are also shown on Figure 7.

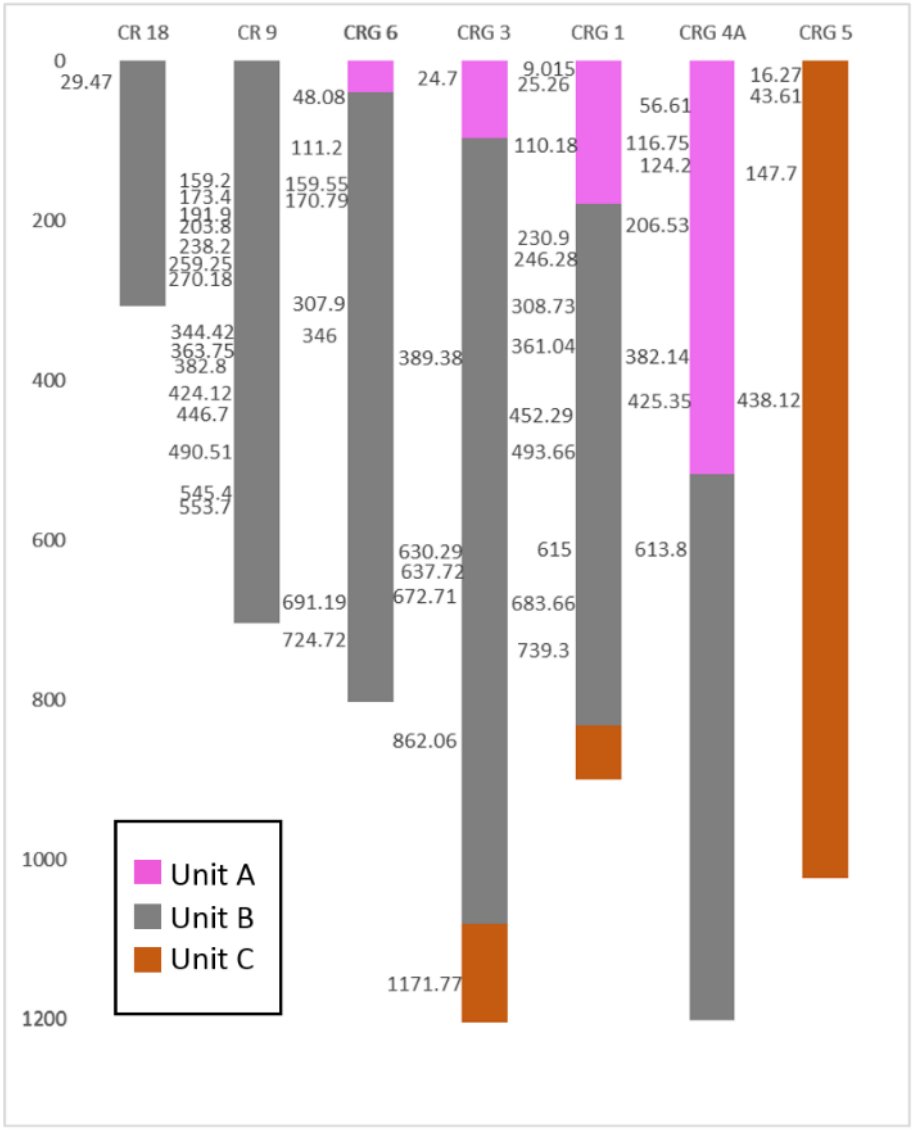


Figure 7. The seven boreholes sampled from the CRL site used in this study aligned along XX' (cross section in Fig. 5B) showing the location of samples for isotopic analyses at different depth. Unit A which is the pink part in the figure indicates the upper garnet-poor gneiss assemblage; unit B which is the gray part on the figure indicates the central garnet-rich gneiss assemblage; and unit C which is the orange part on the figure indicates the lower garnet-poor gneiss assemblage.

With the aid of a petrographic microscope the main rock types from the Chalk River boreholes were examined. Figure 8a presents a calcite vein in bedrock

assemblage A from borehole CRG1 at 25.26 m depth. The bedrock is gneissic and contains no garnets. Both Figures 8b and c are from bedrock assemblage B (borehole CRG3 at 389.38 m and 862.06 m respectively) and Figure 8c shows a calcite vein in borehole CRG3 at 862.06 m depth. Garnets and biotite appear in the thin sections of the samples shown in both of these figures. Figure 8d from borehole CRG3 at 1171.77 m depth is contained in bedrock assemblage C. The brown mineral is biotite and the mineral to the left above biotite is hornblende. In assemblage C, garnet is much less prevalent or absent compared to assemblage B.

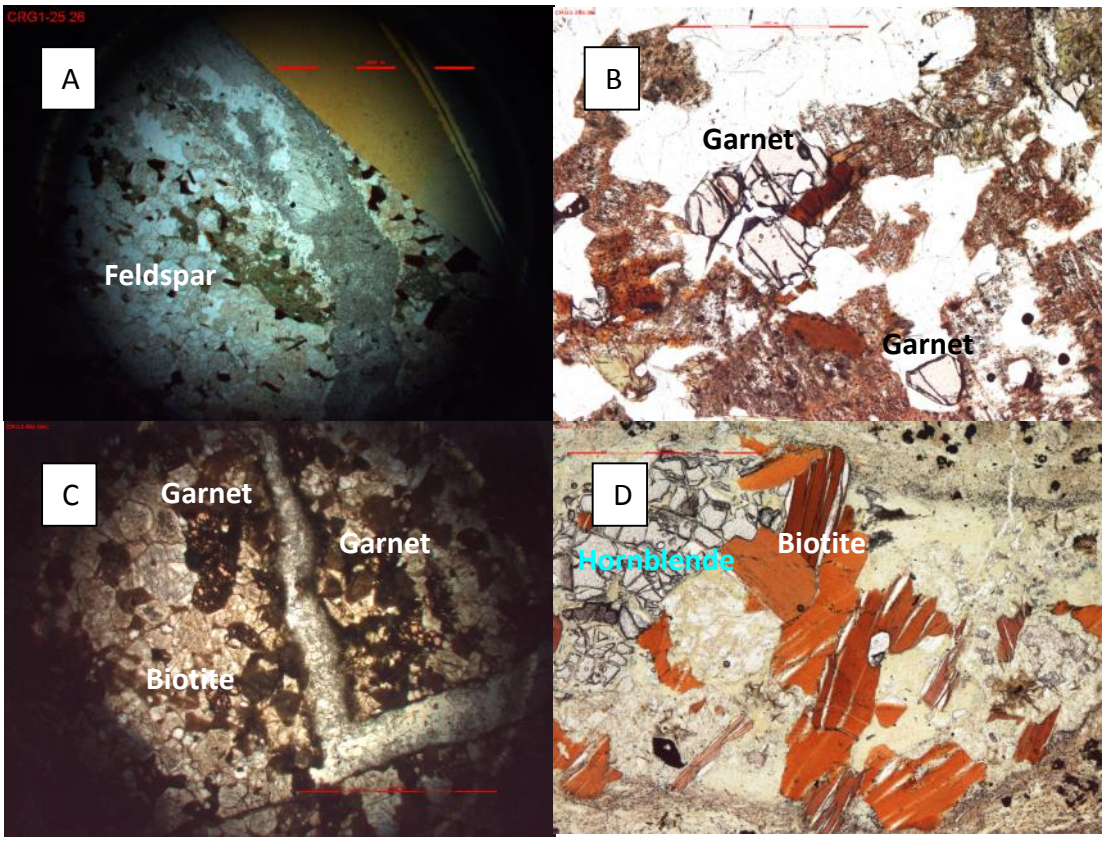


Figure 8. Photographs of typical bedrock samples: (a) is from borehole CRG1 at 25.26 m under polarized light (Unit A); (b) is from borehole CRG3 at 389.38 m under plane light (Unit B); (c) is from borehole CRG3 at 862.06 m under polarized light (Unit B); and (d) is from the borehole CRG3 at 1171.77 m under polarized light (Unit C).

Six dominant fracture minerals are observed in the samples examined from the boreholes used in this study. These include chlorite, quartz, fine-grained calcite,

dolomite, fibrous calcite, and coarse-grained calcite. These minerals are found as single mineral phases in some veins or as combinations of multi-mineral phases in other veins (Table 3). Fractures containing a single mineral phase listed on table 3 appear widely in all seven boreholes sampled. Chlorite is common in multi-mineral fracture assemblages and normally appears older based on petrographic relations than the other minerals in the same vein.

Table 3. Types of minerals found in fracture filled veins from rock cores at CRL.

| **vein type** | **mineral assemblage** |
|---|---|
| Single vein | Chlorite<br>horse tooth quartz (crystalline quartz)<br>fine grained calcite<br>Dolomite |
| tectonic fracture | quartz & fibrous calcite |
| Multi-mineral vein | chlorite & quartz & calcite<br>chlorite & fine grained calcite & coarse calcite<br>quartz & dolomite & fine to coarse calcite<br>dolomite & calcite<br>fine & coarse calcite |
| single vein | coarse grained calcite |

Figure 9 presents microscopic views of examples of different types of vein fillings observed under polarizing and non-polarizing light in thin sections. Calcite mineralogy occurs in many fractures, sometimes as a mono mineral fracture filling and in other cases filling gaps between other fracture minerals (Fig. 9a). An example of a fibrous calcite appears in borehole CRG1 at 615 m depth and is cut and displaced by another fracture (Fig. 9b). The fibrous calcite in this figure experienced strong

distortion and may have undergone post depositional deformation during a later stage tectonic event as described for the area by Perkins (1998). The fracture seems younger than the fibrous calcites because it cuts across and does not show the same deformation as the fibrous calcite. The example shown on Figure 9c from borehole CRG6 at 395.7 m depth includes chlorite and calcite in a vein. The calcite in the vein appears to have formed after the chlorite because chlorite formed alongside bedrock.

Figure 9d shows the morphology of crystalline quartz in a fracture at 307.9 m depth in borehole CRG3. There is calcite in the vein on both sides of the quartz. It may be because the fracture developed space on both sides of the quartz and the calcite formed after the quartz or the quartz may have formed after the calcite from a very different solution. Results from fluid inclusion analyses will show that some examples of quartz filling have a lower formation temperature than the calcite. Figure 9e shows a fracture from borehole CRG3 at 1171.11 m depth, which is the deepest sample in this study. The vein in borehole CRG3 at 1171.11 m is highly deformed showing mylonitization at the edge of the fracture (Fig. 9e). Bedrock is incised by the fracture as shown on the hand specimen and the bedrock is different and distinct on either side of the fracture (Fig. 9f). Thin sections in the photo on the right (Fig. 9f) show the difference between the two bedrock types on either side of the fracture. On the right side is a regular garnet-poor gneiss (Unit C) and the left is a highly metamorphosed gneiss. The vein in CRG3 at 1171.11 m is separating the two different bedrock types and therefore represents structural movement followed by later dominantly calcite

fracture infilling. This calcite is a distinct end member for $\delta^{13}C$ and $\delta^{18}O$ isotopic values ($\delta^{13}C$ is -5.27 ‰ and $\delta^{18}O$ is -16.05 ‰) in CRG3 as shown on Figure 14a.

Figure 9g shows displacement of a fracture from borehole CR9 at 238.2 m depth. Aspects of the morphological relationships are enhanced by using alizarin red dye to identify different generations of calcite. The calcite in the fracture probably precipitated from an earlier hydrothermal fluid and the dye results clearly show that the fluid channeled from the outside of the quartz mineralization to the inside of the fracture through cracks between the quartz crystals (Fig. 9g). Homogenization temperature (Th) of quartz fluid inclusions were greater than 200 $^{o}$C, and higher than any calcite values. The emplacement of calcite after quartz mineralization is favoured as the quartz in this example formed at a higher temperature and therefore is older than the calcite mineralization. The hydrothermal fluid may have flowed through fractures to the middle of the veins resulting in the calcite appearing in the middle although a three dimensional view of the fracture might show additional migration routes for the depositional fluids. This may also be an explanation for the calcite emplacement on either side of the quartz mineralization shown on Figure 9d. The thin section shown on Figure 9h is enhanced by the use of alizarin dye and the white mineral in the picture is dolomite.

Figure 9h shows two specific calcite types, left is an example of metasomatic calcite, which means the calcite was in the process of replacing dolomite. The right photo of Figure 10g is an example of a vuggy calcite that formed in an environment

having enough space to allow the growth of the crystalline calcite shape shown in the photo.

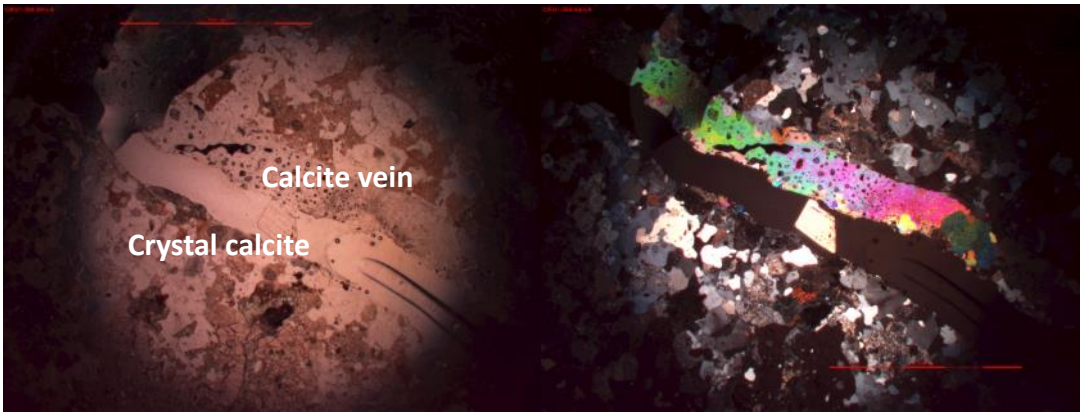


Figure 9a. Photograph of calcite vein next to a void in borehole CRG1 at 366.04 m depth, left photo is under plane light and right photo is under polarized light.

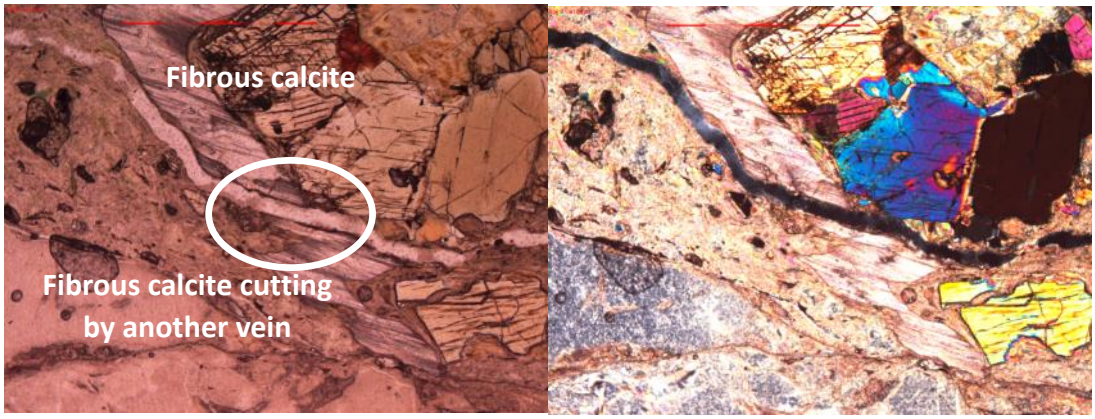


Figure 9b. Fibrous calcite vein cut by fractures in borehole CRG1 at 615 m depth, left photo is under plane light and right photo is under polarized light.

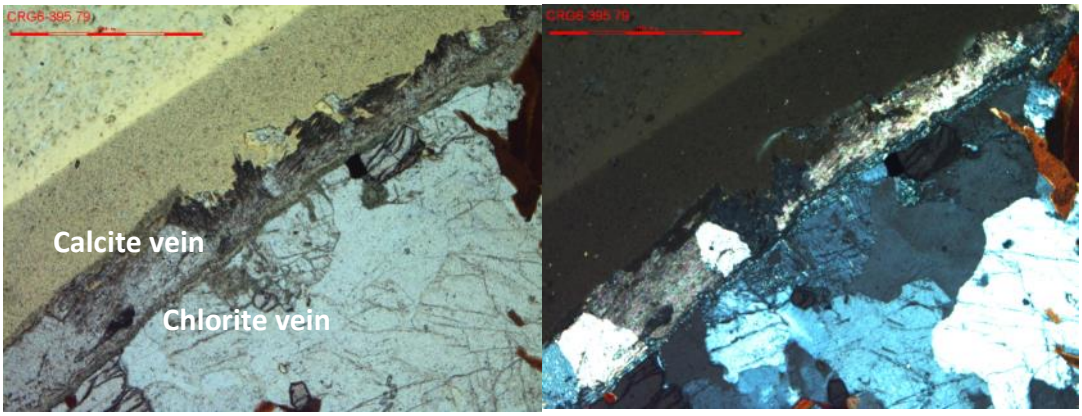


Figure 9c. Chlorite vein associated with calcite vein in borehole CRG6 at 395.79 m depth, left photo is under plane light and right photo is under polarized light.

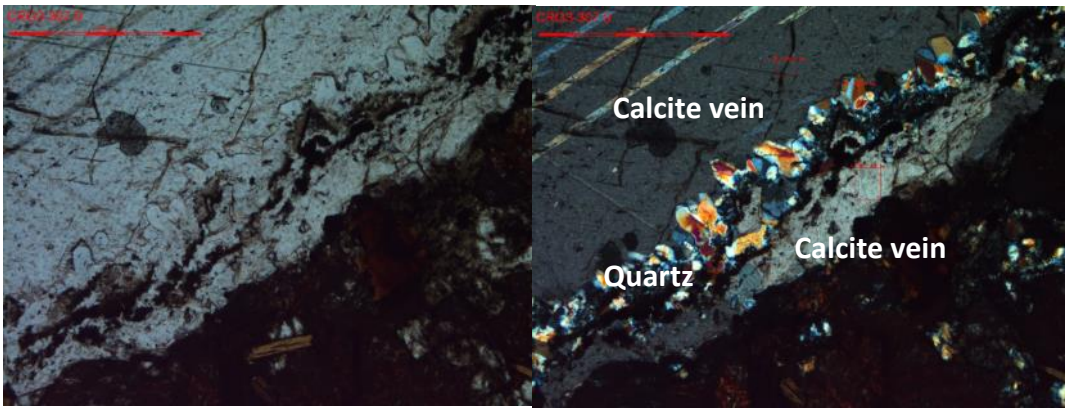


Figure 9d. Quartz vein enclosed by calcite veins in borehole CRG3 at 307.9 m, left photo is under plane light and right photo is under polarized light.

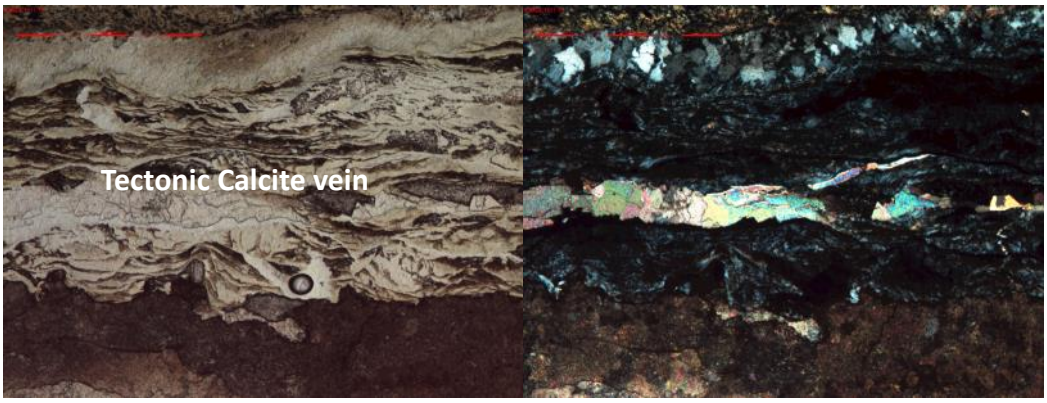


Figure 9e. A highly deformed tectonic vein which shows mylonization from borehole CRG3 at 1171.77 m depth, left photo is under plane light and right photo is under polarized light.


Figure 9f. Hand specimen showing different bedrock types separated by calcite filled fracture in a thin section from borehole CRG3 at 1171.77 m depth.

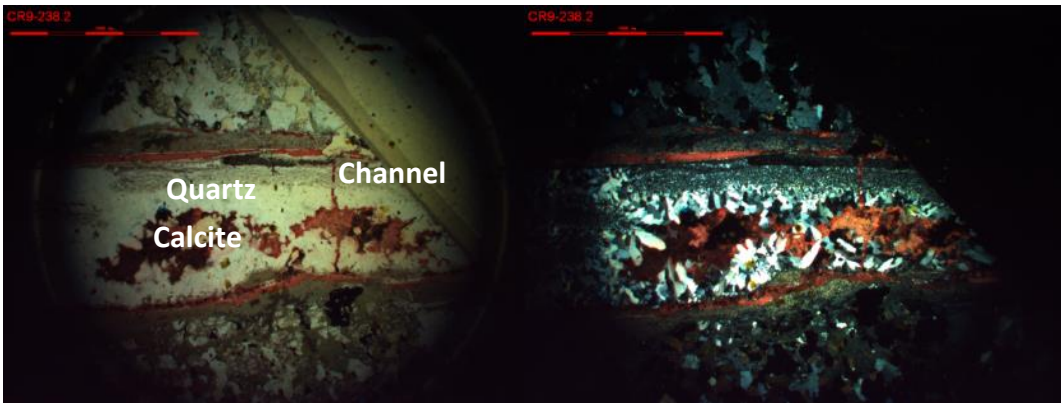


Figure 9g. Calcite veins dyed by alizarin red from borehole CR9 at 238.2 m depth showing calcite crystals grown in a void, left photo is under plane light and right photo is under polarized light.

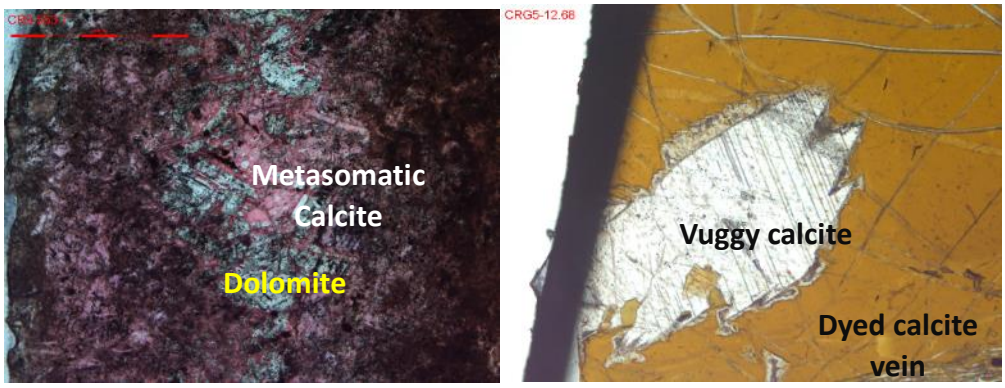


Figure 9h. Metasomatic calcite found in borehole CR9 553.7 m (left) and vuggy calcite found in borehole CRG5 12.68m (right), both photos under plane light.

Chlorite formed close to the boundaries of many fractures, as thin alteration zones (Fig. 9c, g). Quartz also appears in several samples (Fig. 10d, g) which usually formed in separate layers from the calcite mineralogy and in some cases appeared to be mylonitic, showing a very fine-grained, layered appearance on fracture boundaries (Fig. 9g). This situation seems to be evidence of an early ductile, high strain event that occurred at the site. Other quartz grains formed as crystals in void spaces and may be indicative of a separate crystallization episode (Fig. 9d, g). As both quartz and chlorite mineralization usually occur on the boundaries of fractures, it suggests they probably formed earlier than calcite in fractures. Dolomite in fractures appears to have been

altered by calcite in some instances as an early phase (Fig. 10c) and in other instances as a later phase based on relationships to the younger pervasive calcite mineralogy (Fig. 9h and Fig. 10e). Therefore, most chlorite, quartz and dolomite are defined as early fracture mineral phases and in general appear to have formed before the majority of the calcite mineralogy. Mono mineral fractures containing higher temperature silicates such as chlorite and quartz were not chosen for examination in detail during the study. These fractures in hand specimen appeared to be sealed and relatively older than the calcite filled fractures.

Cathode luminescence (CL) was used to differentiate calcite generations which are formed at different stages in a fracture or vug. CL was also useful to distinguish relationships between dolomite and calcite. Figure 10 shows CL images together with the corresponding polarizing microscope images of several samples shown as examples of various types of calcite found at the site.

Figure 10a shows a crystalline calcite from 366.04 m depth in borehole CRG1, which formed beside the calcite vein in the fracture. It is a light vermillion in color. In the CL picture the right part of the vermillion colored mineral is fine-grained calcite and the left part is an example of a large crystalline calcite grain (Fig. 10b). Calcite appears in the crystal lining on Figure 10b and it seems clearly lighter in color than the fine-grained calcite. Figure 10c shows that calcite formed beside the dolomite and there appears to be a metasomatic reactions into fractures within the dolomite. Metasomatic calcite is used in context here to define a calcite that forms during a hydrothermal event cogenically with dolomite. This is based on petrographic

relationships and as shown later based on similar fluid inclusion filling temperatures (Th) although these two mineral phases had different salinity (Tm) relationships. This may indicate that several hydrothermal solutions were mixing in the fracture during the time of mineral formation. In a similar case the metasomatism seems less developed as shown on Figure 10c. On Figures 10c and 10d coarse grain calcites appear as two different colors under CL, one is light vermilion (Calcite A) and the other is dark vermilion (Calcite B). The dark vermillion calcite seems clear under polarizing light while the light vermillion calcite contain dark impurities (Fig. 10d, e). Residual dolomite sometimes appears in these calcites. Comparing to Figure 10c, the dolomite shown on Figure 10e is almost completely converted to calcite and only small amounts of dolomite still remain (Fig. 10e).

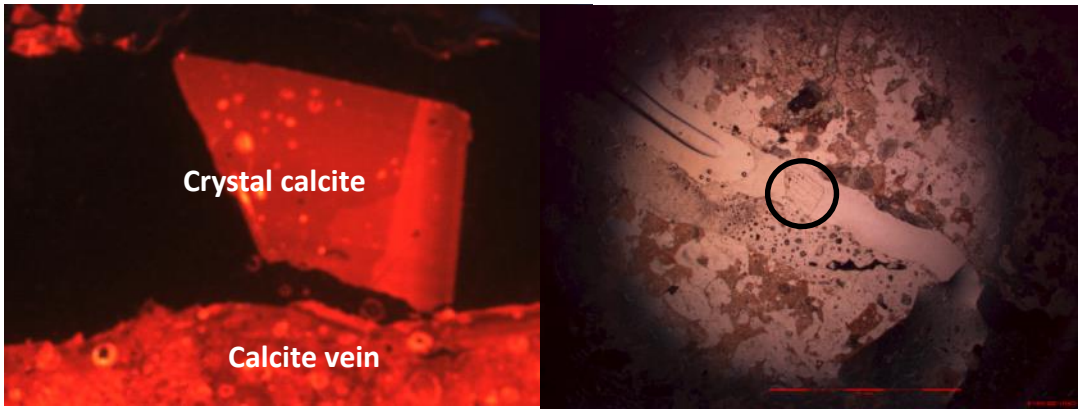


Figure 10a. Crystalline calcite close to the vein, from borehole CRG1 at 366.04 m depth. Left photo is from cathode luminescence (CL) and right is that calcite under orthogonal microscope.

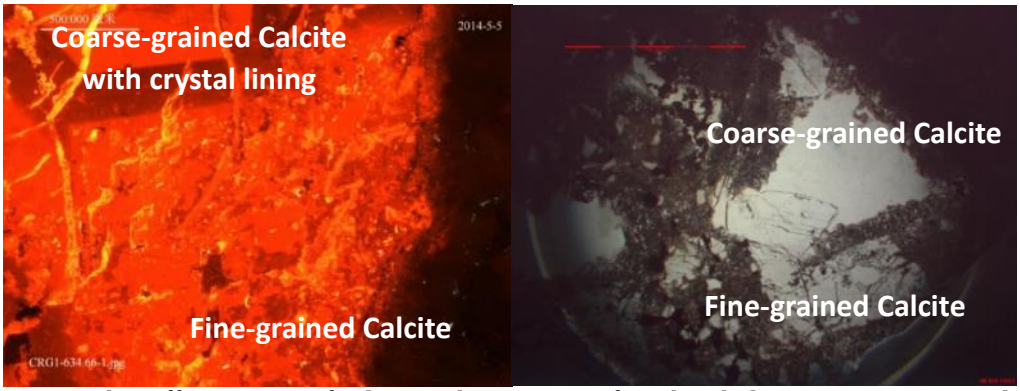


Figure 10b. Different types of calcite in the same vein from borehole CRG1 at 634.66 m depth.

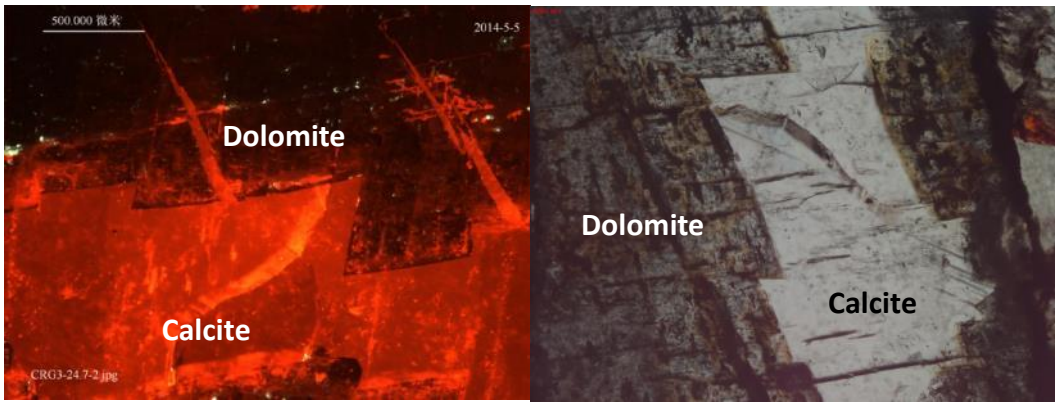


Figure 10c. Metasomatic dolomite in association with calcite from borehole CRG3 at 24.7 m depth.

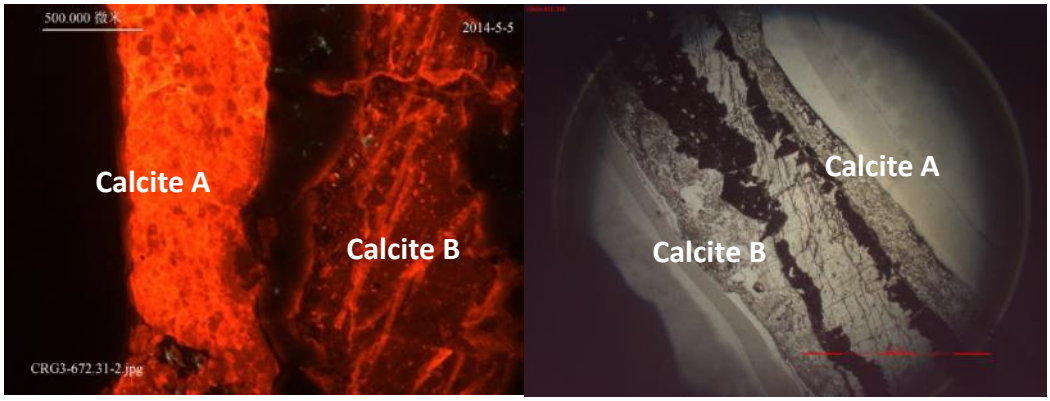


Figure 10d. Coarse-grained calcite showing two episodes of emplacement from borehole CRG3 at 672.31 m depth

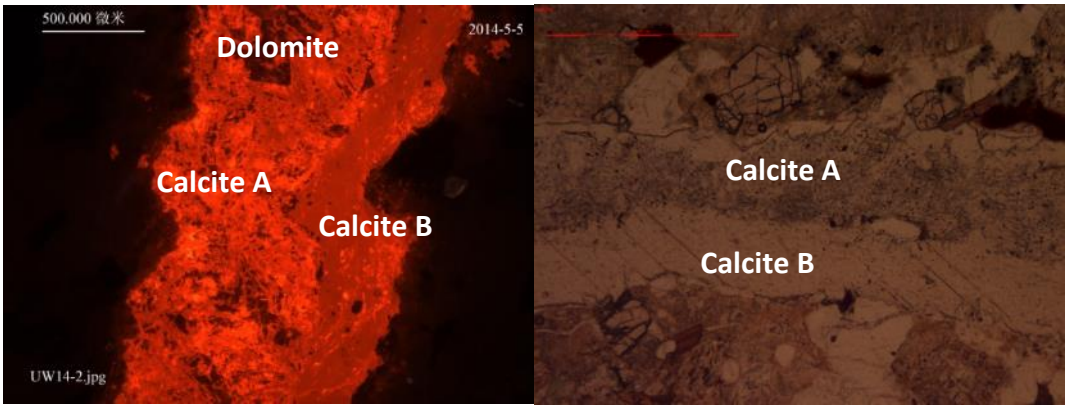


Figure 10e. Coarse-grained calcite within two episodes of mineral fillings in one vein shown from borehole CRG6 at 159.55 m depth. Also shown dolomite (left photo) partially replaced by calcite.

By using petrographic relationships, four types of calcite are defined in this study, (a) fibrous calcite (Fig. 9b, e), (b) metasomatic calcite (Fig. 9h, Fig. 10c), (c) crystalline

calcite (coarse-grained and fine-grained calcite in samples), and (d) vuggy calcite (Fig. 9h). Vuggy calcite is a form of coarse-grained calcite that was found in only a few fractures in boreholes CRG5 at 12.67m and CRG3 at 346m (Fig. 9h). Globally calcite infillings of this variety are not common in crystalline rocks because it formed in cave and shows crystalline shape. Vuggy calcites have only been noted at two other locations, the Lupin Mine, Nunavut (Stotler et al. 2010) and the Ylivieska, Finland site (Ruskeeniemi et al., 1996). Calcite is extensively distributed as a fracture mineral and is used here to record evidence of geologic stability and fluid events at the CRL site. The present study focused mainly on the calcite mineralogy to search for the presence of fracture minerals representative of lower temperature relatively young fluid events. Previous studies have used calcite fracture mineralogy to define processes such as hydrothermal fluid flow and other more recent hydrogeochemical events such as meteoric water intrusion to depth in crystalline rocks (Clauer et al., 1989; Frape et al., 1992; Blyth et al., 2009; Neymark et al. 2013). Table 4 summarizes the results for isotopic analyses, fluid inclusion measurements and calculations for calcite formation water $^{18}O$ and salinity.

Table 4. Homogenization temperature (Th), melting temperature (Tm), eutectic melting temperature (Te), salinity, $\delta^{18}O$-$\delta^{13}C$, and strontium isotopic ratios of the calcite types identified in this study. *Calculated $^{18}O$ of water is based on $^{18}O$ stable isotopic measurements of calcite and Th, the points are shown on Figure 18. *Calculated salinity is based on equation 1. Samples which have Tm lower than -22.8 also use equation 1 to estimate the salinity.

| Borehole | Depth (mabl) | Calcite type | $^{13}C$ (‰ VPDB) | $^{18}O$ (‰ VPDB) | Th (ºC) | Tm (ºC) | Te (ºC) | $^{87}Sr/^{86}Sr$ | *Calculated $^{18}O$ of water (SMOW) | *Calculated salinity (% wt) |
|---|---|---|---|---|---|---|---|---|---|---|
| CRG1 | 615.00 | Fibrous | -7.71 | -15.31 | 80.1 | -3.8 | | 0.71278 | -5.00 | 6.14 |
| | | calcite | -7.64 | -15.82 | 90.1 | -5.5 | | 0.70952 | -3.50 | 8.54 |
| CRG3 | 1171.77 | | -4.91 | -15.32 | | | | 0.70910 | | |
| | | | -5.27 | -16.05 | | | | | | |
| CRG5 | 16.27 | | -7.26 | -11.63 | 124 | 0 | -29 | 0.70942 | 5.00 | 0.00 |
| | | | -7.65 | -10.66 | 78 | -2 | -56 | 0.70849 | 0.00 | 3.37 |
| | | | -7.67 | -9.36 | 78 | -14 | -57 | | 1.00 | 17.92 |
| CRG6 | 724.72 | metasomatic | -5.03 | -15.08 | 77.2 | -37.2 | -47.2 | | -4.00 | 34.35 |
| | | calcite | -4.64 | -14.98 | 72.7 | -29.3 | -51.3 | | -5.50 | 28.74 |
| CR9 | 553.70 | | -5.12 | -11.98 | 73 | -20 | -46 | | -2.50 | 22.66 |
| | | | -8.59 | -14.66 | 90 | -19 | | | -2.50 | 21.94 |
| CRG3 | 672.31 | vug calcite | -8.60 | -9.32 | 89 | -38 | -57 | | 3.50 | 35.00 |
| CRG5 | 12.68 | | -9.04 | -7.73 | 85 | -38 | | | 4.50 | 35.00 |
| CRG6 | 346.00 | | -7.47 | -10.59 | 85.4 | -31 | | | 1.50 | 29.85 |
| CRG6 | 182.04 | Crystal | -7.16 | -12.77 | 82 | -7 | -38 | 0.70899 | -2.00 | 10.49 |
| | | calcite | -13.34 | -11.21 | 84 | -2 | -33 | 0.70904 | 0.00 | 3.37 |
| CRG6 | 111.22 | | -7.33 | -12.80 | 89.5 | -21.3 | | 0.70889 | -0.50 | 23.56 |
| CRG1 | 25.26 | | -7.13 | -14.14 | 79 | -6 | -56 | | -4.50 | 9.21 |
| | | | -6.51 | -9.72 | 72 | -17 | | | 0.00 | 20.43 |
| CRG1 | 366.04 | | -5.61 | -16.04 | 113 | -2 | -23 | 0.70905 | -2.00 | 3.37 |
| CRG1 | 493.65 | | -5.84 | -15.20 | 86.3 | -1.2 | -24.8 | 0.70963 | -4.00 | 2.06 |
| | | | -5.84 | -15.26 | 95.4 | -0.8 | | | -3.50 | 1.39 |
| | | | -5.72 | -15.36 | 83.7 | -2.3 | | | -4.50 | 3.85 |
| CRG3 | 133.52 | | -5.72 | -11.81 | 81.3 | -3.7 | | | -0.50 | 5.99 |
| CRG3 | 307.90 | | -4.94 | -14.05 | 70 | -6 | -51 | | -4.50 | 9.21 |
| | | | -8.15 | -10.27 | 67 | -4 | -47 | | -1.00 | 6.43 |
| | | | -6.37 | -14.73 | 75 | -3 | -36 | | -4.50 | 4.94 |
| CRG3 | 389.38 | | -8.35 | -10.31 | 92 | -8 | -26 | | 2.50 | 11.71 |
| | | | -9.77 | -8.43 | 88 | -5 | -26 | | 3.50 | 7.85 |
| CRG3 | 630.29 | | -6.97 | -12.72 | 89.7 | -0.3 | -23 | | -0.50 | 0.53 |
| | | | -8.11 | -10.22 | 101.8 | -3.6 | -25.2 | | 3.50 | 5.85 |
| | | | -6.10 | -15.52 | 92.3 | -2.7 | | | -3.00 | 4.48 |

(Table 4 continue)

| Borehole | Depth (mabl) | Calcite type | $^{13}C$ (‰ VPDB) | $^{18}O$ (‰ VPDB) | Th (°C) | Tm (°C) | Te (°C) | $^{87}Sr/^{86}Sr$ | *Calculated $^{18}O$ of water (SMOW) | *Calculated salinity (% wt) |
|---|---|---|---|---|---|---|---|---|---|---|
| CRG3 | 637.72 | | -6.42 | -15.04 | 106.2 | -0.6 | -25 | 0.70925 | -1.00 | 1.05 |
| | | | -8.35 | -10.60 | 102.3 | -6.3 | | 0.70937 | 3.50 | 9.60 |
| CRG3 | 862.06 | | -5.89 | -14.40 | 85.7 | -0.3 | -25.00 | | -3.00 | 0.53 |
| | | | -5.83 | -14.60 | 108.1 | -0.3 | -24.70 | | -0.50 | 0.53 |
| | | Crystal | -5.83 | -13.63 | 92.4 | -3.1 | | | -1.00 | 5.09 |
| CRG6 | 159.55 | calcite | -7.27 | -13.55 | 90.2 | -3.7 | -38.8 | | -1.50 | 5.99 |
| | | | -7.54 | -11.75 | 81 | -9.1 | -70.1 | | -0.50 | 12.99 |
| CRG6 | 169.12 | | -6.24 | -14.36 | 93.7 | -0.1 | | | -2.00 | 0.18 |
| | | | -7.20 | -12.18 | 90.5 | -14.5 | | | 0.00 | 18.36 |
| CRG6 | 170.79 | | -8.15 | -10.90 | 88 | -8 | -36 | | 1.50 | 11.71 |
| | | | -10.42 | -8.35 | 72 | -11 | -25 | | 1.50 | 15.04 |
| CRG6 | 440.20 | | -6.38 | -13.23 | 79.6 | -9.4 | -71.5 | | -3.00 | 13.33 |
| CRG1 | 493.65 | Crystal | -5.71 | -15.23 | 192.3 | -1.6 | -25.4 | | 5.00 | 2.72 |
| | | calcite | -5.59 | -15.40 | 197.1 | -0.9 | -24.8 | | 5.00 | 1.56 |
| | | (high Th) | -5.68 | -16.17 | 179.6 | -0.7 | | | 3.50 | 1.22 |
| | | | -5.84 | -15.20 | 199 | -2.2 | | | 5.50 | 3.69 |
| CRG4A | 613.79 | | -7.74 | -10.30 | 197.3 | -4.7 | -25.5 | | 11.00 | 7.44 |
| | | | -8.06 | -12.48 | 181.2 | -1.7 | | | 7.50 | 2.89 |
| CR18 | 28.14 | Crystal | -5.05 | -13.24 | 81 | -33 | -55 | | -3.00 | 31.21 |
| CRG3 | 637.72 | calcite | -6.42 | -15.04 | 91.7 | -36.7 | | | -3.00 | 33.95 |
| CRG6 | 111.22 | (low Tm) | -7.33 | -12.80 | 85.6 | -31.4 | -45.9 | | -1.00 | 30.12 |
| CRG6 | 159.55 | | -6.62 | -12.34 | 86 | -29 | | | -0.50 | 28.54 |
| CRG6 | 724.72 | | -5.03 | -15.08 | 79.6 | -38.9 | -59.8 | | -5.00 | 35.77 |
| | | | -4.64 | -14.98 | 75.5 | -39.4 | -59.8 | | -4.50 | 36.21 |

**Results of fluid inclusion analyses**

More than 120 fluid inclusion analyses were obtained from a number of primary fluid inclusions found in the different varieties of calcite samples (Appendix 2). Fluid inclusion analyses are used to further categorize the calcite varieties using homogenization temperature (Th) and salinity (Tm). The major distribution of fluid inclusion homogenization temperatures aggregate in a range from 70 ℃ to 110 ℃ (Fig. 11). Three lower values for homogenization temperature were found in fluid inclusions from calcite samples in borehole CRG3 at 307.9 m and 389.38 m depth and several elevated homogenization temperature values were obtained from fluid inclusions occurring in borehole CRG1 at 493.65 m depth and borehole CRG4A at 613.79 m depth. While the range of measured temperatures was from 20 to 200 ℃ closer inspection of the lower temperature fluid inclusions show that they are secondary inclusions occurring along fracture planes in the minerals examined and therefore cannot be used as reliable formation temperature indicators. Figure 12 shows the low temperature fluid inclusions discovered in borehole CRG3 at 389.38m (Fig. 12a and b) compared to normal primary fluid inclusions (Fig.12c). The formation of low temperature fluid inclusions often occurs because the calcite formed small stress fractures at some time in the past and the fluid leaked from a primary inclusion or are due to fluids from external sources and calcite rehealing (Gonzalez et al., 2003). Low temperature fluid inclusions were reported in a previous study and reported as evidence of recent low temperature fluid events at the site (Bukata 2000). The author suggests that those data results may have been similar to the samples analyzed in this study.

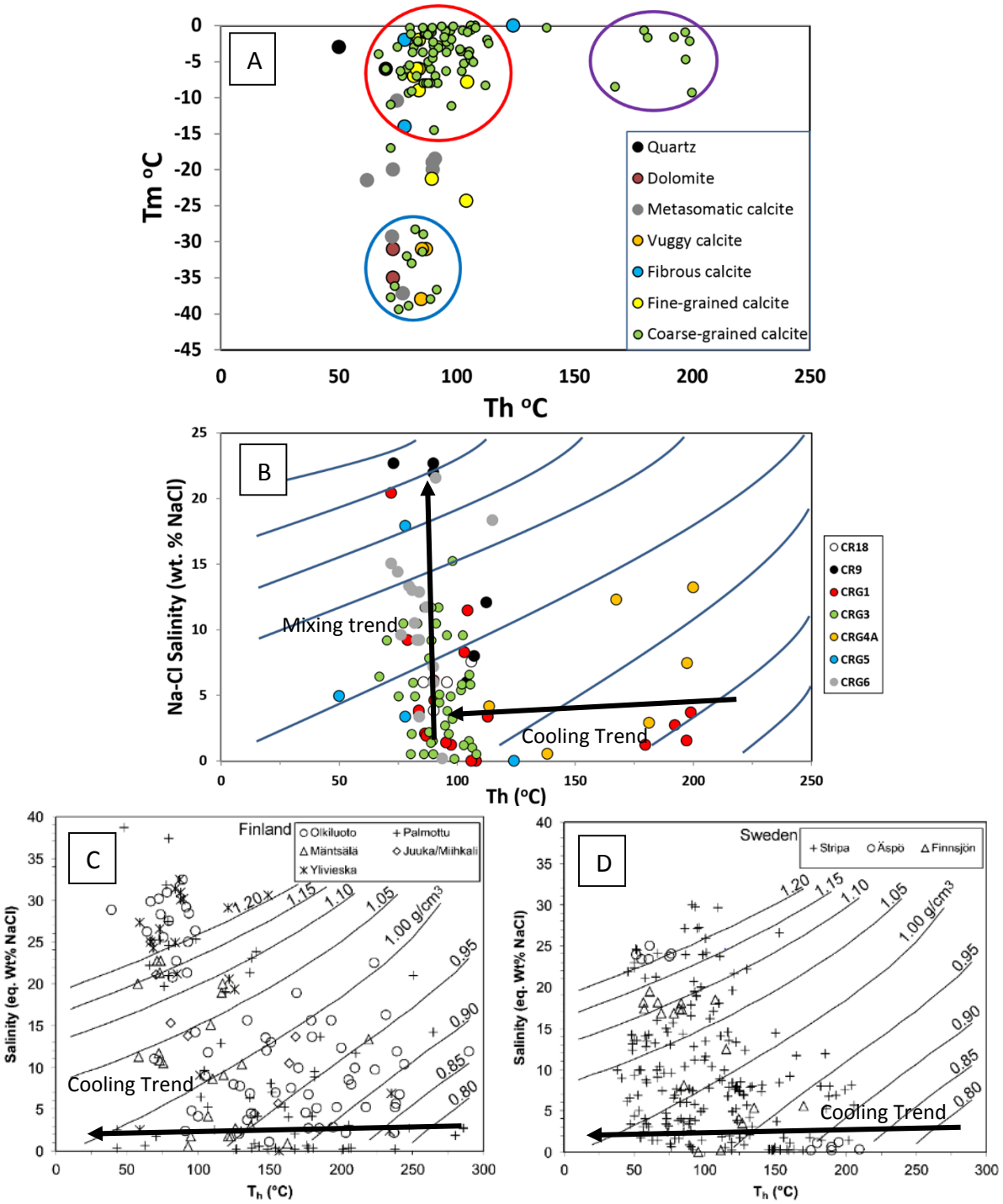


Figure 11. (a) Homogenization temperature (Th) vs. melting temperature (Tm) of all fluid inclusion results. Results categorized by mineral type. (b) Salinity versus homogenization temperature plot of fluid inclusions from the CRL site. (c) and (d) salinity versus homogenization temperature plot of fluid inclusions from the Finland and Sweden sites. Samples are categorized for the different boreholes from the site. Density lines ($g/cm^3$) have been constructed after the equation of Zhang and Frantz (1987) for the Na-Cl-$H_2O$ system.

Melting temperatures (Tm) were also measured in order to ascertain the possible salinity of the parent fluid from which the calcites formed. The salinity of fluid

inclusions is related to the melting temperature (Tm) which is referenced to Laoult's Law (1880). The calculation is based on the equation from Hall et al. 1988 for calculating NaCl weight content by melting temperature. Equation 1 is for a NaCl weight content calculation and Table 3 shows the calculated results.

$$W = 1.76958 * Tm - 0.042384Tm^2 + 0.00052778Tm^3 \qquad \text{Equation 1}$$

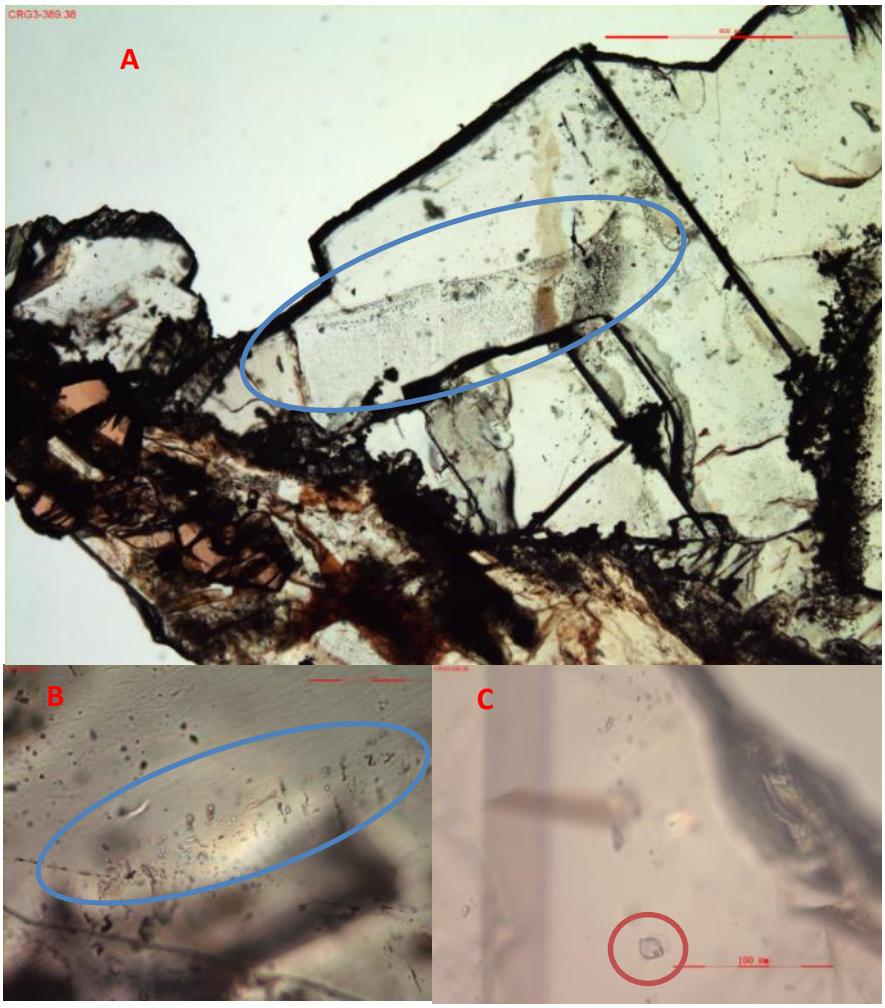


Figure 12. Picture of fluid inclusions in CRG3 at 389.38m under the polarization microscope. (a) (top) shows a series of secondary fluid inclusions at 10X zoom; (b) (bottom left) is the secondary fluid inclusions at 500X zoom (note the linear healed fracture along which the inclusions are distributed); (c) (bottom right) show a primary fluid inclusion at 500X zoom (note: only data from primary inclusions are used in this study).

Salinity of the samples measured from this study ranged from 0 to 36.21 wt. % (Table 4). The frequency of the salinities found in the study are shown on Figure 11b. Very low melting temperatures around -33 ℃ occur in some samples and would indicate a high salinity solution, most likely Ca-Na-Cl (Roedder 1984; Blyth et al., 1998 and 2009; Drake et al., 2009). However, most values are in a narrow range between -10 ℃ to 0 ℃. All data measured for this study are shown in Table 4. Previous studies suggested that recrystallization of hydrothermal calcite by low salinity water or precipitation from meteoric water during plutonic cooling was a major process to produce the lower salinity (0-1 wt. % NaCl) inclusions (Bukata, 2000, Blyth et al., 2009). The assumption was that salinity between 1 and 6 wt. % indicates calcite formation under conditions that precipitated calcites from fresh ground water or a dilute seawater, for example Champlain Sea waters (Bottomley 1987; Bukata 2000). However, these low salinity inclusions had homogenization temperatures (Th) that ranged from 50 ℃ to 200 ℃. In fact most of the higher temperature inclusions measured in this study are in the group of low salinity samples. There is no evidence of elevated thermal events during the recent glacial period in this area that would support the proposed calcite precipitation or dissolution re-precipitation model propose by previous authors.

Fluid inclusions that contain salinities between 1 to 7 wt. % from the CRL site are widely distributed in the different boreholes. They are probably from a thermal cooling and precipitation event which would result in a decreasing calcite salinity during precipitation as has been shown in similar studies (Blyth et al., 2004 and 2009).

Salinities of more than 7 wt. % most likely indicate formation of calcite under elevated temperature conditions from fluids similar to those found in crystalline rocks or basinal brines as discussed in other studies (Frape et al., 1984; Gascoyne et al., 1987).

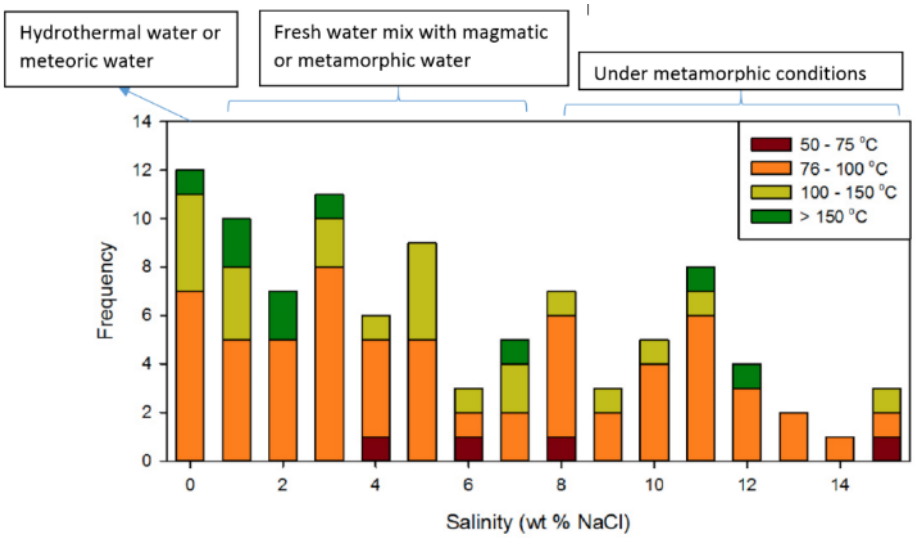


Figure 13. Salinity (as wt. % NaCl) of fracture calcite fluid inclusion data calculated from the cooling (melting) temperature (Tm) of fluid inclusions. Salinity categorized on the top is based on a classification of potential source fluids from Bukata (2000).

No fluid inclusions could be found in chlorite and a limited number of fluid inclusions were found in minerals such as quartz and dolomite. Some quartz such as from borehole CR9 at 238.2 m depth had measured homogenization temperature higher than 200 ºC. In this case it suggests the quartz formed during a higher temperature event which probably was earlier than calcite formation. Fibrous calcites occur in a range of Th from 78 to 128ºC and Tm from 0 to -14 ºC (Fig. 11). Therefore, they formed at elevated temperatures from mixtures of different salinity fluids. Metasomatic calcites have homogenization temperature (Th) and melting temperature (Tm) that ranged from 62.1 to 90 ºC and -19 to -37.2 ºC, respectively. Most of the metasomatic calcite has melting temperature lower than -22.9 similar to the dolomite.

That melting temperature suggests a fluid other than Na-Cl, possibly Ca-Na-Cl as the parent fluid (Blyth et al., 2000 and Blyth et al., 2004). Most fluid inclusion measurements were obtained from crystalline calcite. Crystalline calcite can be divided into three parts by fluid inclusion homogenization temperature (Th) and salinity (Tm) (Fig. 11a), which are elevated temperature (67 $^{o}$C to 113 $^{o}$C) low salinity calcite (red circle), elevated temperature (73.7 $^{o}$C to 91.7 $^{o}$C) high salinity calcite (blue circle) and higher temperature (167.3 $^{o}$C to 200 $^{o}$C) low salinity calcite (purple circle) (Table 4). The salinities of these groups suggest parent fluids of formation that may include fresh groundwater mixed with saline fluids to generate the wide range of salinities. Homogenization temperatures (Th) and melting temperatures (Tm) of vuggy calcite ranged from 85 $^{o}$C to 89 $^{o}$C and -31 $^{o}$C to -38 $^{o}$C, respectively. They are similar to the crystalline calcite within the blue circle group (Fig. 11a). The elevated salinity for samples in the blue circled group and vuggy calcite also suggests a Ca-Na-Cl parent fluid as suggested by authors from results of other studies (Blyth et al., 2000 and Blyth et al., 2004).

Figure 11b shows the salinity of calcites versus homogenization temperature applied to investigate possible cooling trends and mixing of different fluids during calcite formation. Curve lines of equal density are constructed based on Zhang and Frantz (1987). Previous studies have shown that horizontal trends in data are due to cooling trends as the hydrothermal or higher temperature fluid cooled and precipitated calcite (Blyth et al., 2009). Under these conditions, the salinity of the parent solution trapped in the inclusions when the calcite precipitates would generally remain the same

while the homogenization temperature decreases (Zhang and Frantz 1987; Blyth et al., 2009). Only a few weak cooling trends could be found in fluid inclusions from calcite samples at the CRL site, unlike other sites reported from previous studies such as Palmottu in Finland and Stripa in Sweden (Fig. 11c and d) (Blyth et al., 2009). From the cooling data calculations and Th measurements the CRL site backs the higher temperature (>250$^{o}$C) calcites found at many other sites worldwide. These higher temperature calcites found at other sites are often interpreted as associated with the late stage cooling of the plutonic rock mass (Frite et al., 1987; Blyth et al., 2009). In the present study, calcites from borehole CRG1, CRG4A and CRG5 show evidence of a weak cooling trends in a few of the low salinity samples (Fig. 11b). Otherwise, calcites in this study show mainly vertical salinity trends which suggest based on other studies that the parent waters of formation of these calcites are mixtures of different salinity fluids (Blyth et al., 2000, 2004 and 2009). Samples from borehole CRG4A show a vertical mixing trend at homogenization temperatures from 160 to 200 $^{o}$C. The high-temperature elevated-salinity of the formation fluids suggests that they could be mixtures of hydrothermal and metamorphic fluids (Bukata 2000; Blyth et al., 2009). Other calcites have mixing trends at homogenization temperatures from 70 to 120 $^{o}$C. Therefore, the source fluids of the high salinity groundwaters are most likely evaporated seawater or basinal brines as shown in other similar studies (Sandstrom et al., 2009; Blyth et al., 2009).

**Isotopic results for $^{13}C$-$^{18}O$**

The origin and evolution of fracture calcite mineralogy has been studied using a variety of analytical tools. The stable isotopic ($\delta^{13}C$ and $\delta^{18}O$) values have been widely applied in investigating calcite genesis in crystalline rocks (Tullborg, 1989b; Bottomley and Veizer, 1992; Blyth et al., 1998, 2004, 2009; Sandstorm et al., 2009). Based on the petrographic analyses, carbonate material was chosen for stable isotopic analyses from the mineralogical morphologies found in the cores (Fig. 5). Over 150 samples were analyzed and the isotopic results are shown on Figure 14a. Results for $\delta^{13}C$ range from -3 to -14‰ VPDB with a statistical average value of -6.93‰ VPDB; while $\delta^{18}O$ results range from -8 to -21‰ VPDB with a statistical average of -13.02‰ VPDB and a standard deviation of 2.22‰.

Fibrous calcites in samples from boreholes CRG1 at 615 m and CRG3 at 1171.77 m depth have similar carbon and oxygen isotopic signatures (Fig. 14a and b). The $\delta^{13}C$ values of these calcites range from -4.91 to -7.88 ‰ (VPDB) and the $\delta^{18}O$ values range from -15.32 to -17.34 ‰ (VPDB) (Fig. 14b). However, similar calcite found in borehole CRG5 at 16.27 m had different isotopic ranges. The $\delta^{13}C$ values of these calcites range from -7.26 to -7.67 ‰ (VPDB) and the $\delta^{18}O$ values ranged from -9.36 to -11.63 ‰ (VPDB). Metasomatic calcites are mainly found in borehole CR9 at 663.7 m and CRG6 at 724.72 m in association with dolomite (Fig. 9h and Fig. 10c). The $\delta^{13}C$ values of these calcites ranged from -4.64 to -8.59 ‰ (VPDB) and the $\delta^{18}O$ values range from -11.98 to -15.08 ‰ (VPDB) (Fig. 14b). Elevated-temperature, low-salinity crystal calcite (red circle on Fig. 11) has the $\delta^{13}C$ values from -5.61 to

-10.42 ‰ (VPDB) and the $\delta^{18}O$ values ranged from -8.35 to -16.04 ‰ (VPDB). Elevated-temperature, high-salinity crystal calcite (blue circle on Figure 11) has the $\delta^{13}C$ values from -4.64 to -8.60 ‰ (VPDB) and $\delta^{18}O$ values from -12.34 to -15.04 ‰ (VPDB). The higher-temperature, low-salinity crystal calcite group (purple circle on Figure 11) has $\delta^{13}C$ value of these calcites from -5.59 to -8.06 ‰ (VPDB) and the $\delta^{18}O$ values from -10.03 to -16.17 ‰ (VPDB). The vuggy calcite found in a few samples from boreholes CRG3 at 672.31 m, CRG5 at 12.68 m and CRG6 at 346 m (Fig. 9h) have $\delta^{13}C$ values from -7.47 to -9.04 ‰ (VPDB) and $\delta^{18}O$ values from -9.32 to -10.59 ‰ (VPDB).

The bedrock at CRL has three recognized rock assemblages that may have a relationship to the fracture calcites (Thivierge et al., 2011). The isotopic values of fracture minerals from different rock assemblages are presented on Figure 14c. Isotopic data from shallow depths of Unit A are only from a few cores covering a relatively small isotopic range. Unit B, which includes most of the fractures containing calcites, contains the depleted values of $\delta^{18}O$ from the CRG1 core and one of the depleted values of $\delta^{13}C$ from CRG6. The results for data from Unit C are limited as well, due to a smaller number of fractures and fractures containing calcite in the cores at depth. Calcites in Unit C are found at greater depths than other units (Fig. 7), and they have more depleted $\delta^{13}C$ values than other calcites (Fig. 14c). Those calcites with more depleted $\delta^{13}C$ values may be a result of a depleted organic such as methane source during formation. Some calcites found at the CRL site have $\delta^{13}C$ values of approximately -6‰ (VPDB) similar to mental carbon and $\delta^{18}O$ values as low

as -22‰ (VPDB). As stated previously high temperature (>250°C) calcites were not found at the site and although some carbon isotopic values are similar to mental carbon values a strong relationship could not be established to mental derived carbon sources (-6‰) in the formation of CRL calcites.

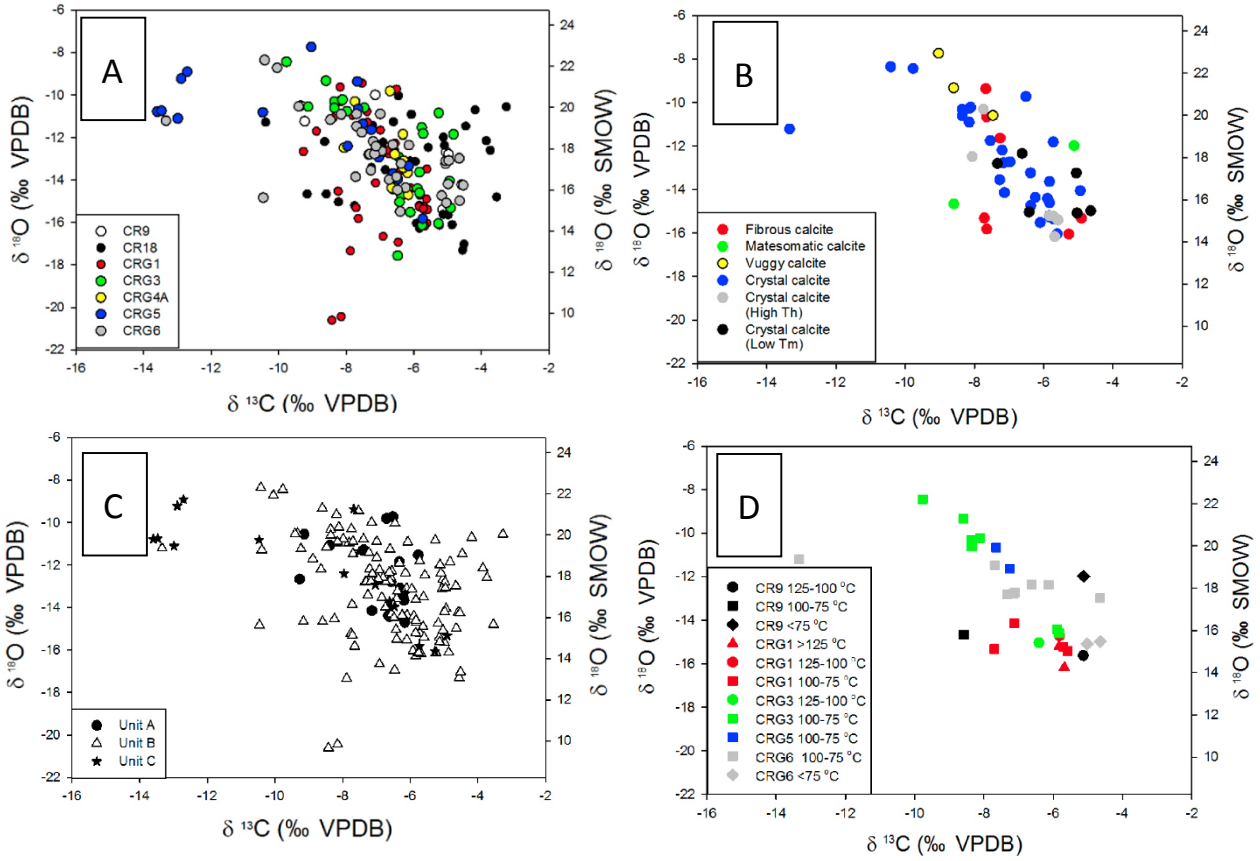


Figure 14. (a) $\delta^{13}C$ and $\delta^{18}O$ isotopic measurements for calcite fracture mineral samples selected from cores at the CRL site, Chalk River, Canada (for location of samples see Figure 5). (b) $\delta^{13}C$ and $\delta^{18}O$ isotopic measurements of calcites categorized by calcite types where fluid inclusion results have been determined. (c) $\delta^{13}C$ and $\delta^{18}O$ isotopic measurements of calcites categorized by the different gneiss assemblages found in each borehole. Gneiss assemblages defined by Thivierge et al. (2011). (d) $\delta^{13}C$ and $\delta^{18}O$ isotopic measurements of calcites categorized by boreholes and homogenization temperature (Th).

### $\delta^{18}O$ geothermometry results and analyses

In many early studies of calcite geothermometry, the $\delta^{18}O$ value of the formation water was assumed and using isotopic fractionation values between water and calcite

the temperature of calcite formation was calculated (Blyth et al., 1998, 2004, 2009; Drake et al., 2009; Sandstrom et al., 2009). Calcite geothermometry $\delta^{18}O$ values can be calculated more correctly by using the homogenization temperature (Th) of fluid inclusions and the $\delta^{18}O$ stable isotopic value of calcite in order to constrain the $\delta^{18}O$ value of the water of formation (Fig. 15). Figure 15 includes the vertical axis for $\delta^{18}O$ value of calcite and the horizontal axis for the temperature of the solution in degrees Celsius determined by fluid inclusion homogenization values (Th) (Blyth et al., 2009). Curved lines on Figure 15 are established by experimental results to determine $\delta^{18}O$ fractionation factors between water and calcite (O'Neil et al., 1969; Mook et al., 1974). All results in Table 4 are estimated using Figure 15. Results of geothermometry $\delta^{18}O$ of calcite can be used to comment on and possibly refine the type of fluid from which the calcite precipitated (Fig. 15) (Kyser 1987; Blyth et al., 1998, 2004, 2009).

The fluid of formation of the fibrous calcites occurs over a large range of geothermometry $\delta^{18}O$ values, which varied from 5 to -5 ‰ (SMOW). Therefore, the parent water can be meteoric water, evaporated seawater, hydrothermal water and metamorphic water depending on temperature values (Fig. 15). The salinity of these calcites varies from 0 to 15.02 wt. % and the homogenization temperatures (Th from 78 to 128 $^{o}$C) are not as high as would be expected in a metamorphic water. The possible parent waters for fibrous calcite are evaporated seawater mixed with meteoric water or hydrothermal fluids (Fig. 16) (Kyser et al., 1987; Blyth et al., 1998). $\delta^{18}O$ values calculated for waters of formation for metasomatic calcite ranged from -2.5 to -6 ‰ (SMOW) (Table 4). In addition, the salinity of these calcites suggest that the

parent fluid could have an elevated salinity and possibly be a Ca-Na-Cl fluid. Therefore, parent water of the metasomatic calcite probably is a mixtures of meteoric water and high salinity sedimentary basinal or a shield brines (Fig. 16) (Blyth et al., 1998 and 2004). The calculated geothermal source water for the crystalline calcites has an elevated-temperature, low salinity (red circle on Figure 11) and a calculated $\delta^{18}O$ signature of -4.5 to +3.5 ‰ (SMOW) (Table 4). Calcites in this group have a wide range of $\delta^{18}O$ water isotope values which span the range from hydrothermal, meteoric, basinal brines, metamorphic, and seawater as discussed by previous researchers (Fig. 16) (Blyth et al., 1998). Considering the Th and salinity results discussed earlier, the parent water of this group most likely formed from a mixture of fluids in which one end member was a more dilute recharge water. Crystal calcites with elevated-temperatures and high-salinity (blue circle on Figure 11) have a $\delta^{18}O$ signature of -5 to -0.5 ‰ (SMOW) (Table 4). Negative $\delta^{18}O$ signatures of geothermal water and high Ca-Na-Cl salinity of this group suggest it probably has a component of meteoric water mixed with basinal or crystalline shield brine as the parent water (Fig. 16)(Blyth et al., 2004 and 2009). Crystal calcite in higher-temperature, low-salinity (purple circle on Figure 11) had the most positive $\delta^{18}O$ signature in this study which ranged from +3.5 to +11 ‰ (SMOW). The salinity of this group is from 0 to 7.33 wt. %. Therefore, the parent water of this group probably includes a mixture of hydrothermal fluid recharged from dilute evaporated waters such as seawater or sedimentary basinal fluid. Calculation of the isotopic value for waters of formation for the vuggy calcites gives $\delta^{18}O$ isotopic signatures between +1.5 to +3.5‰ (SMOW), and these calcites contain

an elevated Ca-Na-Cl salinity as discussed early. The parent water of the vuggy calcite is possibly an evaporated sedimentary basinal brine or a saline crystalline rock shield brine (Fig. 16) (Blyth et al., 1998, 2000 and 2004).

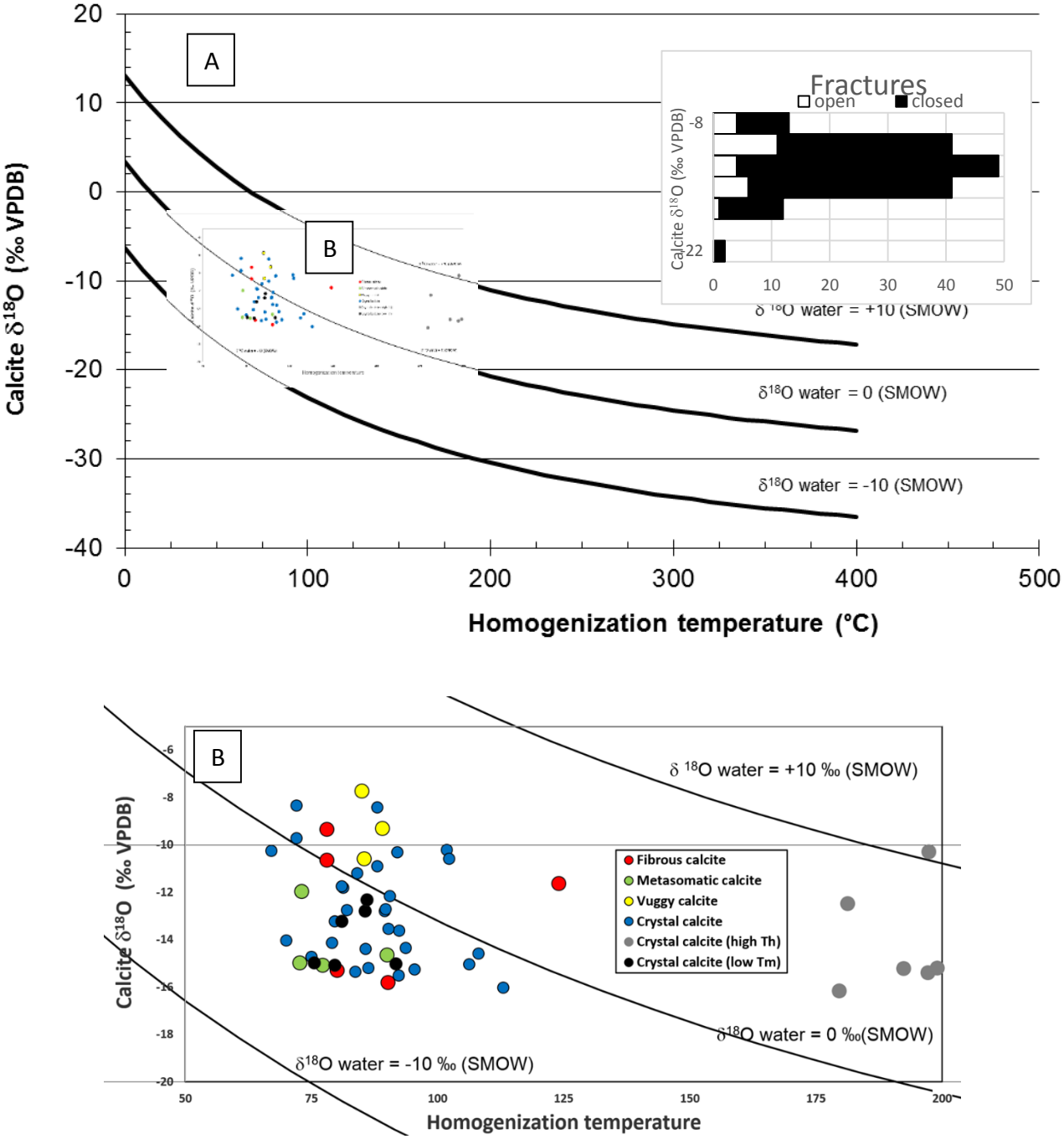


Figure 15. Plot (a): $\delta^{18}O$ plot which includes the calcite $\delta^{18}O$ as Y axis and temperature ($^{o}C$) as X axis. The curved lines represent the $\delta^{18}O$ of the fluid environment from which a calcite would have formed in equilibrium. Plot edited from Blyth et al., 2009. Plot (b): data from Table 4 are added to the plot from (a) and data categorized by calcite types.

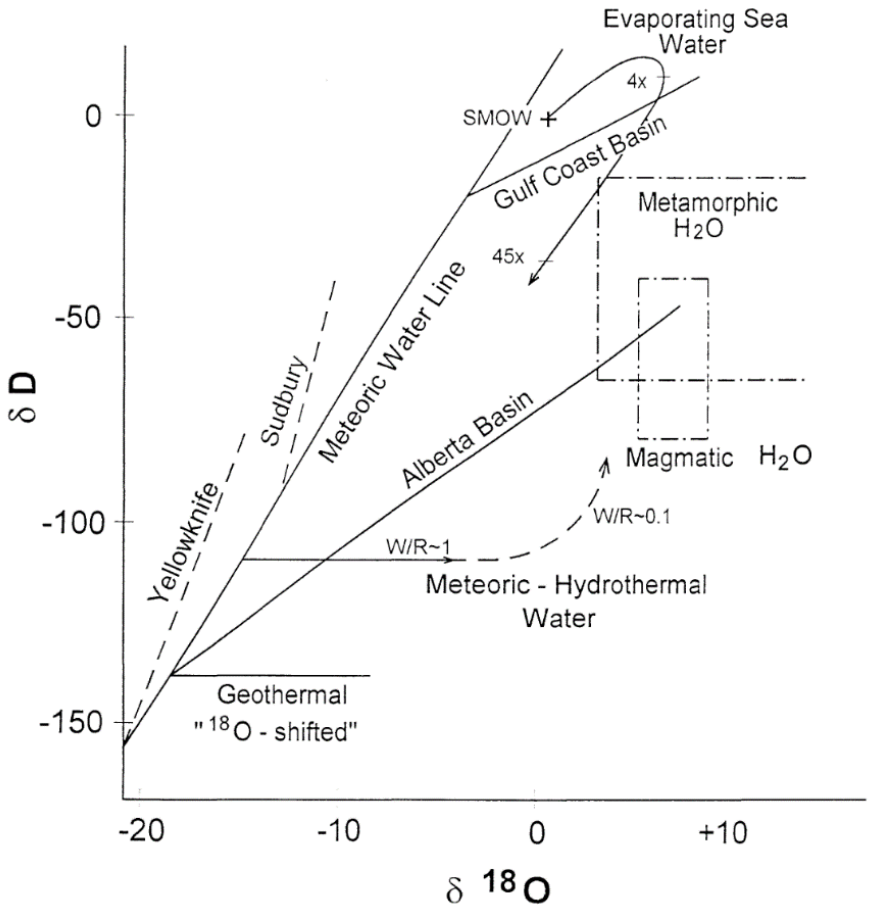


Figure 16. $\delta^{18}O$ and $\delta D$ values of various fluids associated with isotopic processes and end members. Trends in isotopes of magmatic and metamorphic water, evaporated seawater, and meteoric hydrothermal water are shown on the plot (Kyser 1987; Blyth et al., 2009).

**Strontium results and analyses**

Strontium isotopic ratios have been applied to fracture mineral studies to investigate the degree of water/rock interaction and origin of fluids. The majority of samples from the CRL site analyzed for $^{87}Sr/^{86}Sr$ ratios contain values between 0.708 and 0.710 as shown on Figure 17. Strontium values for the bedrock gneisses yielded $^{87}Sr/^{86}Sr$ ratios of 0.71085 to 0.72313 which is more elevated than most of the calcites in this study (Appendix 5) (Bottomley et al. 1987; Bottomley et al. 1992; Blyth et al.

2009). The variations of the strontium isotope ratios between the bedrock and calcites suggests that water/rock interaction and exchange with calcite forming fluids was limited at the site. Another interpretation of the calcites with lower $^{87}Sr/^{86}Sr$ ratios than the bedrock would be that the formation age of calcite is much younger than the bedrock and the Rb decayed to Sr has not had sufficient time to produce high $^{87}Sr/^{86}Sr$ ratios. The elevated strontium ratios of crystal calcite samples from borehole CRG1 at 110.18 m, CRG5 at 438.12 m and CRG6 at 48.04 m may also be partially due to inclusions of minerals such as K-feldspar or phyllosilicates with more concentrated levels of radiogenic $^{87}Sr$ than the other calcite varieties as seen in a number of other studies (Fig. 17) (McNutt et al., 1990; Blyth et al., 2009; Sandstrom and Tullborg 2009). Presently groundwaters at the site have $^{87}Sr/^{86}Sr$ ratios of 0.70920 to 0.70929 which is similar to some of the calcite. For example, calcites in borehole CR9 at 700.76 m and CRG6 at 637.73 m have strontium ratios of 0.709267 and 0.709253 respectively. Strontium ratio of these calcites overlap with the present groundwater signatures found at 600 to 700 m depth. However, calcite from borehole CRG3 at 637.72 m depth has a measured homogenization temperature (Th) between 102 and 106 $^{o}C$. Thus, they cannot precipitate from the present groundwater. The calcites, in this case, have undergone a degree of dissolution, and the groundwaters are in equilibrium with and reflecting the Sr isotopic signatures of the adjacent fracture minerals.

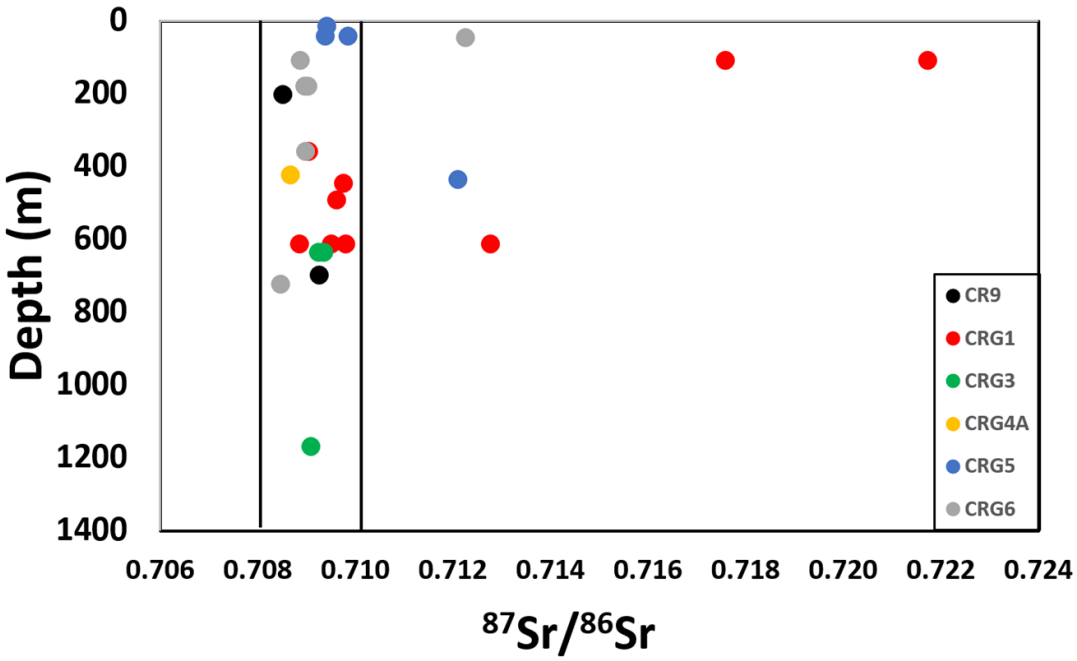


Figure 17. Strontium isotopic ratios organized from table 4. Data categorized by borehole and depth.

For the different calcite type, there a limited number of strontium ratios as shown on Table 4. The fibrous calcite has strontium ratios of 0.70952 and 0.70910 for CRG1 at 615 m and CRG3 at 1171.77 m respectively (Fig. 17, Table 4). Low ratios of these calcites and the fluid types discussed earlier suggest they may have precipitated from fluids that could have been derived from Paleozoic sedimentary rocks or a similar Paleozoic seawater source as described at other sites in other studies (Drake and Tullborg 2009). The metasomatic calcite sample from borehole CRG6 at 724.72 m has a strontium ratio of 0.70849 (Table 4). This is the least radiogenic strontium ratio found in calcite from this study. This ratio is similar to the strontium ratios of Precambrian-Cambrian boundary (McArthur et al., 2012). Elevated formation temperature (Th) and elevated salinity (Table 4) of these calcites suggest that parent waters probably was influenced by the heated and evaporated ocean water at

Precambrian-Cambrian time based on Seawater curve (McArthur et al., 2012). Therefore, the metasomatic calcites may have formed during an early tectonic orogeny (Fig. 4) which means it is the earliest calcite occurring at the CRL site. Crystal calcites have a wide range of strontium isotopic ratios from 0.70853 to 0.72172 (Fig. 17). Few elevated strontium ratios were found suggest limited water/rock interaction as descending or recharging waters interacted with the host rock and incorporated the more radiogenic geochemical characteristics of the host geology. Similar situations have been discussed in the literature involving the influence of descending oceanic water or fluid from overlying Paleozoic sediments of marine origin at other sites (Drake and Tullborg 2009).

**Elemental geochemistry results and analyses**

Geochemical analyses were used in this study in order to assess the relationship between bedrock and calcite and to investigate if the formation environment of minerals was oxidizing or reducing. Analyses involved uranium-thorium ratios and rare earth elements (REE).

The Thorium/uranium ratio of a calcite is applied to analyze the redox environment of calcite formation. In natural groundwater, thorium occurs in the $Th^{4+}$ redox state and redox changes are insignificant. However, uranium is sensitive to redox changes due to the insoluble $U^{4+}$ transferred from the fluid under reducing conditions (Brennecka et al., 2011). Therefore, under reducing conditions uranium relative to thorium partitions to the solid phase and Thorium/uranium ratio will increase (Bukata

2000; Romaniello et al., 2013). Limited Th and U data measured in this study from ten calcite samples are available to calculate the Thorium/uranium ratios (Fig. 18). The average thorium concentration of bedrock and calcite is 6.2 and 2.5 ppm, respectively and the average uranium concentration of bedrock and calcite is 1.8 and 1.3 ppm, respectively. Borehole CR9 at 203.8 m depth contained the most elevated thorium and uranium in both bedrock and calcite samples analyzed. The bedrock in boreholes CRG3 at 1171.77 m, CRG5 at 152.33 m, CRG6 at 48.08 m, and CRG6 at 101.44 m were found to have elevated thorium at concentration that were more than 10 ppm. The bedrock in borehole CRG4A at 613.79 m depth contained elevated uranium (4.6 ppm). The bedrock and calcite samples have different Thorium/uranium ratios, which also shows that the bedrock may not be a major source of these elements during calcite formation or that water/rock interactions were limited. Previous studies of seawater redox conditions over time suggest that the redox boundary between oxidizing and reducing conditions is a thorium/uranium ratio of 1 (Brennecka et al., 2011; Romaniello et al., 2013). At the CRL site, most calcites had Thorium/uranium ratios ranging from 0.50 to 12 with some very elevated ratios occurring in calcites from boreholes CRG1 at 110.18 m and CRG5 at 43.61 m. These Thorium/uranium results suggest the majority of calcite seems to precipitate under more reducing environment. However, a pegmatite intrusion occurring at the CRL site at these depths has elevated Th and U values and is therefore most likely to be a major source of these elements during hydrothermal leaching and calcite formation. The pegmatite at CRL site may influence the Thorium/uranium ratios of calcite.

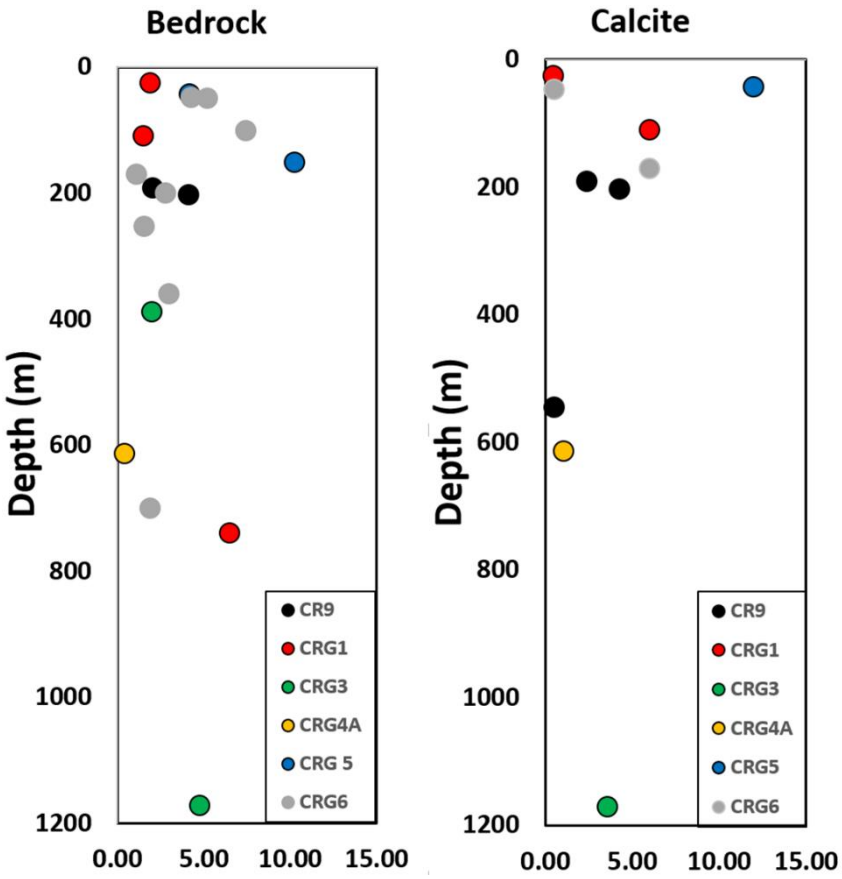


Figure 18. Plot of Thorium/uranium for bedrock and calcite from the CRL site. Plot constructed based on table 5 and all data analyzed by Actlabs.

REE data effectively assists analyses of fracture mineral origin and the degree to which the bedrock may geochemically contribute to fracture mineral formation (Cherniak, 1998; Habermann et al., 1996). Original concentrations of REE measurements can be found in Appendix 4. REE analyses use the chondrite-nomalized pattern instead of original concentration to eliminate the odd-even effect of the results (Lentz, 1998; Panahi et al., 2000). All REE measurements can be normalized to a chondrite standard to show enrichment and depletion of light rare earth elements (LREE) which include elements from La to Eu and heavy rare earth elements (HREE) which includes elements from Gd to Lu. Elevated LREE because of

complexation by $HCO_3^-$ and by organic molecules tend to bond more strongly to the REEs with increasing atomic number (Sandstorm and Tullborg 2009). Thus, the LREE enrichment seen in the calcite is interpreted as a result of the higher solubility of the heavy REE (HREE) complexes in fluid phase. Previous studies at other sites believed that earlier calcites contain higher LREEs because the HREE is more difficult to precipitate with calcite than the LREE and results in the LREE precipitating first with calcite phase (Sandstorm and Tullborg 2009).

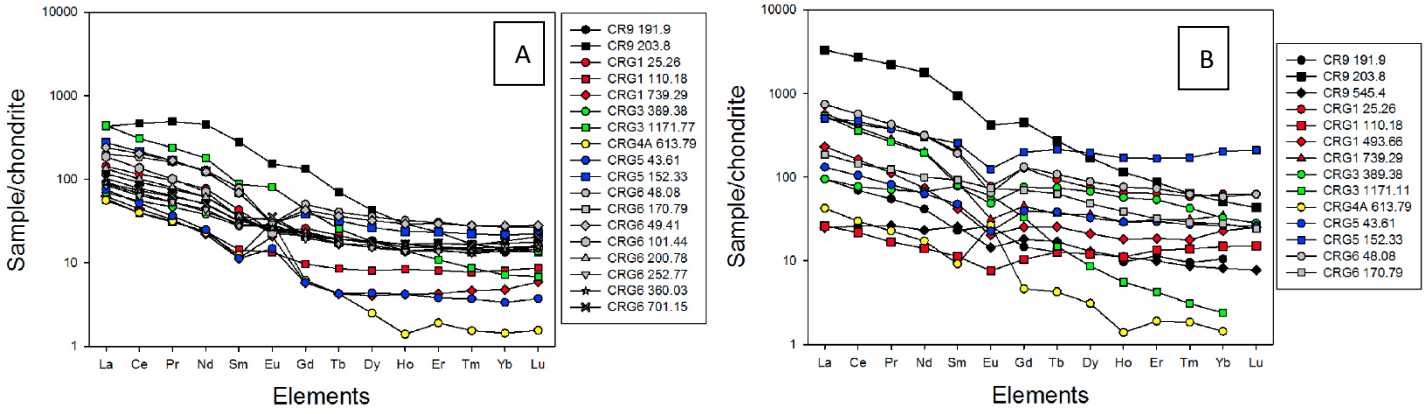


Figure 19. Chondrite normalized plots of REE concentrations in (A) calcite samples and (B) bedrock samples from the CRL site. The REE concentration was measured at Actlabs Ontario, Canada. Chondrite normalized calculation following rules from Panahi et al., (2000) and Lentz (1998).

As shown on Figure 20, most bedrock and calcite samples analyzed show LREE enrichment at the CRL site. The relationship between the calcite fracture fillings and the bedrock is apparent and indicates that the REE elements in the calcites were most likely derived from interaction with the bedrock. Except for calcite samples from borehole CRG1 at 110.18 m, all other calcite and bedrock samples contain a

LREE/HREE ratio more than 1 as shown on the Figure 19 (left part from elements La to Eu is higher than the right part from elements Gd to Lu). This is especially true for borehole CRG3 at 1171.77 m where the LREE/HREE value is 20.93 (Appendix 3). The REE enrichment and LREE/HREE ratios suggest partitioning of REE's to calcite from bedrock. In similar studies this suggests a hydrothermal origin (Sandstrom et al., 2009; Neymark et al., 2013).

Except for one sample, calcites analyzed at the CRL site for REEs contained a similar trend but slightly different REE pattern compared to the adjacent host bedrock. Water/rock interaction between the hydrothermal fluids involved in calcite formation and the bedrock was not extreme enough to leach the rock sufficiently to establish equilibrium or a strong enrichment of REE's in the calcite during formation. The one exception occurs in borehole CRG4A at 613.79 m depth (Fig. 20d). Based on fluid inclusion analyses this sample is part of the higher-temperature, low-salinity (181.2 $^{o}$C to 197.3 $^{o}$C and 2.88 to 7.33 wt. %, respectively) crystal calcite group. The calcite in this sample has a similar REE pattern to the adjacent bedrock and appears to indicate that the calcite geochemistry at this depth may have been highly influenced by the bedrock. Moreover, this calcite has a positive europium anomaly suggesting a higher temperature hydrothermal origin (Prudencio et al., 1994). As discussed earlier, the parent waters of this calcite were interpreted as a mixture of hydrothermal water and an evaporated seawater or sedimentary basinal fluid.

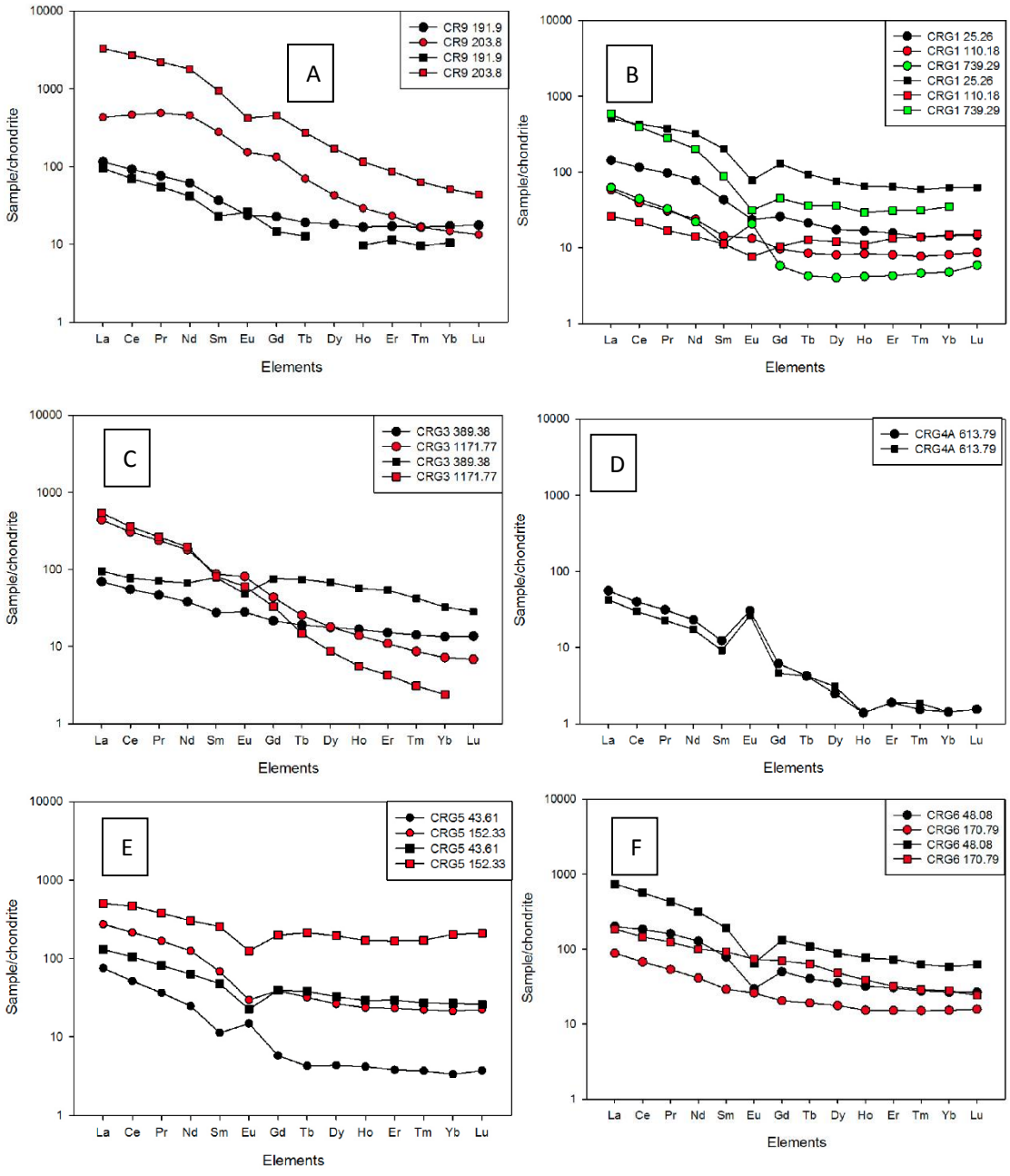


Figure 20. REE data for calcite and bedrock from each core sampled at CRL. Circles are bedrock and squares are calcite. The sample color was used for samples from the same depth.

Europium anomalies are applied to analyze the relationship between calcite and bedrock and the cerium anomalies are applied to analyze the redox environment. δEu is calculated by the equation 2 and δCe is calculated by the equation 3.

$$\delta Eu = Eu/(Sm * Gd)\text{^}(\frac{1}{2}) \qquad \text{Equation 2}$$

$$\delta Ce = Ce/(La * Pr)\hat{}(\frac{1}{2}) \quad \text{Equation 3}$$

Except for boreholes CR9 at 191.9 m, CRG3 at 1171.77 m and CRG4A at 613.79 m, calcite from most samples analyzed contain δEu less than 1. Calcites with negative europium anomalies suggest $Eu^{2+}$ in solution which is difficult to substitute for $Ca^{2+}$ in calcite because it is too large (Eby 1975). Both bedrock and calcite from borehole CRG4A at 613.79 m have higher δEu values at 3.31 and 3.84 respectively. Calcite in CRG4A contained enrich europium probably because it was influenced by the bedrock. For the limited REE data, crystalline calcites represent six of the samples that have negative cerium anomalies and the other seven samples of crystalline calcites have positive cerium anomalies (Appendix 4). Cerium precipitates in oxidizing conditions but is soluble in reducing conditions (Prudencio et al., 1994). Positive cerium anomalies indicate the calcite formed under oxidizing environment otherwise it formed under reducing environment. Therefore, results of cerium anomalies suggest calcites have been precipitated from both oxidizing and reducing.

Overall, the Sr isotopic ratios, Thorium/uranium ratios and REE results were evaluated as indicators of water/rock interaction and the influence of the bedrock on calcite mineralogical formation. Strontium and REE patterns analyses indicated that formation of many of the calcites involved interaction with the crystalline bedrock, but the degree of water/rock interaction was less than observed at other sites studied worldwide. Most likely the lower formation temperatures at the site are a factor in the degree of water/rock interaction. Thorium/uranium ratios suggest the calcite formed in reducing environment may due to the uranium concentration increased in fracture

minerals by pegmatite. Therefore, calcite perhaps be formed under both oxidizing and reducing groundwater according to cerium anomaly analyses.

# Summary

The study aimed to assess the long term stability of the bedrock found at the Chalk River Laboratory as a potential site for low and intermediate radioactive waste storage. The aim was to specifically analyze and categorize the fracture mineralization to specifically determine if there was any evidence for young or very recent hydrogeochemical events recorded in the mineral phases.

Hand specimen examination of core and later petrographic examination showed that early phase mineralogy such as chlorite and quartz were found in sealed veins and appeared to be quite old compared to later stage mineralization based on crosscutting and other emplacement relationships. Some quartz and chlorite veins contained calcite and in a few cases dolomite and were often highly deformed suggesting an earlier emplacement compared to the later stage dominantly calcite mineralogy. Fluid inclusions found in dolomite were elevated in temperature (Th around 70$^{o}$C), but had the highest salinity (Tm = -38$^{o}$C ≈ 35 wt. %) found in any mineral phases. Calcites associated with the dolomite were found to have the same temperatures of formation, but lower salinity and were interpreted as metasomatic calcites.

This study mainly focused on the analyses and interpretation of calcite mineralogy from the CRL site which can be categorized into four main types that include (a) metasomatic calcite, (b) fibrous calcite, (c) crystalline calcite, and (d) vuggy calcite. Crystalline calcite can be further categorized by fluid inclusion results into (i) an elevated-temperature, low salinity group; (ii) an elevated-temperature, high-salinity group; and (iii) a higher-temperature, low-salinity group. Low salinity inclusions

were interpreted as containing Na-Cl fluids system and high salinity inclusions were assumed to contain Ca-Na-Cl fluids based on melting temperatures and background methodologies (Roedder 1984). Fluid inclusion results indicate that all calcites examined at the CRL site were formed at elevated temperature (Th > 60$^{o}$C) which suggest that the calcite at the site could not have precipitated during a low temperature event such as a glacial intrusion. Young calcite suggested by other previous researches such as Bukata (2000) and Neymark et al., (2013) probably do not exist at the CRL site. Low temperature fluid inclusions examined during the study were secondary in nature and not representative of the true temperature of formation. As well, the elevated temperatures and interpreted hydrothermal regimes for all calcite varieties would constrain the timing for calcite emplacement to be possibly 100's of millions of years ago when either major tectonic or intrusive events impacted the regional bedrock regime. Absolute ages for calcite emplacement could not be done in this study and in general such techniques are not widely used at this time.

Isotopic analyses of the calcites allowed calculations of the isotopic composition of the fluids of formation using fluid inclusion temperature (Th) to constrain the calcite formation temperatures. This allowed the author to calculate the $\delta^{18}O$ values of the parent waters from which the calcite formed. Different salinity calcites were used to interpret mixing trends that were found based on fluid inclusion analyses at the study site, and indicate the parent waters could include evaporating seawater, basinal brines and/or shield brines. Metamorphic and magmatic fluids probably did not play a role

in calcite formation because the formation temperatures (Th) of the samples were all lower than 200$^{o}$C.

Several other techniques such as strontium isotopic ratios, Thorium/uranium ratios and rare earth element analyses were used to further confirm the extent of water/rock interaction and the geochemical relationship of calcite formation to the bedrock. Strontium ratios suggest that different calcites at the CRL site probably had been precipitated during the Paleozoic time and agreed that the metasomatic calcites may be the earliest formed calcite. This was based on the low $^{87}Sr/^{86}Sr$ ratios for most calcite where there has been too short a time period for $^{87}Rb$ decay to $^{87}Sr$. However, an alternative explanation could be a lack of interaction with the radiogenic bedrock. This is partially supported by the low hydrothermal temperatures of formation of calcites and other geochemical parameters analyzed. Thorium/uranium ratios are interpreted that the calcites in this study have formed in both oxidizing and reducing fluids which are similar to the results of rare earth elements analyses. Both strontium ratios and REE patterns suggest the water-rock interaction are limited at this site and most calcites were not significantly influenced by the bedrock.

Based on the findings and the tectonic history of the site, the majority of calcite found at the CRL site would most likely be precipitated during the Paleozoic. Hydrothermal and meteoric water results in the elevated formation temperature, evaporating seawater results in the elevated Na-Cl salinity, and basinal or shield brines results in the elevated Ca-Na-Cl salinity. The different types, homogenization

temperatures and salinities found in the various calcite groups indicate the subsurface environment has changed at various times in the past.

Finally, although analyses of the present day fluids at the site were not part of this study, the author can comment that dissolution of calcite by various present day fluids in a few major fracture has led to some of these fluid taking on isotopic and geochemical characteristics of the mineral phases. However, these fluids do not appear to have precipitated any new young low temperature mineral phases.

# Reference


Barnaby, R. J., & Rimstidt, J. D., 1989. Redox conditions of calcite cementation interpreted from Mn and Fe contents of authigenic calcites. Geological Society of America Bulletin, 101(6), 795-804.

Blyth, A., Frape, S.K., Blomqvist, R., Nissinen, P., McNutt, R., 1998. An isotopic and fluid inclusion study of fracture calcite from borehole OL-KR1 at the Olkiluoto site, Finland. Posiva Oy. Report 98-04.

Blyth, A., Frape, S.K., 1999. Assessment of the past thermal and chemical history of fluids at the Palmottu research site, by combining fluid inclusion and isotopic investigations of fracture calcite. The Palmottu Natural Analogue Project. Geol. Surv. Finland. Technical Report 99-07.

Blyth, A., Frape, S.K., Ruskeenemi, T., Blomqvist, R., 2004. Origins, closed system formation and preservation of calcites in glaciated crystalline bedrock: evidence from the Palmottu natural analogue site, Finland. Appl. Geochem. 19, 675–686.

Blyth, A.R., Frape, S.K., & Tullborg, E.L., 2009. A review and comparison of fracture mineral investigations and their application to radioactive waste disposal. Applied Geochemistry, 24(5), 821-835.

Bolduc, A. M., Ross, M., 2001 Surficial geology, Lachute-Oka, Que ̓bec. Geol Surv Can, Open File 3520

Boyko-Diankonow, M., and Terasmae, J., 1975. Palynol- ogy of Holocene sediments in Perch Lake, Chalk River, Ontario. In Hydrological studies on a small basin on the Canadian Shield. Edited by P. J. Bany. Atomic Energy of Canada Limited, Ottawa, Ont., Publication No. AECL 5041111, pp. 189-220.

Bottomley, D.J., 1987. The isotope geochemistry of fracture calcites from the chalk river area, Ontario, Canada. Appl. Geochem. 2, 81–91.

Bottomley, D.J., Veizer, J., 1992. The nature of groundwater in fractured rock: evidence from the isotopic and chemical evolution of recrystallized fracture calcites from the Canadian Precambrian Shield. Geochim. Cosmochim. Acta 56, 369–388.

Brennecka, G. A., Herrmann, A. D., Algeo, T. J., & Anbar, A. D., 2011. Rapid expansion of oceanic anoxia immediately before the end-Permian mass extinction. Proceedings of the National Academy of Sciences, 108(43), 17631-17634.

Bukata, A.R. 2000. Recrystallization of fracture-infilling calcite: evidence from δ18O, δ13C, Thorium/uranium Ages and fluid incluisons. M.Sc. thesis. Trent University.

Carlson, R. W., Hafner, R. S., & Lake, W. H. 1996. Transport and storage of radioactive materials--1996. PVP-Volume 334 (No. CONF-960706--). American Society of Mechanical Engineers, New York, NY (United States).

Catto, N.R., Patterson, R.J., and Gorman, W. A. 1981. Late Quaternary marine sediments at Chalk River, Ontario, Canada. Canadian Journal of Earth Sciences, 18, pp. 1261-1267.

Catto, N. R., Patterson, R. J., & Gorman, W. A. 1982. The late Quaternary geology of the Chalk River region, Ontario and Quebec. Canadian Journal of Earth Sciences, 19(6), 1218-1231.

Cherniak, D.J., 1998. REE diffusion in calcite. Earth and Planetary Science Letters, 160(3), 273-287.

Clauer, N., Frape, S.K., Fritz, B., 1989. Calcite veins of the Stripa granite (Sweden) as records of the origin of the groundwaters and their interactions with the granitic body. Geochim. Cosmochim. Acta 53, 1777–1781.

Cloutier, V., Lefebvre, R., Therrien, R., & Savard, M. M. 2008. Multivariate statistical analysis of geochemical data as indicative of the hydrogeochemical evolution of groundwater in a sedimentary rock aquifer system. Journal of Hydrology, 353(3), 294-313.

Davidson, A., 1998. Geological Map of the Grenville Province, Canada and Adjacent Parts of the United States of America. Geol. Surv. Can. Map 1947A, Scale 1:2,000,000

Davidson, A., van Breemen, O., 1988. Baddeleyite–zircon relationships in coronitic metagabbro, Grenville Province, Ontario: implications for geochronology. Contrib. Mineral. Petrol. 100, 291–299.

Dorobek, S.L., 1987, Petrography, geochemistry and origin of burial diagenetic facies, Siluro-Devonian Helderberg Group, Central Appalachians: Am. Assoc. Petroleum Geologists Bull., v. 71, p. 492-514.

Drake, H., and Tullborg, E. L. 2009. Paleohydrogeological events recorded by stable isotopes, fluid inclusions and trace elements in fracture minerals in crystalline rock, Simpevarp area, SE Sweden. Applied Geochemistry, 24(4), 715-732.

Easton, R.M., 2000. Metamorphism of the Canadian Shield, Ontario, Canada. II. Proterozoic metamorphic history. Can. Mineral. 38, 319–344

Eby G. N. (1975) Abundance and distribution of rare earth elements and yttrium in the rocks and minerals ofthe Oka carbonatite complexl Quebec. Geochim. Cosmochim. dcta 39, 597-620.

Frape, S.K., Fritz, P., & McNutt, R. T. 1984. Water-rock interaction and chemistry of groundwaters from the Canadian Shield. Geochimica et Cosmochimica Acta, 48(8), 1617-1627.

Frape, S.K., Fritz, P., Kamineni, D.C., Gibson, I.L., 1992. In: Davis, S.N., Nordstrom, D.K. (Eds), Hydrogeochemical Investigations in Boreholes at the Stripa Mine: the Hydrochemical Advisory Group and their Associates. Swedish Nuclear Fuel and Waste Management Company (SKB) Report 92-19, pp. 30–63.

Fritz, P., Fontes, J.-Ch., Frape, S.K., Louvat, D., Michelot, J.-L., Balderer, W., 1989. The isotope geochemistry of carbon in groundwater at Stripa. Geochim. Cosmochim. Acta 53, 1765–1775.

Gascoyne, M., Davison, C. C., Ross, J. D., & Pearson, R. 1987. Saline groundwaters and brines in plutons in the Canadian Shield. Saline Water and Gases in Crystalline Rocks, 33, 53-68.

González-Partida, E., Carrillo-Chávez, A., Grimmer, J. O. W., Pironon, J., Mutterer, J., & Levresse, G. 2003. Fluorite deposits at Encantada–Buenavista, Mexico: products of Mississippi Valley type processes. Ore Geology Reviews, 23(3), 107-124.

Habermann, D., Neuser, R. D., & Richter, D. K. 1996. REE-activated cathodoluminescence of calcite and dolomite: high-resolution spectrometric analysis of CL emission (HRS-CL). Sedimentary Geology, 101(1), 1-7.

Hall, D.L., Sterner, S.M., Bodnar, R.J., 1988. Freezing point depression of NaCl–KCl–H2O solutions. Economic Geology 83, 197–20

Hemming, N. G., Meyers, W. J., & Grams, J. C., 1989. Cathodoluminescence in diagenetic calcites: the roles of Fe and Mn as deduced from electron probe and spectrophotometric measurements. Journal of Sedimentary Research, 59(3).

Kamo, S.L., Heaman, L.M., Lumbers, S.B., 1989. Age for a lamprophyre dyke, Callander Bay, Ontario: use of Ti-bearing minerals as a potential geochronometer. Geol. Assoc. Can. Program Abstr. 14, A4

Kamo, S.L., Krogh, T.E., Kumarapeli, P.S., 1995. Age of the Grenville dyke swarm, Ontario–Quebec: implications for the timing of Iapetan rifting. Can. J. Earth Sci. 32, 273–280.

Ketchum, J.W.F., Davidson, A., 2000. Crustal architecture and tectonic assembly of the Central Gneiss Belt, Grenville Province, Canada: a new interpretation. Can. J. Earth Sci. 37, 217–234.

Kyser, T.K., 1987. Equilibrium fractionation factors for stable isotopes. In: T.K. Kyser (ed.). Mineralogical Association of Canada -Short course in Stable Isotope Geochemistry of Low Temperature Fluids, Volume 13.

Larson, S.A., Tullborg, E.-L., 1984. Fracture fillings in the gabbro massif of Taavinunnanen, northern Sweden. SKB/KBS Technical Report TR84-08.

Lentz, D. (1996). U, Mo, and REE mineralization in late-tectonic granitic pegmatites, southwestern Grenville Province, Canada. Ore Geology Reviews,11(4), 197-227.

Li, W., Franklyn, M.T., McNutt, R.H., Gascoyne, M., Kamineni, D.C., Frape, S.K., 1989. A Sr isotopic study of the Eye-Dashwa Pluton, Ontario and the Lac du Bonnet Pluton, Manitoba: plagioclase/water reaction. In: Miles, D.L. (Ed.), Proc. 6th Internat. Symp. (Water–Rock Interaction (WRI-6). A.A). Balkema, Rotterdam, pp. 41–444.

Li. Y., 2013. The Geochemical and Isotopic Evolution of Groundwater in Crystalline Rock of the Chalk River Nuclear Laboratories, Ontario. B.Sc. thesis. University of Waterloo.

Lyon, G. L., & Giggenbach, W. F. 1992. The isotope geochemistry of hot springs gases and waters from Coromandel and Hauraki. In The 14th New Zealand geothermal workshop. Proceedings.

McArthur, J. M., Howarth, R. J., & Shields, G. A. 2012. Strontium isotope stratigraphy. The geologic time scale, 1, 127-144.

McIntosh, J. C., Grasby, S. E., Hamilton, S. M., & Osborn, S. G. 2014. Origin, distribution and hydrogeochemical controls on methane occurrences in shallow aquifers, southwestern Ontario, Canada. Applied Geochemistry, 50, 37-52.

McLelland, J.M., Selleck, B.W., Bickford, M.E., 2010. Review of the Proterozoic evolution of the Grenville Province, its Adirondack outlier and the Mesoproterozoic inliers of the Appalachians. In: Tollo, R.P., Bartholomew, M.J., Hibbard, J.P., Karabinos, P.M. (Eds.), From Rodinia to Pangaea: The Lithotectonic Record of the Appalachian Region. Geol. Soc. Am. Memoir, vol. 206, pp. 1–29.

McNutt, R.H., Frape, S.K., Fritz, P., Jones, M.G., MacDonald, I.M., 1990. The 87Sr/86Sr values of Canadian Shield brines and fracture minerals with applications to groundwater mixing, fracture history, and geochronology. Geochim. Cosmochim. Acta 54, 205–215.

Milton, G.M., 1987. Paleohydrological inferences from fracture calcite analyses: an example from the Stripa Project, Sweden. Appl. Geochem. 2, 33–36.

Milton, G.M. and Brown, R.M., 1987. Uranium series dating of calcite coating in groundwater flow systems of the Canadian Shield. Chemical Geology (Isotope Geoscience Section), 65: 57-65.

Mook, W.G., Bommerson, J.C., Staverman, W.H., 1974. Carbon isotopic fractionation between dissolved bicarbonate and gaseous carbon dioxide. Earth Planet. Sci. Lett. 22, 169–176.

Négrel, P., Casanova, J., Aranyossy, J.F., 2001. Strontium isotopes systematics used to decipher the origin of groundwaters sampled from granitoids: the Vienne case (France). Chem. Geol. 177, 287–308.

Neymark, L. A., Peterman, Z. E., Moscati, R. J., & Thivierge, R. H. 2013. U–Pb, Rb–Sr, and U-series isotope geochemistry of rocks and fracture minerals from the Chalk River Laboratories site, Grenville Province, Ontario, Canada. Applied Geochemistry, 36, 10-33.

O'Neil, J.R., Clayton, R.N., Mayeda, T.K., 1969. Oxygen isotopic fractionation in divalent metal carbonates. J. Chem. Phys. 51, 5547–5558.

Pagel, M., Barbin, V., Blanc, P., and Ohnenstetter, D. (Eds.). 2013. Cathodoluminescence in geosciences. Springer Science & Business Media.

Panahi, A., Young, G. M., & Rainbird, R. H. 2000. Behavior of major and trace elements (including REE) during Paleoproterozoic pedogenesis and diagenetic alteration of an Archean granite near Ville Marie, Quebec, Canada. Geochimica et Cosmochimica Acta, 64(13), 2199-2220

Parent, M., Occhietti, S. 1988. Late Wisconsinian deglaciation and Champlain Sea invasion in the St. Lawrence Valley, Que ́bec. Ge ́ographie physique et Quaternaire 42:215–246

Perkins, D. 1998. Mineralogy. In the Beginning, 17(17), 38.

Potter, R.W., Clynne, M.A., Brown, D.L., 1978. Freezing point depression of aqueous sodium chloride solutions. Econ. Geol. 73, 284–285.

Prudencio, M. I., Gouveia, M. A., & Braga, M. S. 1994. REE distribution as an indicator of the origin of carbonates and silicates in basaltic rocks. In Mineral. Mag., Goldschmidt Conf. (Vol. 58, pp. 744-745).

Roedder, E. 1984. Fluid inclusions (Vol. 12, pp. 79-108). P. H. Ribbe (Ed.). Washington, DC: Mineralogical Society of America.

Romaniello, S. J., Herrmann, A. D., & Anbar, A. D. 2013. Uranium concentrations and 238 U/235 U isotope ratios in modern carbonates from the Bahamas: assessing a novel paleoredox proxy. *Chemical Geology*, *362*, 305-316.

Ruskeeniemi, T., Blomqvist, R., Vuorela, P., Frape, S. K., & Blyth, A. 1996. Silicate geothermometry as an indicator of water-rock interaction processes in the serpentinized mafic-ultramafic intrusion of Ylivieska. Geological Survey of Finland, Espoo (Finland).

Sandstr öm, B., & Tullborg, E. L. (2009). Episodic fluid migration in the Fennoscandian Shield recorded by stable isotopes, rare earth elements and fluid inclusions in fracture minerals at Forsmark, Sweden. Chemical Geology, 266(3), 126-142.

Seguin, A., 1994. Origin of Saline Groundwater in Torbolton Ward, Eastern Ontario. M.Sc. Thesis, University of Ottawa, Ottawa, Ontario, 1 12 pp.

Sims, P.K. and Peterman, Z.E., 1986. Early Proterozoic Central Plains Orogen: a major buried structure in the north-central United States. Geology 14, 488–4

Smellie, J., and Frape, S.k. 1997. Hydrogeochemical aspects of glaciation. In Glaciation and Hydrogeology, Workshop on the impact of climate change & glaciations on rock stresses, groundwater flow and hydrochemistry–past, present and future. SKI Report (Vol. 97, pp. 13-45).

Stotler, R. L., Frape, S. K., & Shouakar-Stash, O. 2010. An isotopic survey of δ 81 Br and δ 37 Cl of dissolved halides in the Canadian and Fennoscandian Shields. Chemical Geology, 274(1), 38-55.

ThermoFinnigan. (2002). Strontium. Triton Hardware Manual (pp. 2.3-20). Bremen, Germany: ThermoFinnigan.

Tullborg, E.L., 1989a. The influence of recharge water on fissure-filling minerals – a study from Klipperås, southern Sweden. Chem. Geol. 76, 309–320.

Tullborg, E.L., 1989b. δ18O and δ13C in fracture calcite used for interpretation of recent meteoric water circulation. In: Miles, D.L. (Ed.), Proc. 6th Inter. Symp. (Water–Rock Interaction (WRI-6). A.A). Balkema, Rotterdam, pp. 95–698.

Van der Pluijm, B.A., & Marshak, S. 2004. Earth structure: an introduction to structural geology and tectonics. New York: WW Norton; 2nd Ed.

Zhang, N. 2016. Fluid inclusion analyses and application of oil and gas basins. Petroleum Industry Press.

Zhang, Y.G., & Frantz, J.D., 1987. Determination of the homogenization temperatures and densities of supercritical fluids in the system NaCl-KCl-CaCl2-H2O using synthetic fluid inclusions. Chemical Geology, 64(3), 335-350.

# Appendix 1

Table of the isotopic data are organized by the core and depth, which means the meter along the borehole length (mable). $\delta^{18}O$ and $\delta^{13}C$ data are under VPDB standard.

| Core | Sample# | Depth | Unit | $\delta^{13}C$ | $\delta^{18}O$ | 87Sr/86Sr | geology |
|---|---|---|---|---|---|---|---|
| | | (mabl) | | (‰ VPDB) | (‰ VPDB) | | |
| CR18 | IS-CR18-01 | 29.47 | B | -5.04 | -12.68 | | White, clean, fine grained. Taken from the cleaner of two calcites |
| CR18 | IS-CR18-01 | 29.47 | B | -5.14 | -15.4 | | Grey/green. Taken from flakey calcite found on the exposed surfaces |
| CR18 | IS-CR18-01 | 29.47 | B | -4.97 | -12.8 | | White, clean, fine grained. Taken from the cleaner of two calcites |
| CR18 | IS-CR18-01 | 29.47 | B | -9.34 | -10.5 | | |
| CR18 | IS-CR18-01 | 29.47 | B | -7.14 | -9.99 | | |
| CR18 | IS-CR18-01 | 29.47 | B | -9.23 | -11.23 | | |
| CR9 | IS-CR9-1 | 159.2 | B | -4.46 | -11.46 | | crystalline, fracture filling, red colour present in some calcite |
| CR9 | IS-CR9-2 | 173.4 | B | -6.72 | -12.6 | | platy, predominant throughout sample, consistent pink colour occuring in host rock, some large whole flakes remain intact when sampled |
| CR9 | IS-CR9-3 | 191.9 | B | -3.85 | -12.15 | | platy, calcite not abundant at surface of core beneath surface |
| CR9 | IS-CR9-3 | 191.9 | B | -5.92 | -16.04 | | platy calcite broken off cleavage plane, green contamination |
| CR9 | IS-CR9-4 | 203.83 | B | -6.11 | -13.1 | | Localized large and small veins containing crystalline calicite, with some yellow contamination near host rock |
| CR9 | IS-CR9-4 | 203.83 | B | -9.16 | -14.66 | | platy calcite broken off cleavage plane, green contamination |
| CR9 | IS-CR9-25 | 238.2 | B | -6.57 | -12.6 | | Crystalline, closed vein calcite, |
| CR9 | IS-CR9-25 | 238.2 | B | -6.45 | -10.03 | | Crystaline, closed vein calcite bordering host rock, red contamination |
| CR9 | IS-CR9-6 | 254.9 | B | -6.91 | -12.22 | | platy calcite broken off cleavage plane, grey contamination |
| CR9 | IS-CR9-7 | 259.25 | B | -5.95 | -13.13 | | platy calcite broken off cleavage plane, red contamination |

| Core | Sample# | Depth | Unit | $\delta^{13}C$ | $\delta^{18}O$ | 87Sr/86Sr | geology |
|---|---|---|---|---|---|---|---|
| | | (mabl) | | (‰ VPDB) | (‰ VPDB) | | |
| CR9 | IS-CR9-7 | 259.25 | B | -8.64 | -12.19 | | platy calcite scratched off cleavage plane |
| CR9 | IS-CR9-8 | 270.18 | B | -4.18 | -10.7 | | platy calcite broken off cleavage plane, heavy grey contamination |
| CR9 | IS-CR9-9 | 352.75 | B | -3.26 | -10.55 | | platy calcite scratched off cleavage plane surrounded by pink red host rock |
| CR9 | IS-CR9-10 | 363.75 | B | -7.22 | -11.42 | | platy calcite scratched off cleavage plane surrounded by pink red host rock |
| CR9 | IS-CR9-11 | 382.8 | B | -5.57 | -12.47 | | platy calcite broken of cleavage plane in one solid piece grey and green contamination |
| CR9 | IS-CR9-12 | 424.12 | B | -5.83 | -16.28 | | platy calcite scrated of surface, yellow contamination prominent throughout |
| CR9 | IS-CR9-14 | 446.7 | B | -7.75 | -15.22 | | platy calcite broken off cleavage plane surrounded by pink host rock |
| CR9 | IS-CR9-26 | 490.51 | B | -5.13 | -15.62 | | platy calcite huge pieces broken off cleavage plane, grey and green contamination |
| CR9 | IS-CR9-27 | 491.85 | B | -4.86 | -16.11 | | Crystalline calcite, from thick branching vein, blue contamination |
| CR9 | IS-CR9-27 | 491.85 | B | -3.73 | -12.6 | | crystalline calcite, from thin closed vein, yellow contaminatino bordering host rock |
| CR9 | IS-CR9-28 | 498.3 | B | -5.24 | -16.13 | | crystalline calcite, thick closed vein, red contamination bordering red host rock |
| CR9 | IS-CR9-29 | 499.5 | B | -3.54 | -14.8 | | platy calcite scratched off cleavage plane, grey contamination |
| CR9 | IS-CR9-30 | 500.31 | B | -4.55 | -17.31 | | platy calcite , grey contamination, huge pieces broken off with small amounts of host rock contamination |
| CR9 | IS-CR9-15 | 521.21 | B | -7.25 | -13.41 | | crystalline calcite, thick closed vein, red and green host rock contamination |
| CR9 | IS-CR9-16 | 545.4 | B | -6.07 | -10.91 | | Crystalline calcite, thick closed vein, large chunks with green and yellow contamination, some host rock contamination |
| CR9 | IS-CR9-16 | 545.4 | B | -6.6 | -11.26 | | mostly platy, and some crystalline calcite, with some red contamination throughout |

| Core | Sample# | Depth | Unit | $\delta^{13}C$ | $\delta^{18}O$ | 87Sr/86Sr | geology |
|---|---|---|---|---|---|---|---|
| | | (mabl) | | (‰ VPDB) | (‰ VPDB) | | |
| CR9 | IS-CR9-17 | 553.7 | B | -5.12 | -11.98 | | crystalline open vein, grey and green contamination in certain areas, |
| CR9 | IS-CR9-17 | 553.7 | B | -8.59 | -14.66 | | crystalline open vein, grey and yellow contamination throughout |
| CR9 | IS-CR9-18 | 560.86 | B | -10.39 | -11.28 | | thick platy calcite with very little contamination, mostly white with slight amound of green |
| CR9 | IS-CR9-19 | 577.06 | B | -5.09 | -12.37 | | thick platy calcite with green and yellow contamination |
| CR9 | IS-CR9-21 | 635.27 | B | -6.6 | -12.77 | | platy calcite scratched off of cleavage plane, grey and green contamination. Some dark grey host rock contamination |
| CR9 | IS-CR9-32 | 700.76 | B | -4.51 | -17.03 | | thick crystalline vein bordered by black rock surrounding vein and very light pink rock containing green and garnets |
| CRG1 | IS-CRG1-01A | 9.015 | A | -7.37 | -11.28 | | |
| CRG1 | IS-CRG1-02A | 25.26 | A | -7.13 | -14.14 | | Larger Crystals, clean, white, some biotite |
| CRG1 | IS-CRG1-02A | 25.26 | A | -6.51 | -9.72 | | Edge material, grey. Taken from the exposed surface one side of the clean fracture calcite |
| CRG1 | IS-CRG1-03A | 110.18 | A | -8.38 | -11.07 | 0.72174 | White, clean, flaking off the top surface |
| CRG1 | IS-CRG1-03A | 110.18 | A | -9.27 | -12.66 | 0.7176 | Brown loose conglomeration containing small calcite crystals |
| CRG1 | IS-CRG1-10A | 230.9 | B | -6.09 | -14.37 | | More abundant, clean, white |
| CRG1 | IS-CRG1-10A | 230.9 | B | -8.88 | -11.7 | | Less common, cntaminated with a pink compound |
| CRG1 | IS-CRG1-11A | 238.62 | B | -7.38 | -10.78 | | White, fine grained, consistent across the fracture |
| CRG1 | IS-CRG1-11A | 238.62 | B | -6.99 | -11.65 | | Massive vuggy crystals of calcite, clean |
| CRG1 | IS-CRG1-12 | 246.28 | B | -6.4 | -13.58 | | Clean distinct calcite type that runs the length of the face side |
| CRG1 | IS-CRG1-12 | 246.28 | B | -8.18 | -9.62 | | Built up and flaking off the host rock, potentially a different calcite type |
| CRG1 | IS-CRG1-13A | 308.73 | B | -7.53 | -9.44 | | White, fine grained, clean, taken from the wide area of the fracture. Surface pock-marked |

| Core | Sample# | Depth | Unit | $\delta^{13}C$ | $\delta^{18}O$ | 87Sr/86Sr | geology |
|---|---|---|---|---|---|---|---|
| | | (mabl) | | (‰ VPDB) | (‰ VPDB) | | |
| CRG1 | IS-CRG1-15 | 361.038 | B | -5.82 | -14.72 | 0.70905 | White, fine grained, clean, consistent. Taken from a wide vein |
| CRG1 | IS-CRG1-16 | 448.565 | B | -5.62 | -14.9 | 0.70978 | White, fine grained clean. Taken from wide section |
| CRG1 | IS-CRG1-16 | 448.565 | B | -5.61 | -13.49 | | Grey, potential host rock contamination. Taken from a narrow vein |
| CRG1 | IS-CRG1-16 | 448.565 | B | -6.74 | -12.76 | | Brown/red, very contaminated. Taken from a narrow vein |
| CRG1 | IS-CRG1-18 | 452.285 | B | -6.55 | -12.27 | | White, clean. Taken from the middle of the main vein |
| CRG1 | IS-CRG1-18 | 452.285 | B | -6.32 | -11.91 | | Greenish white. Taken flaking off the exposed surface of the main vein |
| CRG1 | IS-CRG1-20A | 493.655 | B | -5.71 | -15.23 | 0.70963 | Massive crystals, clean, white, vuggy |
| CRG1 | IS-CRG1-20A | 493.655 | B | -5.59 | -15.4 | | Taken from a very large crystal, taken from the top side |
| CRG1 | IS-CRG1-20A | 493.655 | B | -5.68 | -16.17 | | Same cystal as C, taken from the lower side |
| CRG1 | IS-CRG1-20A | 493.655 | B | -5.84 | -15.2 | | Same crystal as D+C, taken from the "middle" after a break |
| CRG1 | IS-CRG1-21A | 615 | B | -7.88 | -17.34 | | Previously analysed… Green flakey calcite (left sample point) |
| CRG1 | IS-CRG1-21A | 615 | B | -8.24 | -14.53 | | middle sample point |
| CRG1 | IS-CRG1-21A | 615 | B | -7.71 | -15.31 | | right sample point |
| CRG1 | IS-CRG1-21A | 615 | B | -7.64 | -15.82 | | White/pink cleaner calcite scraped from a closed vein |
| CRG1 | IS-CRG1-21A | 615.15 | B | -8.42 | -20.61 | 0.71278 | Serpentinized? Green/white calcite, platey |
| CRG1 | IS-CRG1-21A | 615.15 | B | -8.15 | -20.44 | | Serpentinized? Off white calcite, platey |
| CRG1 | IS-CRG1-21A | 615.15 | B | -8.14 | -10.95 | 0.70952 | Serpentinized? Green/white calcite, platey |
| CRG1 | IS-CRG1-21A | 615.15 | B | -7.81 | -10.95 | | Serpentinized? Off white calcite, platey |
| CRG1 | IS-CRG1-22 | 683.66 | B | -6.8 | -12.6 | 0.70981 | Greenish calcite abundant in the main vein |
| CRG1 | IS-CRG1-22 | 683.66 | B | -6.22 | -14.38 | | White, brittle, vuggy, clear open spaces |
| CRG1 | IS-CRG1-24 | 739.295 | B | -6.91 | -16.66 | 0.70887 | White/grey in colour, scraped from the middle of the large main vein |
| CRG1 | IS-CRG1-24 | 739.295 | B | -6.46 | -16.94 | | Whiter in colour, scraped from the border of the vein where contant is |
| CRG3 | IS-CRG3-1A | 24.7 | A | -5.76 | -11.52 | | Type 1, lower vein (mic pic), appears to be contaminated. Fine grained |

| Core | Sample# | Depth | Unit | $\delta^{13}C$ | $\delta^{18}O$ | 87Sr/86Sr | geology |
|---|---|---|---|---|---|---|---|
| | | (mabl) | | (‰ VPDB) | (‰ VPDB) | | |
| CRG3 | IS-CRG3-1A | 24.7 | A | -9.13 | -10.55 | | Type 2, edge calcite. Some scaly some finer grained |
| CRG3 | IS-CRG3-4A | 389.38 | B | -8.35 | -10.31 | | White crystalline calcite vein, not regular, chaos |
| CRG3 | IS-CRG3-4A | 389.38 | B | -7.98 | -10.76 | | White calcite vein |
| CRG3 | IS-CRG3-9A | 630.29 | B | -6.97 | -12.72 | | White calcite vein |
| CRG3 | IS-CRG3-9A | 630.29 | B | -8.11 | -10.22 | | White crystalline calcite vein(very obvious huge vein127). Some grey and pink stuff grow in it. |
| CRG3 | IS-CRG3-9A | 630.29 | B | -6.1 | -15.52 | | White, clean, coarse and light grained cacite in a thick vein (representative) |
| CRG3 | IS-CRG3-10A | 637.721 | B | -6.42 | -15.04 | 0.70925 | Large crystal only |
| CRG3 | IS-CRG3-10A | 637.721 | B | -8.35 | -10.6 | 0.70937 | Small crystal only |
| CRG3 | IS-CRG3-11A | 672.71 | B | -8.6 | -9.32 | | White crystalline calcite inside the green calcite vein |
| CRG3 | IS-CRG3-13A | 862.06 | B | -5.89 | -14.4 | | Contaminated calcite in the main vein, scraped from the base of core |
| CRG3 | IS-CRG3-13A | 862.06 | B | -5.83 | -14.6 | | Scraped from the open channel coarse grain calcite |
| CRG3 | IS-CRG3-13A | 862.06 | B | -5.83 | -13.63 | | Scraped from fine graned calcite in the open channel (mic pic) |
| CRG3 | IS-CRG3-16A | 1171.77 | C | -4.91 | -15.32 | 0.7091 | Massive blocky clean calcite |
| CRG3 | IS-CRG3-16A | 1171.77 | C | -5.27 | -16.05 | | finer grained calcite |
| CRG4A | IS-CRG4A-01 | 56.61 | A | -6.32 | -11.84 | | Flakey calcite |
| CRG4A | IS-CRG4A-02 | 115.75 | A | -6.56 | -12.79 | | Type 1, the dominant type of what looks like two layered types |
| CRG4A | IS-CRG4A-02 | 116.75 | A | -6.18 | -13.66 | | Type 2, the less dominant type (greenish) |
| CRG4A | IS-CRG4A-02 | 117.75 | A | -6.3 | -13.09 | | Flakey calcite on the top of the core section (greenish) |
| CRG4A | IS-CRG4A-03 | 124.2 | A | -6.56 | -13.87 | | White clean, very thin vein (left) |
| CRG4A | IS-CRG4A-03 | 124.2 | A | -6.31 | -13.43 | | White/green scaly calcite seems to be inter-layered (right) |
| CRG4A | IS-CRG4A-04 | 206.532 | A | -6.19 | -14.45 | | White, clean, crystal type. Taken from the main vein |
| CRG4A | IS-CRG4A-05 | 382.14 | A | -6.7 | -9.81 | | White, clean. Taken from the main vein |

| Core | Sample# | Depth | Unit | $\delta^{13}C$ | $\delta^{18}O$ | 87Sr/86Sr | geology |
|---|---|---|---|---|---|---|---|
| | | (mabl) | | (‰ VPDB) | (‰ VPDB) | | |
| CRG4A | IS-CRG4A-07 | 425.35 | A | -6.61 | -14.43 | 0.70868 | White, clean. Taken from the edge of the main vein |
| CRG4A | IS-CRG4A-08 | 425.95 | A | -6.16 | -14.7 | | White, fine grained, clean. Taken from the middle of a wide part of a vein |
| CRG4A | IS-CRG4A-10 | 613.795 | B | -7.74 | -10.3 | | White, massive, crystal, vuggy, taken from an open cavern |
| CRG5 | IS-CRG5-24A | 16.27 | C | -7.67 | -9.36 | 0.70942 | White, clean, massive, crystal, vuggy. Taken from an open channel |
| CRG5 | IS-CRG5-24A | 16.27 | C | -7.51 | -11.35 | | |
| CRG5 | IS-CRG5-01 | 43.61 | C | -12.71 | -8.9 | 0.70939 | White, fine grained, clean. Taken from the middle of a wide deposit |
| CRG5 | IS-CRG5-01 | 43.61 | C | -12.89 | -9.22 | | White, fine grained, clean. Taken from the edge of a wide deposit |
| CRG5 | IS-CRG5-01 | 43.61 | C | -10.47 | -10.81 | 0.70987 | Red tint, relatively clean. Scraped from the exposed surface of the vein |
| CRG5 | IS-CRG5-03 | 147.7 | C | -7.96 | -12.4 | | White, fine grained, clean. Taken from the cleaner of two types within the fractures |
| CRG5 | IS-CRG5-03 | 147.7 | C | -5.73 | -15.83 | | Surface green/white flakey calcite |
| CRG5 | IS-CRG5-03 | 147.7 | C | -7.03 | -12.93 | | Side, interlayered flakey calcite |
| CRG5 | IS-CRG5-04 | 152.33 | C | -6.61 | -13.7 | | White, massive spherical crystals, vuggy |
| CRG5 | IS-CRG5-04 | 152.33 | C | -6.47 | -13.95 | | White, smaller spherical crystals, vuggy |
| CRG5 | IS-CRG5-04 | 152.33 | C | -6.15 | -13.34 | | White, fine grained, clean. Taken from the closed vein |
| CRG5 | IS-CRG5-05A | 438.12 | C | -13.6 | -10.78 | 0.71211 | White, clean, large crystal within the main vein |
| CRG5 | IS-CRG5-05A | 438.12 | C | -12.99 | -11.1 | | White clean, fine grained. Taken from the edges of the main vein |
| CRG5 | IS-CRG5-05A | 438.12 | C | -13.47 | -10.74 | | Pink, clean, large crystal |
| CRG6 | IS-CRG6-04 | 48.08 | B | -10.46 | -14.83 | | White, clean, fine grained. Taken from the main vein |
| CRG6 | Is-CRG3-20 | 96.33 | B | -6.56 | -14.31 | | Scraped from the exposed surface, potentially flakey clacite |
| CRG6 | Is-CRG3-21 | 96.63 | B | -5.75 | -16.13 | | White, clean, fine grained. Taken from the main vein |
| CRG6 | IS-CRG6-05 | 111.2 | B | -7.1 | -12.71 | | |
| CRG6 | IS-CRG6-05 | 111.2 | B | -7.33 | -12.8 | | |

| Core | Sample# | Depth | Unit | $\delta^{13}C$ | $\delta^{18}O$ | 87Sr/86Sr | geology |
|---|---|---|---|---|---|---|---|
| | | (mabl) | | (‰ VPDB) | (‰ VPDB) | | |
| CRG6 | IS-CRG6-06 | 116.9 | B | -6.73 | -13.98 | | Pink calcite vein grow inside the white vein |
| CRG6 | IS-CRG6-07 | 123.26 | B | -6.51 | -13.84 | | huge bunch of calcite crystal in the core, large crastals |
| CRG6 | Is-CRG3-22 | 127.72 | B | -5.26 | -10.84 | | Green flaky calcite, found grow between the body rock and white calcite. |
| CRG6 | Is-CRG3-23 | 133.6 | B | -5.72 | -11.81 | | Large vuggy clean calcite, found in the ceter of the core |
| CRG6 | IS-CRG6-08 | 149.84 | B | -6.95 | -12.64 | | White crystalline calcite vein, very thick |
| CRG6 | IS-CRG6-08 | 149.84 | B | -7.69 | -10.89 | | Thick white crystalline calcite along the whole core, very thick relative to green vein |
| CRG6 | IS-CRG6-09 | 159.55 | B | -6.62 | -12.34 | | White crystalline calcite vein |
| CRG6 | IS-CRG6-09 | 159.55 | B | -6.14 | -12.36 | | Medium vuggy clean calcite, found internal the white vein |
| CRG6 | IS-CRG6-09 | 159.55 | B | -7.69 | -11.47 | | Green flaky calcite, found on the ends of the core |
| CRG6 | IS-CRG6-01 | 169.123 | B | -7.2 | -12.18 | | White crystalline vein calcite (thin veins) |
| CRG6 | IS-CRG6-01 | 169.123 | B | -6.24 | -14.36 | | Large vuggy clean calcite, found internally |
| CRG6 | IS-CRG6-02 | 170.79 | B | -6.48 | -14.47 | | White, clean, fine grained. Taken from the exposed sections of the closed vein calcite |
| CRG6 | IS-CRG6-02 | 170.79 | B | -8.15 | -10.9 | | Grey/brown, crumbly, seems to dominate |
| CRG6 | IS-CRG6-02 | 170.79 | B | -10.42 | -8.35 | | White, clean, fine grained. Taken from the middle of the closed vein calcite |
| CRG6 | IS-CRG6-02 | 170.79 | B | -10.05 | -8.71 | | White/Grey, flakey. Scraped from the exposed side of a previously closed |
| CRG6 | IS-CRG6-10 | 182.04 | B | -7.16 | -12.77 | | White, clean, large crystal, vuggy. Open channel |
| CRG6 | IS-CRG6-10 | 182.04 | B | -13.34 | -11.21 | | White, clean, large crystal, vuggy. Open channel |
| CRG6 | IS-CRG6-11 | 217.15 | B | -8.47 | -11.16 | | Two big white crystalline calcite vein |
| CRG6 | IS-CRG6-11 | 217.15 | B | -6.4 | -15.49 | | Large vuggy clean calcite, found internal the white vein |
| CRG6 | IS-CRG6-12 | 219.33 | B | -5.17 | -14.73 | | Very large vuggy clean calcite. Nearly full of the core. Very beautiful |
| CRG3 | Is-CRG3-24 | 307.9 | B | -4.94 | -14.05 | | Pretty slice white calcite verin |

| Core | Sample# | Depth | Unit | $\delta^{13}C$ | $\delta^{18}O$ | 87Sr/86Sr | geology |
|---|---|---|---|---|---|---|---|
| | | (mabl) | | (‰ VPDB) | (‰ VPDB) | | |
| CRG6 | IS-CRG6-15 | 346 | B | -5.05 | -13.1 | | |
| CRG6 | IS-CRG6-15 | 346 | B | -4.53 | -14.25 | | White crystalline calcite. Found alongside green calcite (same vein) |
| CRG6 | IS-CRG6-15 | 346 | B | -4.65 | -12.98 | | Green crystalline calcite. Alongside white |
| CRG6 | IS-CRG6-16 | 348.09 | B | -7.72 | -13.85 | | Pink caclite. Larger crystals, found between green and white |
| CRG6 | IS-CRG6-16 | 348.09 | B | -7.12 | -12.41 | | White crystalline vein calcite (thins but huge part through the core), found at the ende of the core |
| CRG6 | IS-CRG6-17 | 359.62 | B | -9.41 | -10.53 | | Green brunch of calcite, found in the indiddle of the core |
| CRG6 | IS-CRG6-18 | 395.79 | B | -6.99 | -10.89 | | White crystalline calcite vein |
| CRG6 | IS-CRG6-19 | 410.2 | B | -6.38 | -13.23 | | Hard to see. Maybe the very thin white slice/ vein is calcite. White calcite on the slope side run through the whore core(on the surface) |
| CRG6 | Is-CRG3-25 | 463.79 | B | -4.82 | -11.85 | | White crystalline calcite vein |
| CRG6 | IS-CRG6-20 | 691.19 | B | -4.98 | -14.19 | | a slice of white calcite grow in the vein |
| CRG6 | IS-CRG6-20 | 691.19 | B | -4.96 | -13.08 | | very thine green calcite vein |
| CRG6 | IS-CRG6-21 | 724.72 | B | -5.03 | -15.08 | | Huge white crastalline calcite at one edge of the core |
| CRG6 | IS-CRG6-21 | 724.72 | B | -4.64 | -14.98 | | Green flaky calcite, found in the vein separate the wihte and pink (maybe quartzite) |

# Appendix 2

Table of Fluid inclusion data which include the homogeneous temperature and melting temperature, table is organized by fracture mineral type. The equation applied for salinity calculation are W=-1.76958*Tm-0.042384Tm^2+0.00052778Tm^3 which was estimated by Hall et al., 1988 and the calculated range of Tm is from 0 to -20 $^{o}$C.

| Sample | Sample# | Depth(mabl) | Th ($^{o}$C) | Tm ($^{o}$C) | Salinity (%) | Unit | Fracture mineral |
|---|---|---|---|---|---|---|---|
| CRG3 | | 548.4 | 70 | -6 | 8.977656 | B | Quartz |
| CRG5 | IS-CRG5-01 | 43.61 | 50 | -3 | 4.913034 | C | Quartz |
| CRG3 | IS-CRG3-1A | 24.7 | 73 | -31 | | A | Dolomite |
| CRG3 | IS-CRG3-1A | 24.7 | 73 | -35 | | A | Dolomite |
| CRG6 | IS-CRG6-21 | 724.72 | 77.2 | -37.2 | | B | calcite metasomatic dolomite |
| CRG6 | IS-CRG6-21 | 724.72 | 77.2 | -37.2 | | B | calcite metasomatic dolomite |
| CRG6 | IS-CRG6-21 | 724.72 | 62.1 | -21.5 | 13.20869 | B | calcite metasomatic dolomite |
| CRG6 | IS-CRG6-21 | 724.72 | 72.7 | -29.3 | 2.186804 | B | calcite metasomatic dolomite |
| CRG6 | IS-CRG6-21 | 724.72 | 74.8 | -10.4 | 13.2257 | B | calcite metasomatic dolomite |
| CR9 | IS-CR9-17 | 553.7 | 73 | -20 | 14.21576 | B | calcite metasomatic dolomite |
| CR9 | IS-CR9-17 | 553.7 | 90 | -19 | 14.70135 | B | calcite metasomatic dolomite |
| CR9 | IS-CR9-17 | 553.7 | 90 | -20 | 14.21576 | B | calcite metasomatic dolomite |
| CR9 | IS-CR9-17 | 553.7 | 90 | -19 | 14.70135 | B | calcite metasomatic dolomite |
| CRG6 | | 440.2 | 90.9 | -18.5 | 14.8896 | B | calcite metasomatic dolomite |
| CRG5 | | 12.68 | 85 | -38 | | C | vug calcite |
| CRG5 | | 12.68 | 87 | -31 | | C | vug calcite |
| CRG6 | IS-CRG6-15 | 346 | 85.4 | -31 | | B | vug calcite |
| CRG5 | IS-CRG5-24A | 16.27 | 78 | -14 | 15.01863 | C | tectonic calcite |

| Sample | Sample# | Depth(mabl) | Th (°C) | Tm (°C) | Salinity (%) | Unit | Fracture mineral |
|---|---|---|---|---|---|---|---|
| CRG5 | IS-CRG5-24A | 16.27 | 78 | -2 | 3.365402 | C | tectonic calcite |
| CRG5 | IS-CRG5-24A | 16.27 | 124 | 0 | 0 | C | tectonic calcite |
| CRG6 | IS-CRG6-10 | 182.04 | 82 | -7 | 10.12922 | B | fine grained calcite |
| CRG6 | IS-CRG6-10 | 182.04 | 84 | -6 | 8.977656 | B | fine grained calcite |
| CRG6 | IS-CRG6-10 | 182.04 | 84 | -6 | 8.977656 | B | fine grained calcite |
| CRG6 | IS-CRG6-10 | 182.04 | 84 | -2 | 3.365402 | B | fine grained calcite |
| CRG6 | IS-CRG6-10 | 182.04 | 84 | -2 | 3.365402 | B | fine grained calcite |
| CRG6 | IS-CRG6-10 | 182.04 | 83 | -6 | 8.977656 | B | fine grained calcite |
| CRG6 | IS-CRG6-10 | 182.04 | 84 | -9 | 12.10836 | B | fine grained calcite |
| CRG6 | IS-CRG6-10 | 111.22 | 89.5 | -21.3 |  | B | fine grained calcite |
| CRG1 |  | 634.66 | 104.2 | -24.3 |  | B | fine grained calcite |
| CRG1 |  | 634.66 | 104.5 | -7.8 | 10.97362 | B | fine grained calcite |
| CRG6 |  | 440.2 | 79.6 | -9.4 | 12.45064 | B | coarse grained calcite |
| CRG6 | IS-CRG6-21 | 724.72 | 72.1 | -37.7 |  | B | coarse grained calcite |
| CRG6 | IS-CRG6-09 | 159.55 | 90.2 | -3.7 | 5.940475 | B | coarse grained calcite |
| CRG3 |  | 307.9 | 77 | -7 | 10.12922 | B | coarse grained calcite |
| CRG3 |  | 307.9 | 70 | -6 | 8.977656 | B | coarse grained calcite |
| CRG3 |  | 307.9 | 67 | -4 | 6.366398 | B | coarse grained calcite |
| CRG3 |  | 307.9 | 75 | -3 | 4.913034 | B | coarse grained calcite |
| CRG3 |  | 307.9 | 82 | -3 | 4.913034 | B | coarse grained calcite |
| CRG3 |  | 307.9 | 83 | -7 | 10.12922 | B | coarse grained calcite |
| CRG3 |  | 307.9 | 91 | -7 | 10.12922 | B | coarse grained calcite |
| CRG3 | IS-CRG3-13A | 862.06 | 87 | -8 | 11.17384 | B | coarse grained calcite |
| CRG3 | IS-CRG3-13A | 862.06 | 97 | -3 | 4.913034 | B | coarse grained calcite |

| Sample | Sample# | Depth(mabl) | Th (°C) | Tm (°C) | Salinity (%) | Unit | Fracture mineral |
|---|---|---|---|---|---|---|---|
| CRG6 | IS-CRG6-05 | 111.22 | 85.6 | -31.4 | | B | coarse grained calcite |
| CRG6 | IS-CRG6-09 | 159.55 | 86 | -29 | | B | coarse grained calcite |
| CRG6 | IS-CRG6-21 | 724.72 | 79.6 | -38.9 | | B | coarse grained calcite |
| CRG6 | IS-CRG6-21 | 724.72 | 73.7 | -36.2 | | B | coarse grained calcite |
| CRG6 | IS-CRG6-21 | 724.72 | 75.5 | -39.4 | | B | coarse grained calcite |
| CRG1 | | 366.04 | 108 | 0 | 0 | B | coarse grained calcite |
| CRG1 | | 366.04 | 106 | 0 | 0 | B | coarse grained calcite |
| CRG1 | | 366.04 | 113 | -2 | 3.365402 | B | coarse grained calcite |
| CRG1 | | 366.04 | 113 | -2 | 3.365402 | B | coarse grained calcite |
| CR9 | IS-CR9-26 | 490.51 | 104.1 | -3.7 | 5.940475 | B | coarse grained calcite |
| CRG1 | IS-CRG1-02A | 25.26 | 79 | -6 | 8.977656 | A | coarse grained calcite |
| CRG1 | IS-CRG1-02A | 25.26 | 72 | -17 | 15.2409 | A | coarse grained calcite |
| CRG3 | | 548.13 | 89.6 | -0.9 | 1.557906 | B | coarse grained calcite |
| CRG3 | IS-CRG1-02A | 389.38 | 92 | -8 | 11.17384 | B | coarse grained calcite |
| CRG3 | IS-CRG1-02A | 389.38 | 86 | -8 | 11.17384 | B | coarse grained calcite |
| CRG3 | IS-CRG1-02A | 389.38 | 89 | -6 | 8.977656 | B | coarse grained calcite |
| CRG3 | IS-CRG1-02A | 389.38 | 88 | -5 | 7.722328 | B | coarse grained calcite |
| CRG3 | IS-CRG3-11A | 672.31 | 89 | -8 | 11.17384 | B | coarse grained calcite |
| CRG3 | IS-CRG3-11A | 672.31 | 89 | -38 | -22.9188 | B | coarse grained calcite |
| CRG6 | IS-CRG6-02 | 170.79 | 87 | -8 | 11.17384 | B | coarse grained calcite |
| CRG6 | IS-CRG6-02 | 170.79 | 88 | -8 | 11.17384 | B | coarse grained calcite |
| CRG6 | IS-CRG6-02 | 170.79 | 72 | -11 | 13.63444 | B | coarse grained calcite |
| CR18 | | 28.14 | 79 | -32 | -4.068951 | B | coarse grained calcite |
| CR18 | | 28.14 | 81 | -33 | -6.726866 | B | coarse grained calcite |

| Sample | Sample# | Depth(mabl) | Th (°C) | Tm (°C) | Salinity (%) | Unit | Fracture mineral |
|---|---|---|---|---|---|---|---|
| CRG6 | IS-CRG6-09 | 159.55 | 76.3 | -6.3 | 9.334163 | B | coarse grained calcite |
| CRG6 | IS-CRG6-09 | 159.55 | 81 | -9.1 | 12.19564 | B | coarse grained calcite |
| CRG6 | IS-CRG6-09 | 159.55 | 90 | -4.5 | 7.05674 | B | coarse grained calcite |
| CRG3 | IS-CRG1-02A | 389.38 | 16 | 0 | 0 | B | coarse grained calcite |
| CRG3 | IS-CRG1-02A | 389.38 | 23 | 0 | 0 | B | coarse grained calcite |
| CRG3 | IS-CRG3-10A | 637.72 | 95.8 | -2.3 | 3.839401 | B | coarse grained calcite |
| CRG3 | IS-CRG3-10A | 637.72 | 102.7 | -0.7 | 1.217757 | B | coarse grained calcite |
| CRG3 | IS-CRG3-10A | 637.72 | 96.3 | -1.2 | 2.061551 | B | coarse grained calcite |
| CRG3 | IS-CRG3-10A | 637.72 | 91.7 | -36.7 |  | B | coarse grained calcite |
| CRG3 | IS-CRG3-10A | 637.72 | 106.2 | -0.6 | 1.046376 | B | coarse grained calcite |
| CRG3 | IS-CRG3-10A | 637.72 | 105.4 | -3.6 | 5.796567 | B | coarse grained calcite |
| CRG3 | IS-CRG3-10A | 637.72 | 102.3 | -6.3 | 9.334163 | B | coarse grained calcite |
| CRG3 | IS-CRG3-10A | 637.72 | 97.8 | -1.9 | 3.205576 | B | coarse grained calcite |
| CRG3 | IS-CRG3-9A | 630.29 | 104.8 | -0.9 | 1.557906 | B | coarse grained calcite |
| CRG3 | IS-CRG3-9A | 630.29 | 88.7 | -0.8 | 1.388268 | B | coarse grained calcite |
| CRG3 | IS-CRG3-9A | 630.29 | 89.7 | -0.3 | 0.527045 | B | coarse grained calcite |
| CRG3 | IS-CRG3-9A | 630.29 | 101.8 | -3.6 | 5.796567 | B | coarse grained calcite |
| CRG3 | IS-CRG3-9A | 630.29 | 92.3 | -2.7 | 4.458498 | B | coarse grained calcite |
| CRG1 | IS-CRG1-20A | 493.65 | 103.1 | -5.3 | 8.109633 | B | coarse grained calcite (cloudy) |
| CRG1 | IS-CRG1-20A | 493.65 | 97.5 | -0.7 | 1.217757 | B | coarse grained calcite (cloudy) |
| CRG1 | IS-CRG1-20A | 493.65 | 86.3 | -1.2 | 2.061551 | B | coarse grained calcite (cloudy) |
| CRG1 | IS-CRG1-20A | 493.65 | 95.4 | -0.8 | 1.388268 | B | coarse grained calcite (cloudy) |
| CRG1 | IS-CRG1-20A | 493.65 | 83.7 | -2.3 | 3.839401 | B | coarse grained calcite (cloudy) |
| CRG1 | IS-CRG1-20A | 493.65 | 90.3 | -2.8 | 4.610948 | B | coarse grained calcite (cloudy) |

| Sample | Sample# | Depth(mabl) | Th (°C) | Tm (°C) | Salinity (%) | Unit | Fracture mineral |
|---|---|---|---|---|---|---|---|
| CRG1 | IS-CRG1-20A | 493.65 | 86.9 | -1.1 | 1.894551 | B | coarse grained calcite (cloudy) |
| CRG1 | IS-CRG1-20A | 493.65 | 192.3 | -1.6 | 2.720663 | B | coarse grained calcite (clean) |
| CRG1 | IS-CRG1-20A | 493.65 | 197.1 | -0.9 | 1.557906 | B | coarse grained calcite (clean) |
| CRG1 | IS-CRG1-20A | 493.65 | 179.6 | -0.7 | 1.217757 | B | coarse grained calcite (clean) |
| CRG1 | IS-CRG1-20A | 493.65 | 199 | -2.2 | 3.682318 | B | coarse grained calcite (clean) |
| CRG3 | IS-CRG3-13A | 862.06 | 85.7 | -0.3 | 0.527045 | B | coarse grained calcite |
| CRG3 | IS-CRG3-13A | 862.06 | 108.1 | -0.3 | 0.527045 | B | coarse grained calcite |
| CRG3 | IS-CRG3-13A | 862.06 | 92.4 | -3.1 | 5.062665 | B | coarse grained calcite |
| CRG3 | IS-CRG3-13A | 862.06 | 95.6 | -6.3 | 9.334163 | B | coarse grained calcite |
| CRG3 | IS-CRG3-13A | 862.06 | 94.8 | -1.6 | 2.720663 | B | coarse grained calcite |
| CRG3 | IS-CRG3-13A | 862.06 | 98.6 | -0.1 | 0.176534 | B | coarse grained calcite |
| CRG3 | IS-CRG3-13A | 862.06 | 87.9 | -1.3 | 2.227666 | B | coarse grained calcite |
| CRG6 | IS-CRG3-13A | 169.12 | 90.5 | -14.5 | 15.13867 | B | coarse grained calcite |
| CRG6 | IS-CRG3-13A | 169.12 | 93.7 | -0.1 | 0.176534 | B | coarse grained calcite |
| CRG4A | IS-CRG4A-10 | 613.79 | 197.3 | -4.7 | 7.325968 | B | coarse grained calcite |
| CRG4A | IS-CRG4A-10 | 613.79 | 113.6 | -2.5 | 4.150803 | B | coarse grained calcite |
| CRG4A | IS-CRG4A-10 | 613.79 | 200 | -9.3 | 12.36678 | B | coarse grained calcite |
| CRG4A | IS-CRG4A-10 | 613.79 | 167.3 | -8.5 | 11.65506 | B | coarse grained calcite |
| CRG4A | IS-CRG4A-10 | 613.79 | 181.2 | -1.7 | 2.883203 | B | coarse grained calcite |
| CRG4A | IS-CRG4A-10 | 613.79 | 138.2 | -0.3 | 0.527045 | B | coarse grained calcite |
| CR18 | | 28.14 | 85.8 | -3.7 | 5.940475 | B | coarse grained calcite |
| CR18 | | 28.14 | 90.1 | -2.3 | 3.839401 | B | coarse grained calcite |
| CR18 | | 28.14 | 83.7 | -2.2 | 3.682318 | B | coarse grained calcite |
| CR18 | | 28.14 | 82.6 | -28.3 | | B | coarse grained calcite |

| Sample | Sample# | Depth(mabl) | Th (°C) | Tm (°C) | Salinity (%) | Unit | Fracture mineral |
|---|---|---|---|---|---|---|---|
| CR18 | | 28.14 | 95.7 | -3.7 | 5.940475 | B | coarse grained calcite |
| CR18 | | 28.14 | 106.1 | -4.8 | 7.459088 | B | coarse grained calcite |
| CRG1 | IS-CRG1-21A | 615 | 90.1 | -3.8 | 6.083419 | B | coarse grained calcite |
| CRG3 | | 133.52 | 97.9 | -11.2 | 13.76115 | B | coarse grained calcite |
| CRG3 | | 133.52 | 81.3 | -3.7 | 5.940475 | B | coarse grained calcite |
| CRG3 | | 133.52 | 105 | -4.1 | 6.506428 | B | coarse grained calcite |
| CRG3 | | 133.52 | 80.3 | -0.3 | 0.527045 | B | coarse grained calcite |
| CRG3 | | 133.52 | 80.7 | -1.2 | 2.061551 | B | coarse grained calcite |
| CRG3 | | 133.52 | 101.4 | -3.3 | 5.359085 | B | coarse grained calcite |
| CR9 | IS-CR9-32 | 700.76 | 112.3 | -8.3 | 11.4659 | B | coarse grained calcite |
| CR9 | IS-CR9-32 | 700.76 | 107.2 | -5.1 | 7.85244 | B | coarse grained calcite |

# Appendix 3

Table 1: REE data of for bedrock samples from different boreholes, data categorized by borehole and define. All REE data is after chondrited-normalized

| Borehole | CRL ID | Depth | La | Ce | Pr | Nd | Sm | Eu | Gd | Tb | Dy | Ho | Er | Tm | Yb | Lu |
|---|---|---|---|---|---|---|---|---|---|---|---|---|---|---|---|---|
| CR9 | IS-CR9-3 | 191.9 | 116.13 | 92.33 | 76.39 | 61.50 | 36.92 | 23.54 | 22.78 | 19.15 | 18.32 | 16.71 | 17.14 | 16.67 | 17.22 | 17.70 |
| CR9 | IS-CR9-25 | 203.8 | 432.26 | 466.58 | 491.80 | 456.67 | 280.00 | 153.74 | 133.59 | 70.21 | 42.86 | 29.25 | 23.33 | 16.67 | 14.83 | 13.35 |
| CRG1 | IS-CRG1-02A | 25.26 | 143.23 | 115.59 | 97.54 | 77.67 | 43.08 | 23.67 | 25.87 | 21.28 | 17.39 | 16.71 | 15.71 | 13.89 | 14.35 | 14.60 |
| CRG1 | IS-CRG1-03A | 110.18 | 58.39 | 39.48 | 30.82 | 23.83 | 14.36 | 13.33 | 9.65 | 8.51 | 8.07 | 8.36 | 8.10 | 7.72 | 8.13 | 8.70 |
| CRG1 | IS-CRG1-24 | 739.29 | 62.58 | 44.31 | 32.70 | 22.00 | 11.28 | 20.68 | 5.79 | 4.26 | 4.04 | 4.18 | 4.29 | 4.63 | 4.78 | 5.90 |
| CRG3 | IS-CRG3-4A | 389.38 | 69.68 | 55.07 | 46.64 | 38.17 | 27.69 | 28.03 | 21.62 | 19.15 | 17.70 | 16.71 | 15.24 | 14.20 | 13.40 | 13.66 |
| CRG3 | IS-CRG3-16A | 1171.8 | 441.94 | 309.41 | 239.34 | 180.00 | 87.69 | 80.95 | 43.63 | 25.53 | 18.01 | 13.93 | 10.95 | 8.64 | 7.18 | 6.83 |
| CRG4A | IS-CRG4A-10 | 613.79 | 55.81 | 39.98 | 31.48 | 23.17 | 12.31 | 30.61 | 6.18 | 4.26 | 2.48 | 1.39 | 1.90 | 1.54 | 1.44 | 1.55 |
| CRG5 | IS-CRG5-01 | 43.61 | 75.48 | 51.86 | 36.48 | 24.83 | 11.28 | 14.83 | 5.79 | 4.26 | 4.35 | 4.18 | 3.81 | 3.70 | 3.35 | 3.73 |
| CRG5 | IS-CRG5-04 | 152.33 | 275.16 | 216.58 | 168.03 | 125.50 | 68.72 | 29.66 | 39.00 | 31.91 | 26.40 | 23.68 | 23.33 | 22.22 | 21.53 | 22.36 |
| CRG6 | IS-CRG6-04 | 48.08 | 201.29 | 184.41 | 161.48 | 128.33 | 78.97 | 29.66 | 50.19 | 40.43 | 35.71 | 32.03 | 30.48 | 27.78 | 26.79 | 26.71 |
| CRG6 | IS-CRG6-02 | 170.79 | 88.39 | 67.95 | 53.61 | 41.17 | 29.23 | 25.99 | 20.46 | 19.15 | 17.70 | 15.32 | 15.24 | 15.12 | 15.31 | 15.84 |
| CRG6 | PWS-CRG6-2 | 49.41 | 240.00 | 204.21 | 168.03 | 123.00 | 69.23 | 29.39 | 42.86 | 36.17 | 31.99 | 29.25 | 29.52 | 27.78 | 27.75 | 27.95 |
| CRG6 | PWS-CRG6-3 | 101.44 | 187.42 | 136.14 | 100.82 | 71.00 | 35.38 | 22.59 | 21.24 | 17.02 | 16.15 | 13.93 | 14.76 | 14.81 | 14.35 | 15.53 |
| CRG6 | PWS-CRG6-5 | 200.78 | 134.52 | 100.99 | 80.57 | 61.50 | 35.90 | 32.38 | 21.62 | 17.02 | 15.22 | 13.93 | 14.29 | 12.96 | 13.88 | 14.60 |
| CRG6 | PWS-CRG6-6 | 252.77 | 85.16 | 63.86 | 53.44 | 43.50 | 28.21 | 29.12 | 19.69 | 17.02 | 15.22 | 13.93 | 13.81 | 13.27 | 15.31 | 15.22 |
| CRG6 | PWS-CRG6-8 | 360.03 | 90.97 | 73.39 | 62.21 | 51.17 | 31.79 | 25.99 | 23.55 | 19.15 | 18.01 | 16.71 | 15.71 | 13.89 | 14.35 | 15.53 |
| CRG6 | PWS-CRG6-15 | 701.15 | 102.90 | 77.85 | 64.10 | 50.17 | 31.28 | 35.37 | 21.62 | 19.15 | 17.39 | 16.71 | 17.14 | 16.36 | 18.18 | 20.50 |

Table 2: Calculation of REE data from bedrock

| Borehole | CRL ID | Depth | ∑REE | LREE | HREE | LREE/HREE | δEu | Ce/Yb | La/Yb |
|---|---|---|---|---|---|---|---|---|---|
| CR9 | IS-CR9-3 | 191.9 | 552.51 | 406.81 | 145.70 | 2.79 | 0.79 | 5.36 | 6.74 |
| CR9 | IS-CR9-25 | 203.8 | 2625.15 | 2281.05 | 344.10 | 6.63 | 0.74 | 31.46 | 29.14 |
| CRG1 | IS-CRG1-02A | 25.26 | 640.58 | 500.78 | 139.80 | 3.58 | 0.69 | 8.05 | 9.98 |
| CRG1 | IS-CRG1-03A | 110.18 | 247.45 | 180.21 | 67.24 | 2.68 | 1.11 | 4.85 | 7.18 |
| CRG1 | IS-CRG1-24 | 739.29 | 231.42 | 193.55 | 37.86 | 5.11 | 2.42 | 9.26 | 13.08 |
| CRG3 | IS-CRG3-4A | 389.38 | 396.96 | 265.28 | 131.68 | 2.01 | 1.14 | 4.11 | 5.20 |
| CRG3 | IS-CRG3-16A | 1171.8 | 1474.04 | 1339.33 | 134.70 | 9.94 | 1.23 | 43.11 | 61.58 |
| CRG4A | IS-CRG4A-10 | 613.79 | 214.09 | 193.34 | 20.75 | 9.32 | 3.31 | 27.85 | 38.88 |
| CRG5 | IS-CRG5-01 | 43.61 | 247.92 | 214.76 | 33.16 | 6.48 | 1.74 | 15.48 | 22.54 |
| CRG5 | IS-CRG5-04 | 152.33 | 1094.09 | 883.66 | 210.43 | 4.20 | 0.55 | 10.06 | 12.78 |
| CRG6 | IS-CRG6-04 | 48.08 | 1054.26 | 784.14 | 270.12 | 2.90 | 0.46 | 6.88 | 7.51 |
| CRG6 | IS-CRG6-02 | 170.79 | 440.47 | 306.32 | 134.15 | 2.28 | 1.05 | 4.44 | 5.77 |
| CRG6 | PWS-CRG6-2 | 49.41 | 1087.13 | 833.86 | 253.27 | 3.29 | 0.52 | 7.36 | 8.65 |
| CRG6 | PWS-CRG6-3 | 101.44 | 681.14 | 553.35 | 127.79 | 4.33 | 0.80 | 9.48 | 13.06 |
| CRG6 | PWS-CRG6-5 | 200.78 | 569.37 | 445.86 | 123.51 | 3.61 | 1.13 | 7.28 | 9.69 |
| CRG6 | PWS-CRG6-6 | 252.77 | 426.75 | 303.29 | 123.47 | 2.46 | 1.22 | 4.17 | 5.56 |
| CRG6 | PWS-CRG6-8 | 360.03 | 472.43 | 335.52 | 136.91 | 2.45 | 0.94 | 5.11 | 6.34 |
| CRG6 | PWS-CRG6-15 | 701.15 | 508.73 | 361.67 | 147.05 | 2.46 | 1.34 | 4.28 | 5.66 |

Table 3: REE data for calcite samples from the in different boreholes, data categorized by borehole and define. All REE data is after chondrited-normalized

| Borehole | CRL ID | Depth | La | Ce | Pr | Nd | Sm | Eu | Gd | Tb | Dy | Ho | Er | Tm | Yb | Lu |
|---|---|---|---|---|---|---|---|---|---|---|---|---|---|---|---|---|
| CR9 | IS-CR9-3 | 191.9 | 95.48 | 70.17 | 55 | 41.67 | 23.077 | 25.99 | 14.67 | 12.8 | 0 | 9.75 | 11.43 | 9.568 | 10.5 | 0 |
| CR9 | IS-CR9-25 | 203.8 | 3322.58 | 2722.77 | 2230 | 1800 | 948.72 | 421.8 | 455.6 | 274 | 171.7 | 116 | 87.14 | 63.89 | 51.2 | 43.5 |
| CR9 | IS-CR9-16 | 545.4 | 24.84 | 25.99 | 26.39 | 23.33 | 25.641 | 14.42 | 18.15 | 17 | 13.04 | 11.1 | 10 | 8.642 | 8.13 | 7.76 |
| CRG1 | IS-CRG1-02A | 25.26 | 509.68 | 429.46 | 377.9 | 320 | 202.05 | 77.96 | 129 | 93.6 | 75.16 | 65.5 | 64.29 | 58.64 | 62.7 | 62.7 |
| CRG1 | IS-CRG1-03A | 110.18 | 26.13 | 21.91 | 16.89 | 14.17 | 11.282 | 7.619 | 10.42 | 12.8 | 12.11 | 11.1 | 13.33 | 13.89 | 14.8 | 15.2 |
| CRG1 | IS-CRG1-20A | 493.66 | 233.55 | 163.37 | 112.3 | 74.17 | 42.051 | 20.54 | 25.48 | 25.5 | 21.12 | 18.1 | 18.57 | 17.9 | 23 | 25.2 |
| CRG1 | IS-CRG1-24 | 739.29 | 587.10 | 396.04 | 283.6 | 201.7 | 88.718 | 31.29 | 45.17 | 36.2 | 36.02 | 29.2 | 30.95 | 31.17 | 34.9 | 0 |
| CRG3 | IS-CRG3-4A | 389.38 | 95.48 | 77.48 | 71.31 | 67.17 | 78.462 | 48.57 | 76.06 | 74.5 | 67.7 | 57.1 | 53.81 | 42.59 | 32.5 | 28.3 |
| CRG3 | IS-CRG3-16A | 1171.8 | 545.16 | 361.39 | 264.8 | 196.7 | 81.538 | 60.27 | 33.2 | 14.9 | 8.696 | 5.57 | 4.286 | 3.086 | 2.39 | 0 |
| CRG4A | IS-CRG4A-10 | 613.79 | 42.58 | 29.83 | 22.79 | 17.33 | 9.2308 | 26.67 | 4.633 | 4.26 | 3.106 | 1.39 | 1.905 | 1.852 | 1.44 | 0 |
| CRG5 | IS-CRG5-01 | 43.61 | 131.61 | 105.32 | 81.97 | 63.5 | 47.692 | 22.59 | 39.38 | 38.3 | 32.61 | 29.2 | 29.52 | 27.16 | 26.8 | 26.1 |
| CRG5 | IS-CRG5-04 | 152.33 | 506.45 | 466.58 | 380.3 | 305 | 256.41 | 125.7 | 199.6 | 215 | 196.3 | 170 | 167.6 | 171.9 | 205 | 210 |
| CRG6 | IS-CRG6-04 | 48.08 | 741.94 | 570.54 | 428.7 | 315 | 192.31 | 64.76 | 132.4 | 109 | 88.51 | 76.6 | 73.33 | 62.96 | 58.4 | 62.7 |
| CRG6 | IS-CRG6-02 | 170.79 | 187.74 | 146.04 | 124.6 | 100.5 | 92.821 | 73.74 | 70.27 | 63.8 | 48.45 | 39 | 31.9 | 29.01 | 27.8 | 24.2 |

Table 4: Calculation of REE data from calcite

| Borehole | CRL ID | Depth | ∑REE | LREE | HREE | LREE/HREE | δEu | Ce/Yb | La/Yb |
|---|---|---|---|---|---|---|---|---|---|
| CR9 | IS-CR9-3 | 191.9 | 380.097 | 311.387 | 68.71 | 4.532 | 1.3768 | 6.666 | 9.071 |
| CR9 | IS-CR9-25 | 203.8 | 12708.46 | 11445.3 | 1263 | 9.061 | 0.6007 | 53.18 | 64.9 |
| CR9 | IS-CR9-16 | 545.4 | 234.5118 | 140.618 | 93.89 | 1.498 | 0.6587 | 3.195 | 3.054 |
| CRG1 | IS-CRG1-02A | 25.26 | 2528.542 | 1917.01 | 611.5 | 3.135 | 0.471 | 6.852 | 8.131 |
| CRG1 | IS-CRG1-03A | 110.18 | 201.7047 | 97.988 | 103.7 | 0.945 | 0.702 | 1.477 | 1.762 |
| CRG1 | IS-CRG1-20A | 493.66 | 820.8048 | 645.972 | 174.8 | 3.695 | 0.6084 | 7.113 | 10.17 |
| CRG1 | IS-CRG1-24 | 739.29 | 1832.09 | 1588.42 | 243.7 | 6.519 | 0.4674 | 11.34 | 16.81 |
| CRG3 | IS-CRG3-4A | 389.38 | 871.0039 | 438.47 | 432.5 | 1.014 | 0.6287 | 2.381 | 2.935 |
| CRG3 | IS-CRG3-16A | 1171.8 | 1581.908 | 1509.78 | 72.13 | 20.93 | 1.0506 | 151.1 | 227.9 |
| CRG4A | IS-CRG4A-10 | 613.79 | 167.0039 | 148.425 | 18.58 | 7.989 | 3.8469 | 20.78 | 29.66 |
| CRG5 | IS-CRG5-01 | 43.61 | 701.7815 | 452.679 | 249.1 | 1.817 | 0.5188 | 3.931 | 4.912 |
| CRG5 | IS-CRG5-04 | 152.33 | 3575.751 | 2040.49 | 1535 | 1.329 | 0.5513 | 2.278 | 2.473 |
| CRG6 | IS-CRG6-04 | 48.08 | 2976.695 | 2313.24 | 663.5 | 3.487 | 0.3989 | 9.774 | 12.71 |
| CRG6 | IS-CRG6-02 | 170.79 | 1059.87 | 725.434 | 334.4 | 2.169 | 0.9043 | 5.262 | 6.765 |

# Appendix 4

Table of EDAX results which were measured in China. Table is organized by core sample and depth and all elements units are normalize to 100%.

| Sample | Depth (mabl) | Unit | Fracture mineral | O (%) | C (%) | Ca (%) | Mg (%) | Mn (%) | Fe (%) | Na (%) | Al (%) | Si (%) | F (%) | S (%) |
|---|---|---|---|---|---|---|---|---|---|---|---|---|---|---|
| CRG1 | 25.26a | A | dolomite | 61.16 | 22.32 | 8.17 | 7.33 | 0.25 | 0.76 | | | | | |
| CRG1 | 25.26b | A | Metasomatic mineral | 61.4 | 22.8 | 15.51 | 0.14 | 0.15 | | | | | | |
| CRG1 | 25.26c | A | Metasomatic mineral | 61.1 | 22.2 | 16.55 | | 0.15 | | | | | | |
| CRG1 | 25.26d | A | quartz | 66.61 | | | | | | | 0.34 | 33.05 | | |
| CRG1 | 308.73a | B | coarse grain calcite | 60.48 | 20.97 | 18.55 | | | | | | | | |
| CRG1 | 308.73b | B | two different coarse calcite | 60.36 | 20.72 | 18.77 | | 0.15 | | | | | | |
| CRG1 | 308.73c | B | two different coarse calcite | 58.79 | 17.58 | 23.63 | | | | | | | | |
| CRG1 | 308.73d | B | rare earth elements | 57.91 | 18.53 | 19.18 | | 0.2 | | | | | 3.2 | |
| CRG1 | 366.04a | B | coarse grain calcite | 60.58 | 21.16 | 18.25 | | | | | | | | |
| CRG1 | 366.04b | B | fluorite | 41.76 | | 18.95 | | | | | | | 24.1 | |
| CRG1 | 366.04c | B | quartz | 61.99 | | 9.51 | | | 0.58 | | | 20.02 | | |
| CRG1 | 448.56a | B | calcite (in little cave) | 60.91 | 21.81 | 17.28 | | | | | | | | |
| CRG1 | 448.56b | B | chlorite (serpentine） | 61.47 | | 0.19 | 13.2 | | 2.04 | | 0.31 | 22.78 | | |
| CRG1 | 615a | B | calcite which has arranged directional | 62.66 | 25.31 | 12.03 | | | | | | | | |
| CRG1 | 615b | B | quartz (serpentine) | 61.47 | | 0.19 | 13.2 | | 2.04 | | | 22.78 | 0.31 | |
| CRG1 | 615c | B | calcite which has arranged direction | 61.08 | 22.16 | 16.63 | | 0.14 | | | | | | |
| CRG1 | 615d | B | Talc | 60.4 | 20.8 | 18.38 | 0.18 | 0.13 | 0.12 | | | | | |
| CRG3 | 24.7a | A | coarse grain calcite | 60.85 | 21.7 | 17.3 | | 0.15 | | | | | | |

| Sample | Depth (mabl) | Unit | Fracture mineral | O (%) | C (%) | Ca (%) | Mg (%) | Mn (%) | Fe (%) | Na (%) | Al (%) | Si (%) | F (%) | S (%) |
|---|---|---|---|---|---|---|---|---|---|---|---|---|---|---|
| CRG3 | 24.7b | A | Dolomite | 61.7 | 23.4 | 7.1 | 7.12 | 0.13 | 0.56 | | | | | |
| CRG3 | 133.52 | B | calcite (crystal) | 58.1 | 16.2 | 25.45 | | 0.25 | | | | | | |
| CRG3 | 133.52 | B | dolomite | 60.77 | 21.55 | 8.89 | 7.82 | 0.15 | 0.81 | | | | | |
| CRG3 | 133.52 | B | coarse grain calcite | 59.5 | 19.01 | 21.26 | | 0.23 | | | | | | |
| CRG3 | 307.9a | B | fine grain calcite | 61.4 | 22.67 | 15.81 | 0.05 | | | | 0.07 | | | |
| CRG3 | 307.9b | B | fine grain calcite | 61.96 | 23.83 | 14.02 | 0.07 | | | | 0.06 | 0.06 | | |
| CRG3 | 307.9c | B | Fluorite | 39.88 | | 14.85 | | | | | 1.79 | 0.82 | 28.9 | |
| CRG3 | 862.06a | B | calcite (crystal) | 59.41 | 18.48 | 21.6 | 0.06 | 0.22 | | | 0.02 | 0.07 | | 0.13 |
| CRG3 | 862.06b | B | coarse grain calcite | 61.3 | 22.45 | 15.64 | 0.09 | 0.1 | | 0.15 | 0.09 | 0.18 | | |
| CRG3 | 862.06c | B | coarse grain calcite | 62.21 | 23.76 | 12.62 | 0.4 | 0.11 | 0.19 | | 0.27 | 0.39 | | 0.06 |
| CRG3 | 1171.77a | C | calcite which arranged directional | 58.94 | 17.78 | 22.83 | | 0.35 | | | 0.01 | 0.09 | | |
| CRG3 | 1171.77b | C | Calcite | 59.33 | 18.59 | 21.32 | 0.15 | 0.39 | 0.17 | | | 0.06 | | |
| CRG4A | 613.79 | B | calcite | 59.79 | 19.57 | 20.54 | | 0.1 | | | | | | |
| CRG5 | 12.68a | C | Calcite | 61.15 | 22.19 | 15.23 | 0.59 | 0.61 | 0.14 | | | 0.1 | | |
| CRG5 | 12.68b | C | Calcite | 61.68 | 23.22 | 13.22 | 0.94 | 0.58 | 0.2 | | | 0.15 | | |
| CRG5 | 43.61 | C | coarse grain calcite | 61.57 | 22.96 | 15.12 | 0.04 | 0.05 | | | 0.16 | 0.1 | | |
| CRG6 | 182.04a | B | fine grain calcite | 61.7 | 22.84 | 14.34 | 0.25 | 0.07 | | | 0.5 | 0.3 | | |
| CRG6 | 182.04b | B | coarse grain calcite | 60.36 | 20.5 | 18.54 | 0.2 | 0.12 | | | 0.12 | 0.17 | | |
| CRG6 | 219.33 | B | coarse grain calcite | 61.18 | 22.36 | 16.47 | | | | | | | | |
| CRG6 | 219.33 | B | chlorite | 61.03 | 9.94 | 0.66 | | | 4.68 | | 3.29 | 20.41 | | |
| CRG6 | 395.79 | B | coarse grain calcite | 59.65 | 19.31 | 20.8 | | 0.23 | | | | | | |
| CRG6 | 691.19 | B | calcite | 59.72 | 19.44 | 20.16 | 0.18 | 0.51 | | | | | | |
| CRG6 | 691.19 | B | calcite (in little cave) | 59.89 | 19.79 | 20.32 | | | | | | | | |

| Sample | Depth (mabl) | Unit | Fracture mineral | O (%) | C (%) | Ca (%) | Mg (%) | Mn (%) | Fe (%) | Na (%) | Al (%) | Si (%) | F (%) | S (%) |
|---|---|---|---|---|---|---|---|---|---|---|---|---|---|---|
| CR9 | 9.015 | B | calcite (in little cave) | 60.6 | 20.98 | 17.96 | | | | | 0.45 | | | |
| CR9 | 238.2 | B | fine grain calcite | 62.53 | 24.84 | 12.21 | 0.2 | | | | | 0.22 | | |
| CR9 | 553.7a | B | Metasomatic mineral | 61.13 | 22.14 | 16.26 | 0.17 | 0.18 | | | | 0.12 | | |
| CR9 | 553.7b | B | coarse grain calcite | 59.21 | 17.11 | 21.2 | 0.88 | | 0.18 | | 0.24 | 1.19 | | |
| CR9 | 599.85 | B | coarse grain calcite | 61 | 21.84 | 16.71 | 0.31 | | | | | 0.15 | | |
| CR18 | LCR18-3 a | B | dolomite | 61.71 | 23.42 | 7.77 | 6.58 | | 0.52 | | | | | |
| CR18 | LCR18-3 b | B | coarse grain calcite | 60.92 | 21.84 | 17.24 | | | | | | | | |

# Appendix 5

Table of strontium ratios for calcite samples from CRL cores.

| Core | Depth (m) | 87Sr/86Sr |
|---|---|---|
| CR9 | 203.8 | 0.70853 |
| | 700.76 | 0.70927 |
| CRG1 | 110.18 | 0.72174 |
| | 110.18 | 0.71760 |
| | 361.04 | 0.70905 |
| | 448.57 | 0.70978 |
| | 493.66 | 0.70963 |
| | 615 | 0.71278 |
| | 615 | 0.70952 |
| | 615.15 | 0.70981 |
| | 615.15 | 0.70887 |
| CRG3 | 637.72 | 0.70925 |
| | 637.72 | 0.70937 |
| | 1171.77 | 0.70910 |
| CRG4A | 425.35 | 0.70868 |
| CRG5 | 16.27 | 0.70942 |
| | 43.61 | 0.70939 |
| | 43.61 | 0.70987 |
| | 438.12 | 0.71211 |
| CRG6 | 48.08 | 0.71227 |
| | 111.2 | 0.70889 |
| | 182.04 | 0.70899 |
| | 182.04 | 0.70904 |
| | 359.62 | 0.70900 |
| | 724.72 | 0.70849 |

# Appendix 6

Table of Th and U concentration and calculated Thorium/uranium ratios, rock type S for bedrock and R for calcite

| borehole | depth | rock type | Th ppm | U ppm | Thorium/uranium |
|---|---|---|---|---|---|
| CR9 | 191.9 | S1 | 2.9 | 1.4 | 2.07 |
| CR9 | 203.8 | S2 | 21.9 | 5.3 | 4.13 |
| CRG1 | 25.26 | S3 | 1.9 | 1 | 1.90 |
| CRG1 | 110.18 | S4 | 1.8 | 1.2 | 1.50 |
| CRG1 | 739.29 | S5 | 7.8 | 1.2 | 6.50 |
| CRG3 | 389.38 | S6 | 2.2 | 1.1 | 2.00 |
| CRG3 | 1171.77 | S7 | 13.8 | 2.9 | 4.76 |
| CRG4A | 613.79 | S8 | 1.9 | 4.6 | 0.41 |
| CRG5 | 43.61 | S9 | 5 | 1.2 | 4.17 |
| CRG5 | 152.33 | S10 | 11.3 | 1.1 | 10.27 |
| CRG6 | 48.08 | S11 | 10.3 | 2.4 | 4.29 |
| CRG6 | 170.79 | S12 | 0.8 | 0.7 | 1.14 |
| CRG6 | 49.41 | S13 | 6.8 | 1.3 | 5.23 |
| CRG6 | 101.44 | S14 | 11.9 | 1.6 | 7.44 |
| CRG6 | 200.78 | S15 | 4.5 | 1.6 | 2.81 |
| CRG6 | 252.77 | S16 | 1.4 | 0.9 | 1.56 |
| CRG6 | 360.03 | S17 | 3 | 1 | 3.00 |
| CRG6 | 701.15 | S18 | 2.1 | 1.1 | 1.91 |
| CR9 | 191.9 | R1 | 2.4 | 1 | 2.40 |
| CR9 | 203.8 | R2 | 20.6 | 4.8 | 4.29 |
| CR9 | 545.4 | R3 | 0.7 | 1.3 | 0.54 |
| CRG1 | 25.26 | R4 | 0.4 | 0.8 | 0.50 |
| CRG1 | 110.18 | R5 | 3 | 0.5 | 6.00 |
| CRG1 | 493.66 | R6 | 0.2 | < 0.1 | |
| CRG1 | 739.29 | R7 | 0.2 | < 0.1 | |
| CRG3 | 389.38 | R8 | 0.2 | < 0.1 | |
| CRG3 | 1171.77 | R9 | 1.8 | 0.5 | 3.60 |
| CRG4A | 613.79 | R10 | 2.3 | 2.1 | 1.10 |
| CRG5 | 43.61 | R11 | 1.2 | 0.1 | 12.00 |
| CRG5 | 152.33 | R12 | 0.4 | < 0.1 | |
| CRG6 | 48.08 | R13 | 0.9 | 1.7 | 0.53 |
| CRG6 | 170.79 | R14 | 0.6 | 0.1 | 6.00 |